THE EFFECT OF VAPOR-BORNE SOUND ON CONDENSATION HEAT TRANSFER

By

ROBERT LEE LOTT, JR.

Bachelor of Science
Southern Methodist University
Dallas, Texas
1960

Master of Science
University of Arkansas
Fayetteville, Arkansas
1962

Submitted to the Faculty of the Graduate College
of the Oklahoma State University
in partial fulfillment of the requirements
for the degree of
DOCTOR OF PHILOSOPHY
May, 1969

THE EFFECT OF VAPOR-BORNE

SOUND ON CONDENSATION

HEAT TRANSFER

Jerald D. Parker
Thesis Adviser

Ladislaus J. Fila

R. J. Towers

Robert L. Robinson Jr.

D. D. Durham
Dean of the Graduate School

ACKNOWLEDGEMENTS

The author sincerely thanks his thesis adviser, Professor Jerald D. Parker, for the aid, assistance and support received throughout the duration of this study. The author appreciates the efforts and advice of a host of faculty members who have served on his Graduate Committee at various times. These faculty members are Dr. O. H. Hamilton, Dr. R. L. Robinson, Dr. R. L. Panton, Dr. R. L. Lowery, Dr. J. A. Wiebelt, and Professor L. J. Fila.

The author fondly recalls and recognizes the excellent services provided by the Mechanical Engineering Laboratory personnel: Professor F. C. McQuiston, Mr. Jeff Freeman, Mr. George Cooper and Mr. Ray Ashcraft. Without the interest and assistance of these gentlemen, the experimental tasks would have been much more difficult.

The financial assistance which has made this study possible include: a Ford Foundation loan, a teaching assistantship in the Mechanical Engineering Department of Oklahoma State University, a NASA graduate research assistantship, a NDEA Fellowship, an Olin grant and a Vanderbilt University Research Council grant. All of these financial awards are remembered and gratefully acknowledged.

The author feels a special indebtedness to Vanderbilt University for the opportunity to instruct Mechanical Engineering courses while completing this thesis study. The support and encouragement given

the author by Dr. Robert S. Rowe, Dean of Engineering at Vanderbilt University, and Professor Bruce M. Bayer, Chairman of the Mechanical Engineering Department at Vanderbilt University, is valued.

The author must express perpetual gratitude for the patience and love the family has extended during the period of this study. The author's children, Susan Lynn, Robert Paul, Lori Jon and John Milton, have perhaps made the largest contribution to the completion of this thesis by their desire for Daddy to "get through". Personal thanks are bestowed upon the author's wife, Peggy, for her loyal support and understanding, as well as for her expert typing of this manuscript.

TABLE OF CONTENTS

LIST OF TABLES

LIST OF FIGURES

LIST OF FIGURES (Continued)

LIST OF FIGURES(Continued)

LIST OF FIGURES (Continued)

NOMENCLATURE

a	speed of sound
a_0	stagnation speed of sound
A	heat exchanger or condenser surface area
A	constant in temperature dependent viscosity relationship, $\mu = Ae^{B/T}$
A_ℓ	defined by equation 3.53
b	main vortex thickness (Figure 10)
B	constant in temperature dependent viscosity relationship, $\mu = Ae^{B/T}$ (equation A.32)
B_ℓ	defined by equation 3.54
$\overline{B}$	defined by equation A.24
C	property parameter, $\left[\frac{gc_p(\rho - \rho_v)}{4\nu k}\right]^{\frac{1}{4}}$
c_p	specific heat at constant pressure
$c_{p,c}$	specific heat of coolant
c_v	specific heat at constant volume
C_h	correction factor for the average heat transfer
$(C_h)_{Rohsenow}$	correction factor for the average heat transfer coefficient, using Rohsenow's recommendation
C_m	defined by equation A.10
C_T	defined by equation A.14
C_u	defined by equation A.6
C_δ	correction factor for the laminar film thickness, $\delta/(\delta_w)_{Nu}$

C_Γ	correction factor for the condensate mass flow rate, $\Gamma/(\Gamma_w)_{Nu}$
C_θ	$-F_5(z)$ evaluated at $z = 1$
f	frequency
f_o	natural or fundamental frequency
f_p	pulse frequency for siren generated sonic pulsations
F	dimensionless variable, $F(\eta) = \Psi/(x^{3/4} \cdot 4\alpha C)$
$F(\tilde{r})$	defined by equations 3.71 and 3.72
F_r	body force on fluid in radial direction
Fr_x	Froude number, U_∞^2/gx
F_x	body force on fluid in axial direction
$F_1(z)$	defined by equation A.7
$F_2(z)$	defined by equation A.8
$F_3(z)$	defined by equation A.18
$F_4(z)$	defined by equation A.21
$F_5(z)$	defined by equation A.25
g	local gravitational attraction
$g(x,t)$	x and t dependent gravity field
g_c	Newton constant
$G(x)$	gravity field
h	heat transfer coefficient
$\bar{h}$	average heat transfer coefficient
$\tilde{h}$	dimensionless heat transfer coefficient, $\bar{h}/\bar{h}_{Nu}$
h_{fg}	latent heat of condensation
h'_{fg}	$h_{fg} + (3/8)c_p\Delta T$
$h_{f,e}$	specific enthalpy of saturated liquid condensate at the exit temperature

$h_{g,i}$	specific enthalpy of saturated vapor at the inlet temperature
$\bar{h}_{Nu}$	average heat transfer coefficient predicted by Nusselt's theory
$\bar{h}_o$	average heat transfer coefficient without sonic pulsation
$\bar{h}_p$	average heat transfer coefficient with sonic pulsation
$(\bar{h}_w)_{Nu}$	average heat transfer coefficient predicted by Nusselt's theory, with condensate properties evaluated at the condenser wall temperature
h_x	local heat transfer coefficient
H	dimensionless parameter, $(c_p\Delta T)/(Prh_{fg})$
I	acoustic intensity
I_o	reference intensity level
IL	acoustic intensity level, $10 \log_{10} \frac{I}{I_o}$
k	thermal conductivity of the condensate
k_v	ratio of specific heats, c_p/c_v, for the vapor or gas
ℓ_n	Helmholtz resonator neck length
L	condenser length
M	mach number of through flow vapor, $\bar{U}/a$
M_e	mach number of through flow vapor at condenser exit
M_o	acoustic mach number, U_o/a
$M_o^2(\tilde{r})$	$ber_o^2(\tilde{r}) + bei_o^2(\tilde{r})$
$M_1^2(\tilde{r})$	$ber_1^2(\tilde{r}) + bei_1^2(\tilde{r})$
N	dimensionless parameter, $(16g\mu h_{fg}) / (k\Delta TU_\infty^2)$
Nu	Nusselt number
Nu_x	Nusselt number based on x, $\bar{h}x/k$
Nu_L	Nusselt number based on condenser length, $\bar{h}L/k$

P	instantaneous pressure
P'	Pressure deviation from the time-mean value
$\overline{P}$	time-mean pressure
$\overline{P'}$	rms sound pressure
P_o	maximum sound pressure amplitude
P_{ref}	reference value of rms sound pressure used to define the sound pressure level
$\overline{P_n - P_a}$	time-mean difference in pressure between the velocity node and antinode in a resonant tube
ΔP	$\overline{P_n - P_a}$
ΔP	venturi meter pressure difference measurement as indicated in Figures 23 and 24.
Q	heat transfer rate
r	radial distance
$\tilde{r}$	dimensionless radius, $r/\sqrt{\nu_v/\omega}$
r_n	neck radius of Helmholtz resonator
R	tube radius
$\overline{R}$	$R-\delta$, radial distance from tube axis to condensate film surface
$\tilde{R}$	dimensionless tube radius, $R/\sqrt{\nu_v/\omega}$
R_v	gas constant
Re	Condensate Reynolds number, $4\Gamma_s/\mu$
Re_a	air Reynolds number
Re_f	thin-film water flow Reynolds number
Re_{Lx}	liquid Reynolds number, $\rho\mu_\infty x/\mu$
Re_v	vapor Reynolds number $2\bar{\rho}_v\bar{U}_o R/\mu_v$
s	specific entropy

SPL	sound pressure level, $20 \log_{10} (\overline{p'} / p_{ref})$
t	time
T	instantaneous temperature
T'	deviation from time-mean temperature
$\overline{T}$	time-average temperature
T_f	temperature to use for condensate property evaluation
T_v	saturated vapor temperature
T_w	condenser wall temperature
ΔT	$T_v - T_w$
ΔT_c	coolant temperature rise
u	instantaneous velocity of condensate in x direction
u'	deviation of particle velocity of condensate in x direction from the time-mean value
$\overline{u}$	time-mean velocity of condensate in x direction
$\tilde{u}$	dimensionless velocity ratio defined by equation A.35 and A.36
u_v	instantaneous vapor velocity in x direction
u_v'	deviation of vapor velocity in x direction from the time-mean value
$\overline{u}_v$	time-mean vapor velocity in x direction
U_o	maximum acoustic velocity
$\overline{U}_o$	time-mean through flow vapor velocity in x direction at x = 0
$\overline{U}_{o,a}$	time-mean through flow air velocity in x direction
v	instantaneous condensate velocity in y (or radial) direction
v'	deviation of condensate velocity in y (or radial) direction from the time-mean value
$\overline{v}$	time-mean condensate velocity in y (or radial) direction
v_v	instantaneous vapor velocity in y (or radial) direction

v_v'	deviation of vapor velocity in y (or radial direction) from the time-mean value
$\bar{v}_v$	time-mean vapor velocity in y (or radial)direction
$v_{g,i}$	specific volume of saturated vapor at inlet temperature
V_c	volume of Helmholtz resonator
x	distance along condensing surface
$\tilde{x}$	$2\pi x/\lambda$
y	distance normal to condensing surface
z	distance normal to x and y
z	dimensionless distance, $y/\delta(x)$, in Appendix A
Z	the inverse of Froude number, $1/Fr_x$

Greek Letters

α	thermal diffusivity of condensate, $k/\rho c_p$
β	$\frac{T_v}{T_w}\left(1 - \frac{\Delta T}{2T_w}\right) \ell n \frac{\mu(T_w)}{\mu(T_v)}$, equation A.37
γ	r/R
Γ	vapor mass flow rate
Γ_o	vapor mass flow rate at x = 0
Γ_c	coolant mass flow rate
Γ_s	condensate mass flow rate from the test condenser
$(\Gamma_w)_{Nu}$	condensate mass flow rate predicted by Nusselt's theory, with properties evaluated at the condenser wall temperature
Γ_x	excess vapor mass flow rate
δ	condensate film thickness
$\tilde{\delta}$	dimensionless film thickness, δ/δ_{Nu}

δ_{ac}	A.C. boundary layer thickness, $\sqrt{2\nu/\omega}$
$(\delta_w)_{Nu}$	condensate film thickness predicted by Nusselt's theory with condensate properties evaluated at the condenser wall temperature
ϵ	$\left(\sqrt{\nu_v/\omega}\right)/\lambda$
ζ	$\frac{\pi}{2\rho g \lambda \rho_v}\left(\frac{Po}{a}\right)^2$
η	similarity variable, $Cyx^{-1/4}$
θ	dimensionless temperature variable, $T - T_v/\Delta T$
$\theta_0(\tilde{r})$	$\tan^{-1}\frac{bei_o(\tilde{r})}{ber_o(\tilde{r})}$
$\theta_1(\tilde{r})$	$\tan^{-1}\frac{bei_1(\tilde{r})}{ber_1(\tilde{r})}$
κ	wave number, ω/a
λ	acoustic wavelength
μ	dynamic viscosity of the condensate
$\tilde{\mu}$	ratio of $\mu_w/\mu(z)$, equation A.4
μ_h	defined by equation A.31
μ_v	dynamic viscosity of the vapor
μ_w	dynamic viscosity of condensate evaluated at the condenser wall temperature.
μ_I	defined by equation A.31b
μ_δ	defined by equation A.31a
ν	kinematic viscosity of the condensate
ν_o	kinematic viscosity of vapor at stagnation conditions
ν_v	kinematic viscosity of the vapor
ξ	$2x/\lambda$

ρ	condensate density
ρ_v	instantaneous vapor density
ρ_v'	deviation of vapor density from the time-mean value
$\bar{\rho}_v$	time-mean vapor density
σ	shearing stress exerted on the condensate film by the vapor
τ	time period much longer than acoustic time period
φ	angle of condenser inclination with respect to the horizontal
ϕ	velocity potential
ψ	stream function
$\tilde{\psi}$	dimensionless stream function
ω	circular frequency, $2\pi f$
Ω_m	dimensionless size of main vortex, b/R

CHAPTER I

INTRODUCTION

Condensation heat transfer has been a subject of theoretical and experimental investigations for many years. In this thesis, condensation is considered to be the process which describes the transition of a substance from a vapor state to a liquid state. The mechanisms of condensation and the parameters important to the phenomenon are generally accepted as being well known. Yet, whenever a fluid or condition different from those of previous investigations is considered, a study is initiated to determine useful relationships to predict the heat (and mass) transfer rate of the "new" situation. The large number of technical papers concerned with condensation attests to this observation. The reason is simply that no universally applicable model has been devised to account for the 2-phase flow conditions, various body forces, relative importance of possible mechanisms, intermolecular forces and multitude of geometries which may exist for a given condensing situation.

Many industrial applications of condensation processes involve systems with some degree of pulsation in the vapor, or relative vibration motion between the condensing fluid and the surface. In recent years a number of investigators have considered the effect of vibration of surfaces and pulsations in the fluid on heat transfer coefficients. The results of these investigations cover a range of

slight decrease to several hundred percent increase in heat transfer coefficients. Although considerable experimental work on the effect of sound on heat transfer has been performed, the mechanisms which determine the particular results do not appear to be completely understood.

The purpose of this study is to determine the parameters which influence condensation heat transfer when acoustic pressure pulsations are imposed on the condensing vapor and to establish the controlling mechanisms for this process.

CHAPTER II

BACKGROUND INFORMATION AND LITERATURE REVIEW

Filmwise Condensation Heat Transfer

The primary item of interest is the condensation heat transfer rate which may be attained on a cooled surface exposed to an abundant supply of vapor. For utility in designing a condensing heat exchanger, it is desirable to obtain a simplified expression relating the heat transfer rate (Q) to the difference in temperature between the saturated vapor (T_v) and the cooled surface (T_w). Preferably an expression of the form, $Q = hA(T_v - T_w)$, where A is the exchanger surface area, and h is the appropriate proportionality--the heat transfer coefficient. Review of the literature has revealed a number of parameters which may influence the heat transfer coefficient.

Considering filmwise condensation, it has been found that for water and most pure organic fluids, the heat transfer rate is governed primarily by the conduction of thermal energy across the condensate film, with negligible resistance to heat transfer being offered by the vapor-liquid interface or the liquid-exchanger interface. The film thickness depends upon the flow situation experienced by the condensate film. Factors which constitute the flow situation include the vapor flow, body forces, viscous effects and surface forces. These factors depend upon geometry and orientation. The state (and corresponding transport

properties) of the vapor and liquid as well as the temperature of the cooled surface are also involved. It is generally assumed that the thermal resistance offered by the cooled wall and the heat transfer rate on the coolant side of the cooled wall do not limit the condensation heat transfer rate. The validity of this last assumption must be verified for any given condensing situation.

Before considering how sound imposed upon the vapor might affect the filmwise condensation process, a review of the literature concerned with filmwise condensation heat transfer will be presented. The purpose of the review is to consider theoretical models, which delineate the mechanism of filmwise condensation and characterize the relative importance of various parameters, and to consider experimental results.

Nusselt (40) published his theory for condensation of a saturated vapor on a cold surface in 1916. The success of his model in predicting condensation heat transfer rates is such that it continues as a standard comparison for more involved models. The idealized model which Nusselt presented embodies the following assumptions: (1) An abundant supply of saturated vapor with steady temperature T_v condenses on a cold wall of steady uniform temperature T_w. (2) The saturated vapor condenses in a manner which completely wets the cold surface, thereby forming a liuqid film. (3) The condensate film flows due to the influence of gravity. (4) The acceleration terms in the momentum equation are negligible. (5) The vapor shear effect of the condensate film is negligible. (6) The viscous shear effect at the wall is included, with the liquid behaving in a Newtonian manner. (7) The temperature profile across the condensate is linear. (8) Saturation conditions prevail at the liquid-vapor interface. (9) Only the thermal energy associated

with the latent heat of condensation is conducted through the condensate film. (10) The fluid and vapor properties are assumed constant. A schematic representation of the physical model employed by Nusselt is shown in Figure 1.

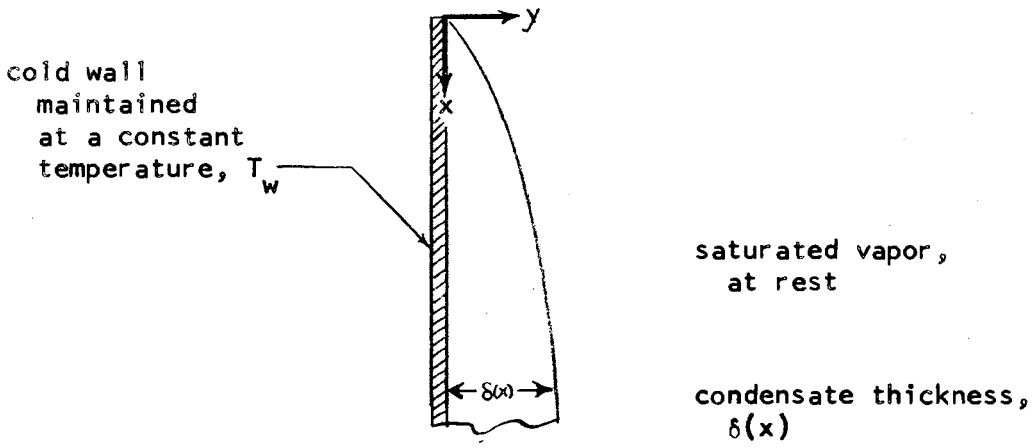

Figure 1. Nusselt's Physical Model of Film Condensation.

Considering a vertical cold wall, the following results can be obtained from the Nusselt model:

$$\text{Condensate velocity, } u(y) = \frac{(\rho-\rho_v)g}{\mu g_c}(\delta y - \tfrac{1}{2}y^2) \tag{2.1}$$

$$\text{Film thickness, } \delta(x) = \left[\frac{4g_c\mu k\Delta T x}{g\rho(\rho-\rho_v)\,h_{fg}}\right]^{1/4} \tag{2.2}$$

$$\text{Mass flow rate, } \Gamma(x) = \frac{\rho(\rho-\rho_v)g}{3\mu g_c}\delta^3(x) \tag{2.3}$$

$$\text{Local heat transfer coefficient, } h(x) = k/\delta(x) \tag{2.4}$$

$$\text{Average heat transfer coefficient, } \bar{h} = \frac{4}{3}k/\delta(L) \tag{2.5}$$

where $\Delta T = T_v - T_w$, and L is the plate length.

If the wall is inclined at an angle φ with the horizontal plane, the $(\rho - \rho_v)$ should be replaced by $(\rho - \rho_v) \sin \varphi$. If the effect of subcooling the condensate is included, then h_{fg} is replaced by $h'_{fg} = h_{fg} + (3/8)c_p \Delta T$. Rohsenow (46) considered the effect of cross-flow of liquid in the condensate and solved the resulting equations by a successive approximations technique to obtain a correction to the Nusselt heat transfer expression. The correction amounts to replacing h_{fg} by the term $(h_{fg} + 0.68\, c_p \Delta T)$. Bromley (6) had earlier arrived at essentially the same result by considering the effect of heat capicity on laminar condensation, as Bromley noted in his discussion of Rohsenow's paper (8). McAdams (35) and Kutateladze (32) recommend that Nusselt's $\bar{h}$ should be increased by a factor of 20 percent to yield predictions more comparable with actual coefficients.

The basic contribution of Nusselt's work was his perceptive observation that the condensation heat transfer rate is controlled predominantly by the thermal resistance of the condensate film, and that the film thickness is coupled with the heat transfer rate and flow situation. These considerations yield a predicted heat transfer rate that is proportional to $(x\Delta T)^{3/4}$, which is in agreement with experimental results.

The analytical efforts dealing with laminar filmwise condensation heat transfer, since Nusselt's successful model, have been directed toward relaxing Nusselt's assumptions. Each assumption which is dropped complicates the resulting mathematical model; and considerable effort, insight and ingenuity have been brought to bear in order to obtain solutions for the differential equations evolved. Rohsenow (46) was able to show that inclusion of condensate cross-flow effect does not

appreciably alter the validity of the linear temperature profile assumption.

Sparrow and Gregg (55) presented a boundary-layer theory type analysis for laminar film condensation on an isothermal vertical plate. Energy-convection and fluid-acceleration terms were retained in their model. The equations representing conservation of mass, momentum and energy of the condensate film are, respectively,

$$\frac{\partial u}{\partial x} + \frac{\partial v}{\partial y} = 0 \ ,$$

$$\rho\left(u \frac{\partial u}{\partial x} + v \frac{\partial u}{\partial y}\right) = g(\rho - \rho_v) + \mu \frac{\partial^2 u}{\partial y^2} \ ,$$

and

$$\rho c_p\left(u \frac{\partial T}{\partial x} + v \frac{\partial T}{\partial y}\right) = k \frac{\partial^2 T}{\partial y^2} \ .$$

The boundary conditions are:

at the wall, $y = 0$; $u = 0$, $v = 0$ and $T = T_w$.

at the liquid-vapor interface, $y = \delta$; $\frac{\partial u}{\partial y} = 0$ and $T = T_v$.

By definition: Stream function, ψ: $u = \frac{\partial \psi}{\partial x}$ and $v = \frac{\partial \psi}{\partial y}$

Independent similarity variable: $\eta \equiv C y x^{-1/4}$, $C \equiv \left[\frac{g c_p (\rho - \rho_v)}{4 \nu k}\right]^{1/4}$

Dependent variables: $F(\eta) \equiv \frac{\psi}{x^{3/4}} \cdot \frac{1}{4\alpha C}$ and $\theta(\eta) \equiv \frac{T - T_v}{T_w - T_v}$,

where $\alpha \equiv \frac{k}{\rho c_p}$.

The momentum and energy equations can be transformed to the following ordinary differential equations:

$$F''' + \frac{1}{Pr}\left[3F''\cdot F - 2(F')^2\right] + 1 = 0$$

$$\theta'' + 3F\theta' = 0 \ ,$$

where Pr represents the Prandtl number, and the prime denoted differentation with respect to η. The transformed boundary conditions are:

$$\text{at } \eta = 0,\ F' = 0, \text{ and } \theta = 1$$

$$\text{at } \eta = \eta_\delta = C\delta x^{-1/4},\ F'' = 0 \text{ and } \theta = 0.$$

The solution of these differential equations depends upon two parameters, Pr and η_δ. By invoking an over-all energy balance, Sparrow and Gregg show that for a given Pr, there is a unique relation between η_δ and $c_p\Delta T/h_{fg}$. The heat-transfer results can be written in terms of the local Nusselt number ($Nu_x = \frac{hx}{k}$):

$$Nu_x \left[\frac{g c_p (\rho - \rho_v) x^3}{4k} \right]^{-1/4} = \left(\frac{d\theta}{d\eta}\right)_o = f\left(Pr, \frac{c_p \Delta T}{h_{fg}}\right) .$$

The solution $\left(\frac{d\theta}{d\eta}\right)_o$, which is a function of Pr and $c_p\Delta T/h_{fg}$, was determined numerically from Prandtl numbers of 1, 10 and 100 for the range $0 < c_p\Delta T/h_{fg} \leq 2$. The representative results presented by Sparrow and Gregg are shown in Figures 2, 3 and 4.

The results of Sparrow and Gregg indicate that a linear temperature profile is a reasonable approximation, and that the effect of the fluid-acceleration terms are negligible for $Pr \geq 1$ coupled with $c_p\Delta T/h_{fg} < 0.4$. Matin (37) demonstrated that a similarity solution employing the techniques of Sparrow and Gregg is possible for a gravity field [G(x)] which varies along the vertical plate such that $G(x) = \text{constant } x^n$, where n is also a constant. This particular gravity field does not represent a realistic situation, and the similarity does not extend to $G(x) = \sum_i A_i x^{ni}$. A_i and n_i are constants for given i.

Koh, Sparrow and Hartnett (29) analyzed laminar film condensation by solving the liquid and vapor boundary-layer type equations

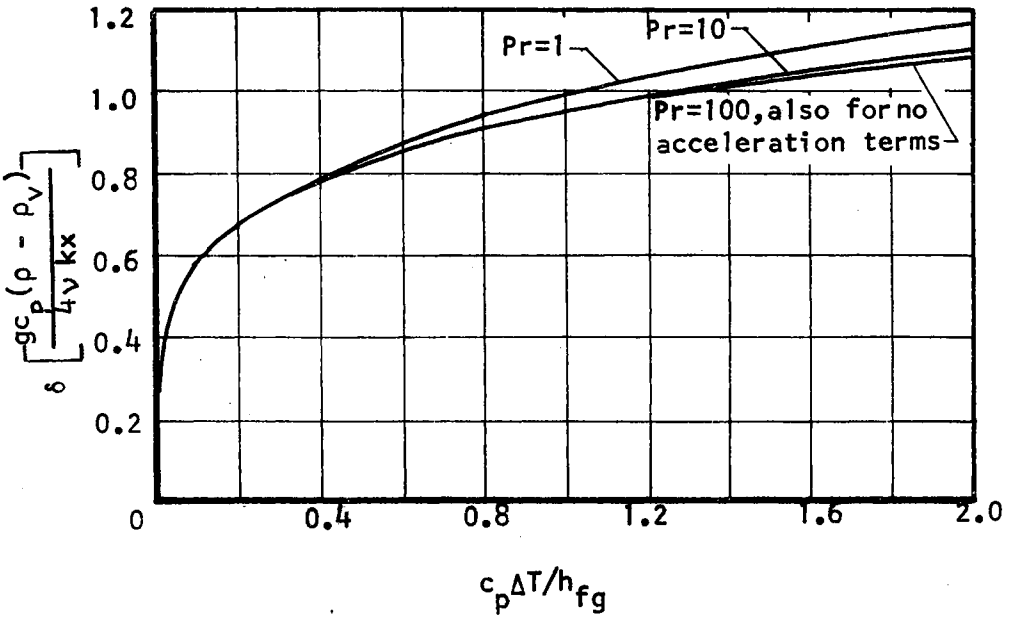

Figure 2. Dimensionless Film Thickness. (Ref. 55)

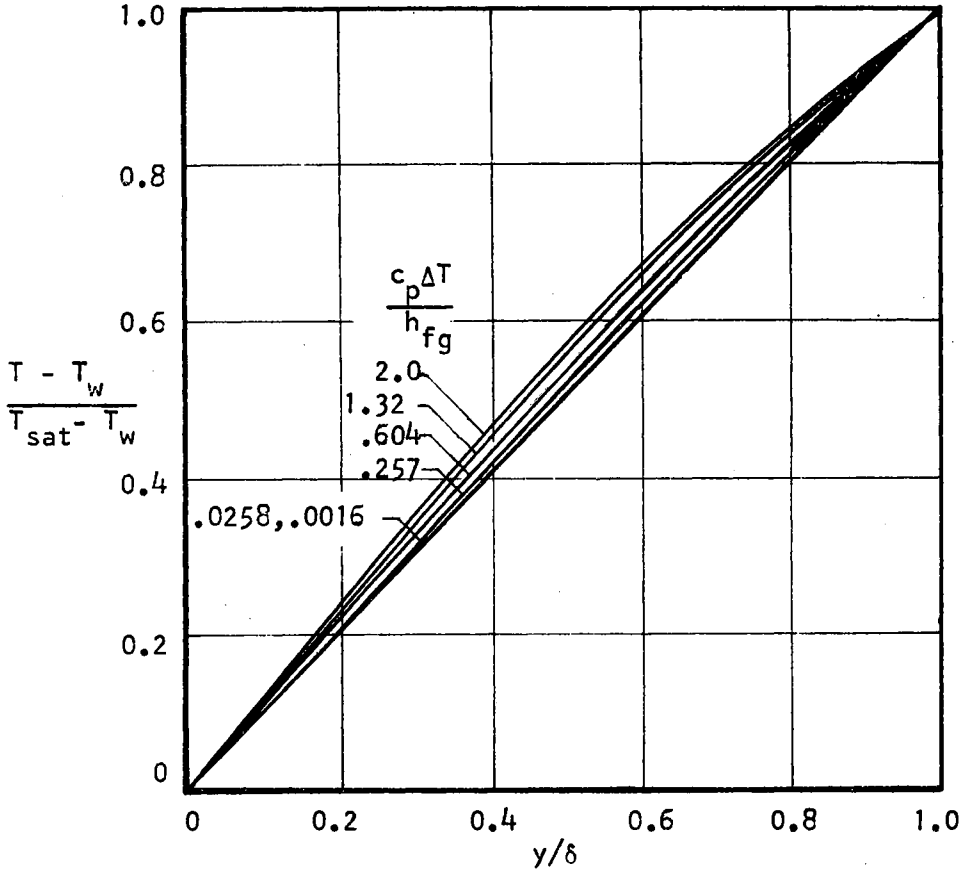

Figure 3. Representative Temperature Distribution from Solutions of Complete Boundary-Layer Equations; Pr=1. (Ref. 55)

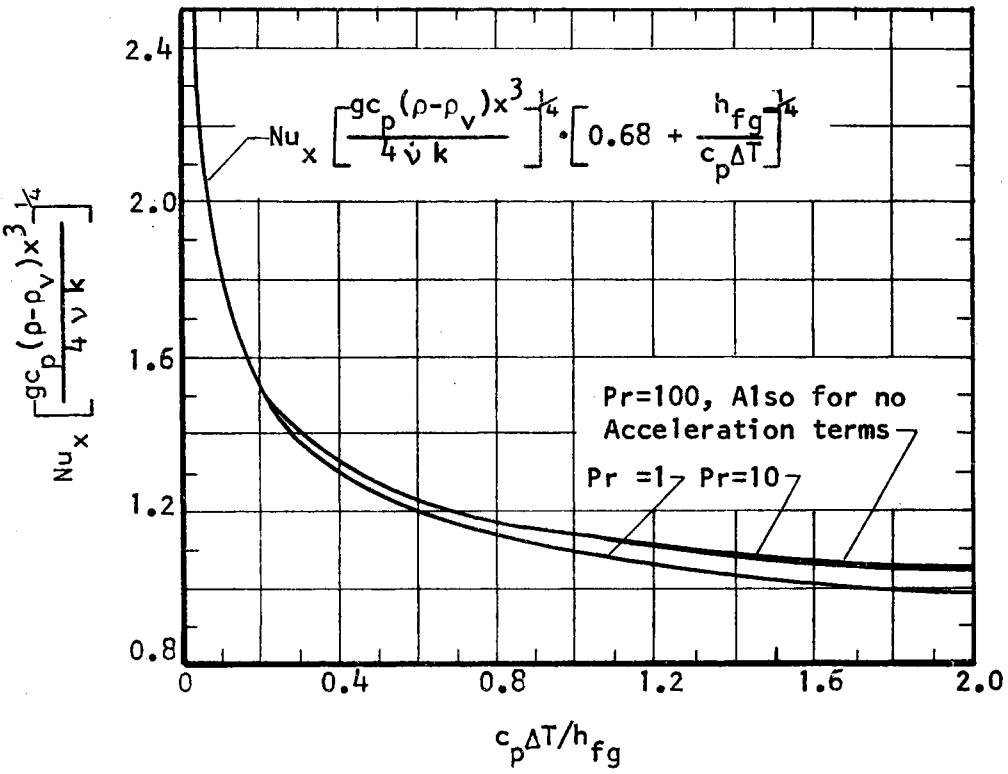

Figure 4. Local Heat Transfer Results from Solutions of Complete Boundary-Layer Equations. (Ref. 55)

simultaneously. This analysis included the effect of vapor drag forces in addition to the energy-convection and fluid-acceleration terms. Their results showed that for large liquid Prandtl numbers, and for small Prandtl numbers coupled with small $c_p\Delta T/h_{fg}$, the interface drag exerted on the liquid by the vapor is negligibly small. They also concluded that terms containing $(\rho\mu)/(\rho\mu)_v$ have no significant effect on film condensation heat transfer. Koh (27) used the integral method to solve the problem considered above. The resulting approximate solution was shown to have a maximum deviation of less than 5 percent from an exact solution. The vapor at infinity was assumed to be at rest in both cases considered by Koh.

Chen (10) considered the same physical situation as described in the preceeding paragraph. Using the dimensionless groups $(c_p\Delta T/h_{fg})$ and $(k\Delta T/\mu h_{fg})$ as perturbation parameters, he employed a perturbation procedure to solve the integral type conservation equations. Chen demonstrated that terms containing $(\rho\mu)_v/(\rho\mu)$ are an order of magnitude less than the wall shear-stress term and consequently neglected these terms in the solution. His results also confirmed that only slight deviation from a linear temperature occurs across the condensate film. However for $(k\Delta T/\mu h_{fg}) > 0.5$, the velocity profile is significantly affected, with a negative velocity gradient at the interface due to vapor drag. The heat transfer results are compared with those of Sparrow and Gregg, and with some liquid metal condensation data. Chen's results are similar to those of Sparrow and Gregg, but consistently lower.

Koh (28) considered the case of forced flow of vapor condensing on a horizontal isothermal plate. The problem was formulated as an exact

boundary-layer solution. The parameters involved are Pr, $[(\rho\mu)/(\rho\mu)_v]^{\frac{1}{2}}$ and $(c_p\Delta T/Pr \cdot h_{fg})$. Numerical solutions of the governing equations led Koh to the conclusion that the energy transfer by convection is negligible for low Prandtl number liquids, but quite important for high Prandtl number liquids.

Shekriladze and Gomelauri (50) discount Koh's (28) conclusion, citing the work of other authors. Shekriladze and Gomelauri present the argument that the condensation process constitutes a vapor "suction" effect, and the magnitude of this effect is sufficient to cause the vapor boundary layer to remain laminar. Assuming the condensate flow is laminar, and that the shearing stress (σ) the vapor exerts on the condensate film depends mainly on the momentum transferred by the "suction" mass, the authors obtain $\sigma = \Gamma(x)(u_\infty - u_\delta)$.

Superimposing a uniform free stream velocity (u_∞) on the physical model shown in Figure 1, the following set of equations result:

$$\mu \frac{d^2u}{dy^2} + \rho g = 0 \ ,$$

$$\frac{d}{dx}\left(\int_o^{\delta(x)} \rho u dy\right) = \frac{k}{\delta(x)} \frac{\Delta T}{h_{fg}} \ ,$$

and $$h_x = \frac{k}{\delta(x)} \ .$$

The boundary conditions are:

For $y = 0$; $u = 0$, $T = T_w$.

For $y = \delta(x)$; $\frac{du}{dy} = \frac{\Gamma(x)}{\mu}(u_\infty - u_\delta)$, $T = T_v$,

with $u_\delta = u(\delta)$.

At $x = 0$; $\delta(x) = 0$.

The solution can be written:

$$h_x = k\left[\frac{\rho u_\infty}{4\mu x}\right]^{\frac{1}{2}}\left[\frac{1+\sqrt{1+Nx}}{2}\right]^{\frac{1}{2}} \tag{2.6}$$

$$\bar{h} = \sqrt{2}\,\frac{k}{3}\left[\frac{\rho u_\infty}{\mu L}\right]^{\frac{1}{2}}\frac{(2+\sqrt{1+NL})}{[1+\sqrt{1+NL}]^{\frac{1}{2}}} \tag{2.7}$$

where: $N = \dfrac{16g\mu h_{fg}}{K\Delta T\, u_\infty^2}$.

Employing the same approach to determine the liquid-vapor interface shearing stress, the authors have determined expressions for heat transfer coefficients for a horizontal isothermal flat plate, a horizontal plate with constant heat transfer rate, and a cylinder in transverse vapor flow. These last three models were shown to compare favorably with data from condensing situations involving significant vapor velocity.

The problem of combined body force and forced convection has also been analyzed by Jacobs (19). Jacobs employed an integral method to reduce the coupled liquid layer and vapor governing equations to a tractable differential equation form which was then numerically integrated to obtain results which were presented in a graphical manner. Jacobs made the following equivalent definitions:

$$Fr_x = \frac{u_\infty^2}{gx}\ ,\quad Re_{Lx} = \frac{\rho u_\infty x}{\mu}\ ,\quad Z = \frac{1}{Fr_x}\ ,$$

$$Nu_x = \frac{h_x x}{k}\ ,\quad H = \frac{c_p \Delta T}{Pr\, h_{fg}}\ .$$

Comparison of the equation developed by Shekriladze and Gomelauri (50) for the same physical situation reveals that their relatively simple

approximation for shearing stress is in agreement with Jacobs' model. The result of Shekriladze and Gomelauri given by Equation 2.6, can be expressed in Jacobs' terminology as

$$Nu_x \left(\frac{Fr_x}{Re_{Lx}}\right)^{\frac{1}{2}} = \tfrac{1}{2}\left(\frac{1}{2Z}\right)^{\frac{1}{2}} \left(1 + \sqrt{1 + \frac{16Z}{H}}\right)^{\frac{1}{2}} \qquad (2.8)$$

Jacobs gave a graphical presentation showing his results for $Nu_x(Fr_x/Re_{Lx})^{\frac{1}{2}}$ verus Z, for H = 0.02468, (ρ/ρ_v) = 210.29, and (ν_v/ν) = 4.495. Jacobs' results for these parameters (which corresponds to Freon 113 condensing with $\Delta T = 40^{\circ}F$) along with the results of Equation 2.8 are shown in Figure 5. The asymptotic slope of the curves at low Z values (corresponding to a forced convection predominant situation) is -0.50. This was observed by Jacobs as being a result of his numerical solution. Considering the asymptotic result for $Z \rightarrow 0$ of Equation 2.8,

$$Nu_x \left(\frac{Fr_x}{Re_{Lx}}\right)^{\frac{1}{2}} \approx \frac{1}{2}\left(\frac{1}{Z}\right)^{\frac{1}{2}} + \frac{Z^{\frac{1}{2}}}{H} \approx \frac{1}{2}\left(\frac{1}{Z}\right)^{\frac{1}{2}} \qquad (2.9)$$

So that for values of Z such that $16\,Z << H$, the asymptotic slope is -0.50 on log-log coordinates. If $16\,Z < H$, then the curve could be approximated by the first expression given in Equation 2.9. For the case of predominant forced convection effect, the results can be reduced to $Nu_x = \tfrac{1}{2}(Re_{Lx})^{\frac{1}{2}}$.

The asymptotic value for $16\,Z >> H$ of Equation 2.8 is

$$Nu_x \left(\frac{Fr_x}{Re_{Lx}}\right)^{\frac{1}{2}} = \frac{1}{\sqrt{2}} \left(\frac{1}{HZ}\right)^{\frac{1}{4}} ,$$

can be written as

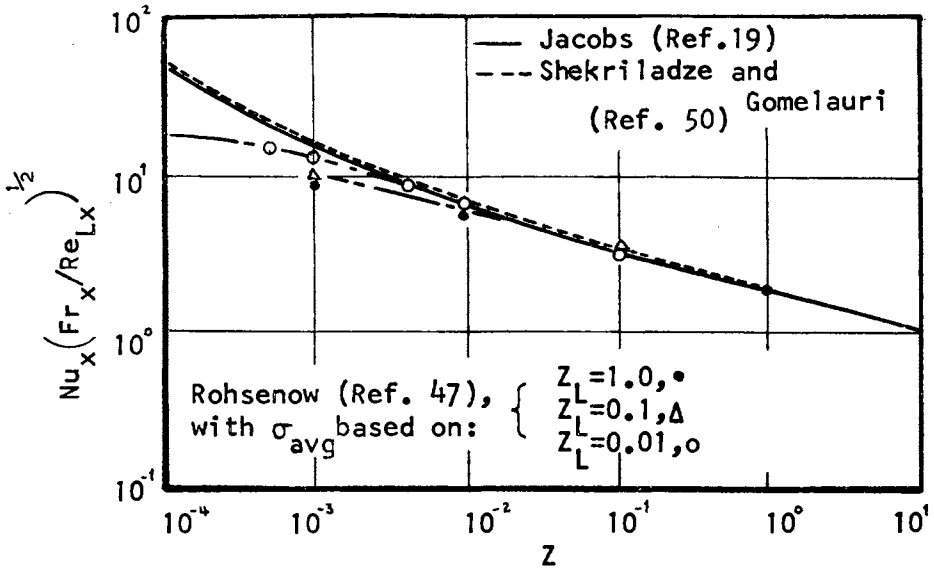

Figure 5. Comparison of Several Investigator's Analytical Results for Combined Body Force with Forced Convection; H=0.02468, ρ/ρ_v=210.29, ν_v/ν = 4.495

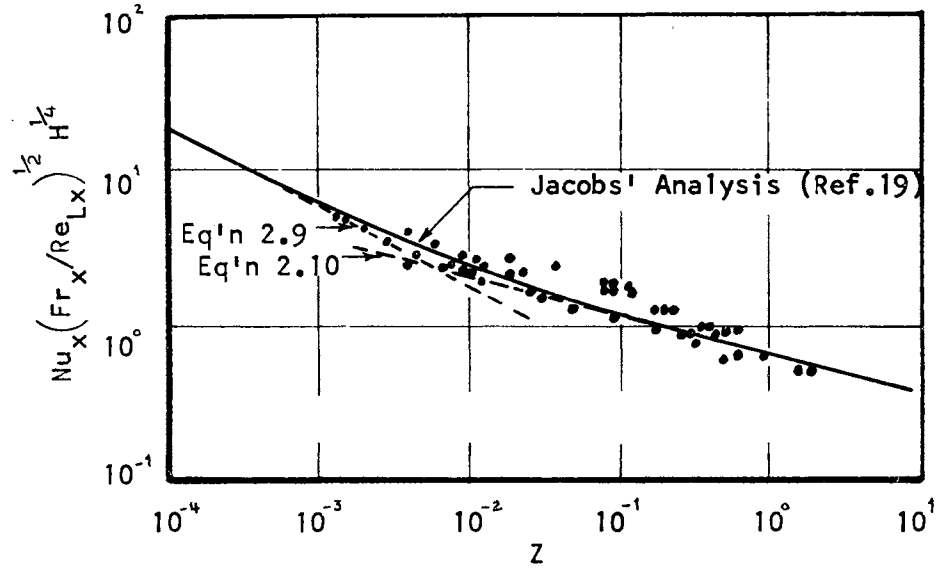

Figure 6. Comparison of Theoretical and Experimental Results for Combined Body Force with Forced Convection; Freon 113.

$$Nu_x \left(\frac{Fr_x}{Re_{Lx}} \right)^{1/2} H^{1/4} = \frac{1}{\sqrt{2}} \left(\frac{1}{Z} \right)^{1/4} . \qquad (2.10)$$

Jacobs (19) presented a graphical comparison of his model with Freon 113 condensing data [Jacobs (20)], in which he used the dimenless grouping $Nu_x \left(\frac{Fr_x}{Re_{Lx}} \right)^{1/2} H^{1/4}$ as a function of Z to correlate the data. These results are shown in Figure 6, along with the asymptotic curves predicted from the results of Shekriladze and Gomelauri. It is evident that the simplified method of determing shear stress is valid for these conditions. It is of particular interest to note that the equations of Shekriladze and Gomelauri appear to be valid for the combined force region as well as for the predominately forced convection region where they demonstrated validity.

A number of the authors have extented their analytical techniques to include the case of laminar condensation on the outside of horizontal tubes; among these are Nusselt (41), Bromley (7), Sparrow and Gregg (56 (56), and Chen (11). Laminar film condensation on inclined cylinders was also considered by Hassen and Jakob (17), with assumptions basically the same as those of Nusselt. They compared their analytical results with data for mean heat transfer coefficients. The actual film coefficients obtained from their experiments were found to be 28 percent to 100 percent higher than theoretical predictions. These deviations were attributed to non-wetting conditions, non-isothermal tubes, contamination and primarily to ripples at the condensate-film surface.

Sparrow and Siegel (58) considered the situation in which the plate temperature, initially the same as that of the vapor, is suddenly dropped. They presented results of their analysis in terms of transient

heat transfer coefficients and time required to achieve steady state for the condensation process.

Chung (12) analyzed laminar film condensation on a vertical plate when subjected to either an arbitrarily time dependent (but continuously differentiable with respect to time) uniform wall temperature or acceleration field parallel to the plate. Utilizing boundary-layer type equations to describe the behavior of the condensate film, non-dimensional variables to implement transformation, and the generalized Taylor series expansion about steady-state solutions, perturbation type equations resulted. A discussion of the effects of various parameters on the results is presented. Utilization of tables and graphs presented would enable the reader to calculate the ratio of unsteady local heat transfer to the hypothetical instantaneous steady-state heat transfer. After attempts to generalize Chung's approach to consider body force fields (g) which were space dependent [i.e., g(x, t)], it was found that g expressed as a function of time (t) only was the sole conceivable dependency whereby the equations could be reduced to tractable form. From consideration of the zeroth and first-order perturbation terms, Chung noted that the time lag was inertia dominated for $Pr \leq 0.1$ and viscous dominated for $Pr \geq 10$. Unfortunately, most fluids of interest fall in the intermediate Prandtl number region where both effects are significant.

The numerous articles which have been concerned with laminar condensation can be attributed in part to the relative ease of mathematically modeling the physical situations. The success of Sparrow and Gregg (55) in expressing the laminar condensation problem in boundary-layer theory type equations led the way for many investigators, since

mathematical techniques developed for boundary-layer problems could be equally well applied to the laminar condensation problem. From these analytical studies, a number of simplifying assumptions have emerged, as well as identification of the mechanisms which govern the heat transfer rate; yet, most investigators are very happy if their results are within 20 percent of the actual case.

The deviation of actual laminar condensation heat transfer coefficients from the theoretical predictions are frequency attributed to ripples, non-wetting, or turbulent film flow, if higher than predicted--and to the presence of non-condensable gases or surface contamination, if lower than predicted. The presence of even a small amount of non-condensable gases has been shown to decrease the heat transfer rate significantly. Literature concerned with the effect of non-condensable gases on condensation heat transfer include the work of Othmer (42), Smith and Robson (51), Votta and Walker (60), Akers et al. (1), Sparrow and Eckert (54), Hampson (16), Sparrow and Lin (57) and Minkowycz and Sparrow (39). An excellent review of condensation heat transfer has been compiled by Wilhelm (61). Wilhelm's literature review includes articles from 1916 through the early part of 1964, and encompasses the areas of kinetic theory, liquid-vapor interfaces, nucleation, dropwise and filmwise (laminar and turbulent) condensation, film flow, contact resistance, and condensation inside horizontal tubes. A somewhat more practice oriented review of condensation heat transfer was presented at the 14th Annual Heat Transfer Conference at Oklahoma State University (15). The intent and accomplishment of the review was to present what we do know for certain and to highlight areas where our ignorance is greatest.

Recently, Soliman et al. (53) proposed a model, which includes friction, momentum and gravity effects for annular flow condensation heat transfer processes. The predicted forces are incorporated in a correlation to predict local heat transfer coefficients. The resulting correlation is reasonably good--when one notes that the Prandtl number range is from 1 to 10 and that the data reflect diverse flow conditions. However, the significant scatter of the data presented serves to emphasize the difficulties which may result from oversimplifying the problem. Kunz and Yerazunis (31) presented a simplified analysis of film condensation inside tubes, and for falling films condensing on vertical surfaces. The comparison of results with data as presented in their paper is reasonably good. The correlations proposed do indicate the proper trend, thus possessing qualitative merit. The ability to predict performance of condensers accurately from the correlations generally available is not too good. Most of the difficulty stems from an inadequate representation of the flow situations.

The assumption of constant properties is made by most investigators. Since the condensate in film condensation is assumed to have a linear temperature distribution between the wall temperature (T_w) and surface temperature (T_v), then the question arises as to the proper temperature(T_f)to use in property evaluation. Kern (23) and Kreith (30) recommend evaluation of properties based on $T_f = \frac{1}{2}(T_v + T_w)$, while Rohsenow and Choi (48) recommend $T_f = T_w + \frac{1}{4}(T_v - T_w)$. The effect of variable fluid properties on laminar condensation is considered in Appendix A.

The methods of irreversible thermodynamics were recently applied to the liquid-vapor phase change by Bornhorst and Hatsopoulos (5).

The condensation process was considered to be a simultaneous flux of energy and mass across the interface, consequently three transport coefficients result. The usual technique involved in determining the coefficients is to conduct experiments. These hypothetical experiments were proposed, primarily to illustrate the physical meaning of the transport coefficients. Employing kinetic theory results to approximate the transport coefficients, it was demonstrated that the surface temperature at the condensate surface may be either higher or lower than the saturated vapor temperature. The results of this analysis are useful primarily in considering the interfacial resistance effect on condensation processes. Interfacial resistance does not appear to be a problem except at very low pressures or for liquid metal condensation. One area of utilization for the methods of irreversible thermodynamics might be the problem of non-condensable gases.

The literature review of laminar condensation has revealed that the local heat transfer coefficient can be determined reasonably well by the relationship, $h_x = k/\delta(x)$, which simply implies that for a given fluid, the heat transfer coefficient depends upon the condensate thickness. Consequently, methods have been proposed to cause thinner films to occur. Kern and Karakas (24) developed equations for the design of machines to implement phase changes. These mechanically aided heat transfer devices are required when very viscous or foamy materials undergo a change of phase; therefore, non-newtonian fluids were considered in their development of equations. Lustenader et al. (34) used wipers to experimentally maintain thin condensate films. Additionally, they investigated fluted surface tubes, which gave high heat transfer coefficients. Their experimental investigation with

water indicated over-all heat transfer coefficients as high as 8000 BTU/hr ft^2 ^oF were obtained by utilizing mechanically thinned films both in evaporation and condensation. An investigation of the effect of strong electric fields on condensation heat transfer was reported by Choi (13). The effect was a significant increase in the condensing heat transfer coefficients, which was attributed to the appearance of instability waves and a reduced average film thickness. Increase in the heat transfer coefficient was as much as 100 percent with 30 KV applied voltage.

Acoustic Phenomena

The terms sound and acoustic are often used interchangeably. Sound, as defined by Beranek (3), is an alteration in pressure, stress, particle displacement or particle velocity which is propogated in an elastic material, or the superposition of such propogated alterations. Acoustics is the science of sound. In this investigation, the propagation as pressure alterations imposed upon a vapor is considered and this is the implication of "sound" in the thesis title.

The assumptions normally involved in defining the acoustic wave equation are: (1) The fluid transmitting the disturbance (or wave) is homogeneous and isotropic. (2) No dissipation occurs (i.e., an isentropic process). (3) Gravitational forces are negligible. (4) The waves are of small enough magnitude, so that only first order terms in the describing differential equations need be considered. Utilization of these assumptions, and application of the conservation laws for mass, momentum and energy allow the derivation of the acoustic wave equation.

$$\frac{\partial^2 \phi}{\partial t^2} = a^2 \nabla^2 \phi$$

Where: ϕ = velocity potential

a = speed of sound

Defining the instantaneous property as being the sum of the time average value (bar superscript) and the instantaneous deviation from the time average value (superscript$'$), the following relations can be written for the instantaneous density (ρ) and pressure (P):

$$\rho(x, y, z, t) = \rho'(x, y, z, t) + \bar{\rho}(x, y, z)$$

$$P(x, y, z, t) = P'(x, y, z, t) + \bar{P}(x, y, z)$$

The pressure deviation from the time average value is the acoustic (sound) pressure. The independent variables (x, y, z) are the rectangular coordinates and the independent variable t is time. Relationships that allow other acoustic variables to be expressed in terms of a wave equation similar to Equation 2.11 are:

$$P' = -\bar{\rho} \frac{\partial \phi}{\partial t} \, , \quad \rho' = \frac{P'}{a^2} \, , \quad u' = \frac{\partial \phi}{\partial x} \, , \quad v' = \frac{\partial \phi}{\partial y} \, ,$$

$$\text{and } w' = \frac{\partial \phi}{\partial z} \, ,$$

where u', v' and w' and the particle velocities due to the acoustic waves in the x, y and z directions, respectively.

The velocity of sound for acoustic waves of ordinary intensity can be predicted with good accuracy by assuming that the compression (and expansion) of the fluid occurs in an isentropic manner. Consequently, the speed of sound is defined as $a = \sqrt{\left(\frac{\partial P}{\partial \rho}\right)_s}$.

For an ideal gas, $a = \sqrt{k_v \frac{\bar{P}}{\rho}} = \sqrt{k_v R_v \bar{T}}$,

where: k_v = ratio of specific heats (c_p/c_v)

R_v = gas constant

$\bar{T}$ = time average temperature

s = entropy

Derivations of the acoutic wave equation and the speed of sound expressions can be found in most acoustics texts, in particular see Kinsler and Frey (26) or Beranek (4).

A plane acoustic wave is the simplest case of wave motion propagation in a fluid media. If the plane wave is considered to be propagated only in the x direction, the three-dimensional wave equation reduces to

$$\frac{\partial^2 \phi}{\partial t^2} = a^2 \frac{\partial^2 \phi}{\partial x^2} ,$$

which has the well known solution $\phi = f_1(at - x) + f_2(at + x)$. A simple harmonic wave has the specific solution, expressed in complex form:

$$\underline{\phi} = \underline{A}e^{j(\omega t - Kx)} + \underline{B}e^{j(\omega t + Kx)} = \underline{\phi}_+ + \underline{\phi}_-$$

where: $\underline{\phi}_+ = \underline{A}e^{j(\omega t - Kx)}$ = velocity potential of wave traveling in + direction

$\underline{\phi}_- = \underline{B}e^{j(\omega t + Kx)}$ = velocity potential of wave traveling in - direction

$\underline{A}$ = complex amplitude of wave traveling in + direction

$\underline{B}$ = complex amplitude of wave traveling in - direction

$\omega = 2\pi f$

f = frequency of vibration

K = wave number = ω/a .

The complex forms of the acoustic variables are

$$\underline{p}' = -\bar{\rho} \frac{\partial \underline{\phi}}{\partial t} = -j\omega\bar{\rho}(\underline{\phi}_+ + \underline{\phi}_-) \qquad (2.12)$$

$$\underline{\rho}' = \frac{\underline{P}'}{a^2} = -j\frac{K}{a}(\underline{\phi}_+ + \underline{\phi}_-) \tag{2.13}$$

$$\underline{u}' = \frac{\partial \underline{\phi}}{\partial x} = -jK(\underline{\phi}_+ + \underline{\phi}_-) \quad . \tag{2.14}$$

The equations which physically correspond to measurable acoustic variables are the real parts of Equations 2.12, 2.13, and 2.14--with the complex constants determined from specified boundary conditions.

Purdy et al. (43) have shown that the criterion for neglecting second order and higher terms is that the Mach number, $M_o = U_o/a_o << 1$, where U_o is the maximum acoustic particle velocity, and a_o is the stagnation speed of sound. This corresponds to the definition that acoustic waves are such that $u' << a_o$, $\rho' << \overline{\rho}$ and $P' << \overline{P}$.

The speed of sound for a mixture of liquid and vapor phases, such as a "wet" vapor is not as easily determinable as for a single phase substance. Karplus (21) presented an equation for the determination of the speed of sound for steam, which takes into account the quality of the steam. His results are shown in Figure 7.

Since the propagation of acoustic waves is not entirely isentropic, a loss of acoustic energy occurs whenever the waves are transmitted through a fluid media. This aspect of acoustics is generally described as absorption of sound waves. This loss can be attributed to viscous dissipation, heat transfer and molecular exchanges of energy--occurring in the fluid itself. Normally the loss of energy within the fluid is a minor contribution to the overall loss when boundaries are present. Since the velocity of the fluid is zero at solid boundaries, significant velocity gradients exist near the walls, causing viscous dissipation of the acoustic energy. Additionally, heat conduction from

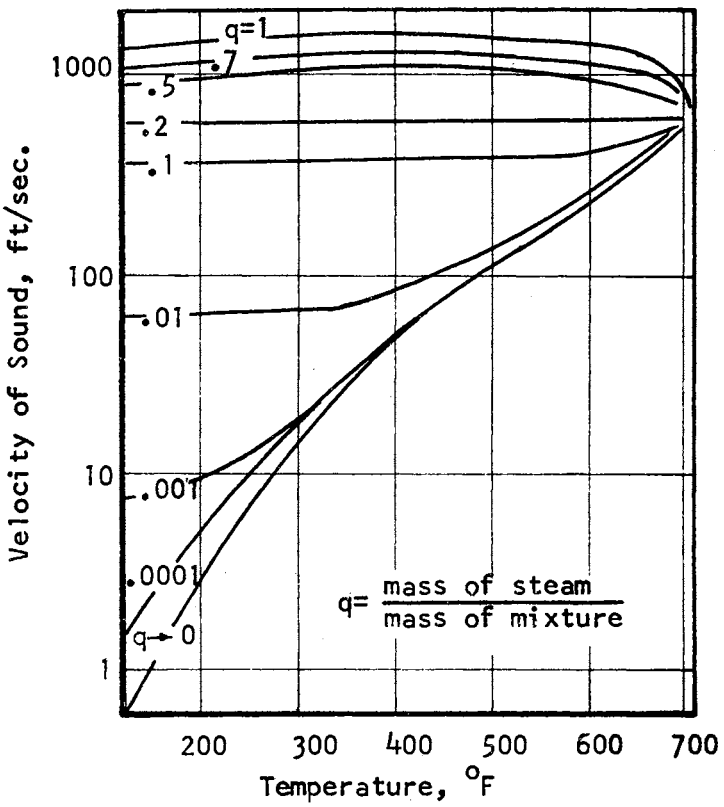

Figure 7. Velocity of Sound in Wet Steam. (Ref. 21)

the fluid medium to the bounding walls cause losses in the acoustic energy. Another source of energy loss is the absorption of acoustic energy by the walls themselves, such as occurs with acoustic insulation. All of the boundary losses depend upon the geometry and wall materials involved, as well as the sound field characteristics. Accurate estimates of these losses rely heavily upon empirical data, with most of the analytical work yielding primarily qualitative results.

The effect of a resonant acoustic field on a liquid layer in a horizontal cylinderical tube has been investigated by Howartson (18) and Barfield (2). Both investigators observed that as the sound pressure level increased, the free surface of the liquid layer assumed a pronounced curvature, as shown schematically in Figure 8a. When the sound pressure level increased to a certain level, an abrupt change in the surface occurred. A thin film of liquid normal to the tube axis was ejected at a velocity antinodal point. A sketch of this is shown in Figure 8b. Both authors reported that multiple ejection sites became active as the sound pressure level was further increased. These ejected thin films were termed spouts by Howartson and curtains by Barfield.

By considering the time average of the resonant sound field, Howartson (18) developed an expression for the time mean pressure difference between the velocity node and the velocity antinode. The resulting equation was

$$\overline{P_n - P_a} = \frac{1}{2} \bar{\rho} U_o^2 \quad , \tag{2.15}$$

where: $\overline{P_n - P_a}$ = time-mean difference in pressure between the velocity node and antinode.

N indicates velocity node and A indicates velocity antinode.

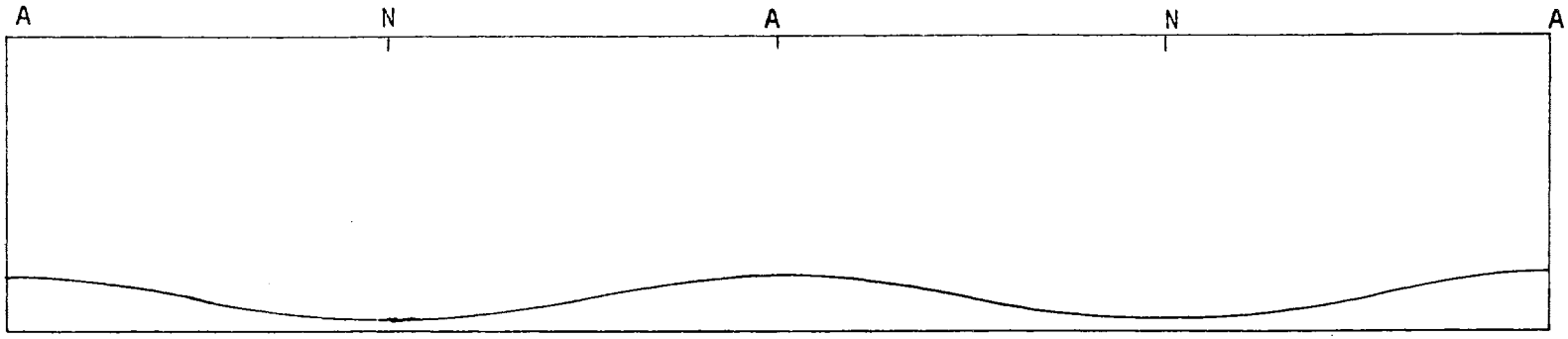

(a) Liquid assumes a sinusoidal shape for moderate sound intensities.

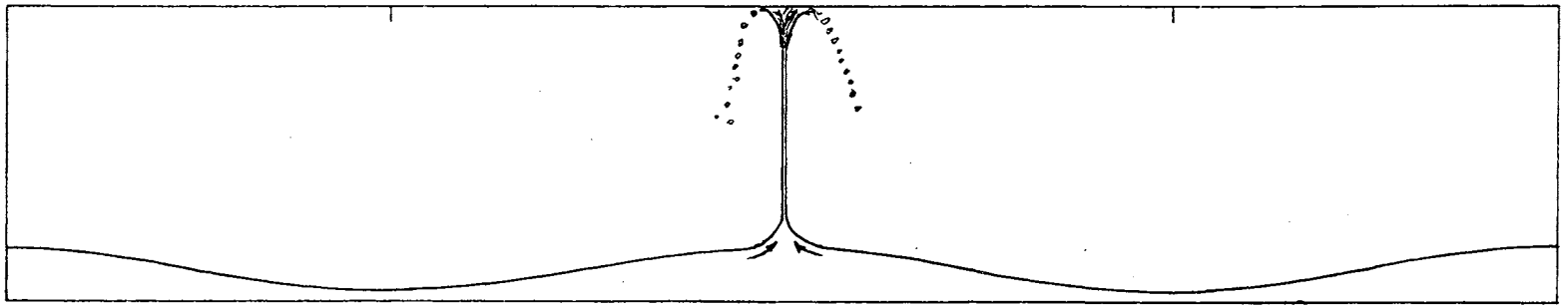

(b) Liquid is ejected at a velocity antinodal location when the sound intensity exceeds a critical value.

Figure 8. Sketch Showing the Effect of a Resonant Air Borne Sound Field on a Horizontal Liquid Layer in a Cylinderical Tube.

Acoustic intensity of a sound wave is defined as the time-average rate of flow of acoustic energy through a unit area normal to the direction of wave propogation. The acoustic intensity (I) of a plane wave traveling in the +x direction can be expressed mathematically as

$$I = \frac{1}{\tau} \int_0^{\tau} P' u' \, dt$$

where τ is a time period much larger than the acoustic time period. The intensity is normally expressed in terms of an Intensity Level (IL) which is defined as

$$IL = 10 \log_{10} \frac{I}{I_o} ,$$

where I_o is a stated reference Intensity. The value of I_o generally used in acoustics employing an air medium is 10^{-16} watts/cm^2. Sound pressure level (SPL) is defined as

$$SPL = 20 \log_{10} \frac{\overline{P'}}{P_{ref}} ,$$

where $$\overline{P'} = \left[\frac{1}{\tau} \int_0^{\tau} (P')^2 \, dt \right]^{\frac{1}{2}} = \text{the rms sound pressure}$$

P_{ref} = a specified rms reference pressure.

Two commonly used values of P_{ref} are 0.0002 dynes/cm^2 for noise level measurements in air, and 1 dyne/cm^2 for underwater acoustic measurements. Although identical values for IL and SPL measurements will occur for progressive plane waves in air (with the above noted reference values), the equivalence is not generally valid for more complex sound fields, nor for fluids other than air. Although Howartson could only obtain an order of magnitude agreement due to his method of measuring the maximum particle velocity, Barfield (2) was able to measure and

confirm Howartson's predicted results. Barfield noted that the pressure distribution along the tube, as reflected by the liquid surface height, appeared to be sinusoidal--before the curtains were formed. Barfield also presented a correlation for the threshold of the curtain formation as a function of the liquid properties, the wavelength and the sound pressure level. Barfield noted that the curtain behavior is independent of the liquid depth (over the liquid depth range investigated), depending only upon the actual sound pressure level in the tube. Barfield presented a good review of Kundt's tube literature.

The effect of a resonant acoustic field on laminar flow in a circular tube was studied by Purdy et al. (43). A mathematical model was formulated in terms of boundary-layer type equations. By employing an order of magnitude analysis, with the assumption that the variables of interest could be represented as the sum of a time-dependent term and a time-average term, the conservation equations were reduced to a tractable form. Appropriate relaxation of boundary conditions along the way allowed the solution to be achieved. The analytical results appear to agree well with experimental results for air. The techniques employed followed those of Purdy et al. (44), for a two dimensional model of the same situation. A masterful solution of the problem yielded results indicative of the secondary flow induced by the resonant acoustic field. The results for the dimensionless time-mean stream function, as determined by Purdy et al. (43), are shown for conditions of no through flow in Figure 9, and for a through flow condition of $M/M_o^2 = 0.3$ in Figure 10. The terms involved with Figure 10 are defined as:

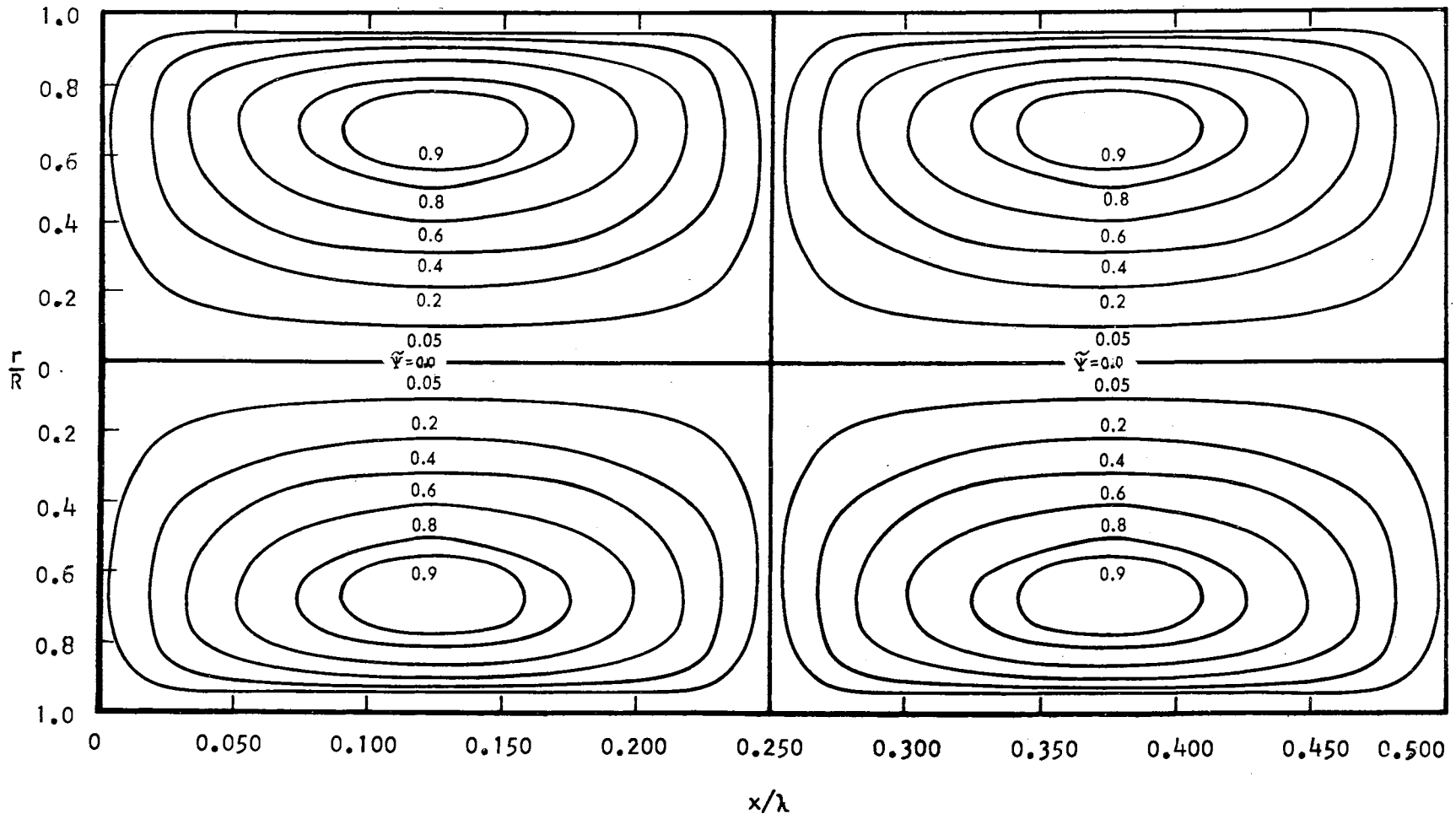

Figure 9. Dimensionless Time-Mean Stream Function for $M/M_o^2 = 0.0$. (Ref. 43)

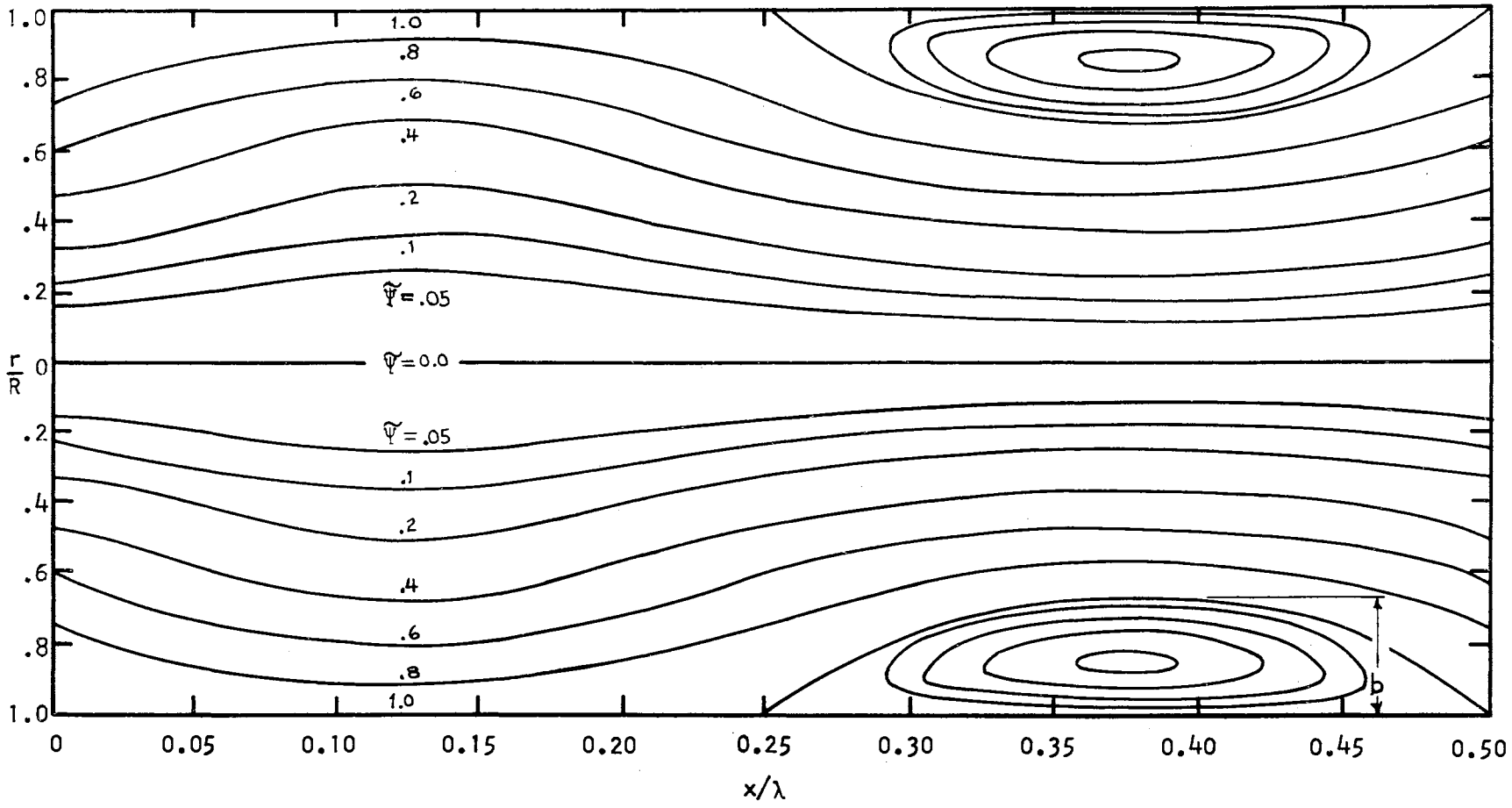

Figure 10. Dimensionless Time-Mean Stream Function for $M/M_o^2 = 0.3$. (Ref. 43)

$M = \bar{U}_v/a_o$

$M_o = U_o/a_o$

a_o = stagnation speed of sound

$\bar{U}_v$ = average through flow velocity

U_o = maximum amplitude of the z component of the time-dependent velocity for an inviscid fluid undergoing resonant acoustic vibrations

$\tilde{\Psi} = \Psi/(\bar{U}_v R^2/2)$, a dimensionless time-mean stream function

Ψ = time-mean stream function

R = tube radius

b = main vortex thickness

The time-mean stream function in the region near the wall is shown in Figure 11 for the through flow condition $M/M_o^2 = 0.3$. The A.C. boundary layer thickness is defined as $\delta_{ac} = \sqrt{2\nu_o/\omega}$, where ν_o is the kinematic viscosity of the fluid at stagnation conditions.

The size of the main vortex was expressed as

$$\Omega_m = 1 - \sqrt{\frac{1}{1 + \frac{3}{8} M_o^2/M}}$$

with $\Omega_m = b/R$. The analytical expression results and the comparative experimental data of Purdy et al. (43) are shown in Figure 12. This gives an indication of the extent of secondary flow induced by the resonant sound field. Purdy summarized the region of applicability by noting that the flow situation must satisfy the following conditions:

$$M_o << 1, \quad |M| \leq M_o^2 \quad \text{and} \quad R/\lambda << 1 .$$

It was the opinion of Barfield (2) that the analytical results of Purdy et al. (43) were inadequate to explain the effect of a resonant

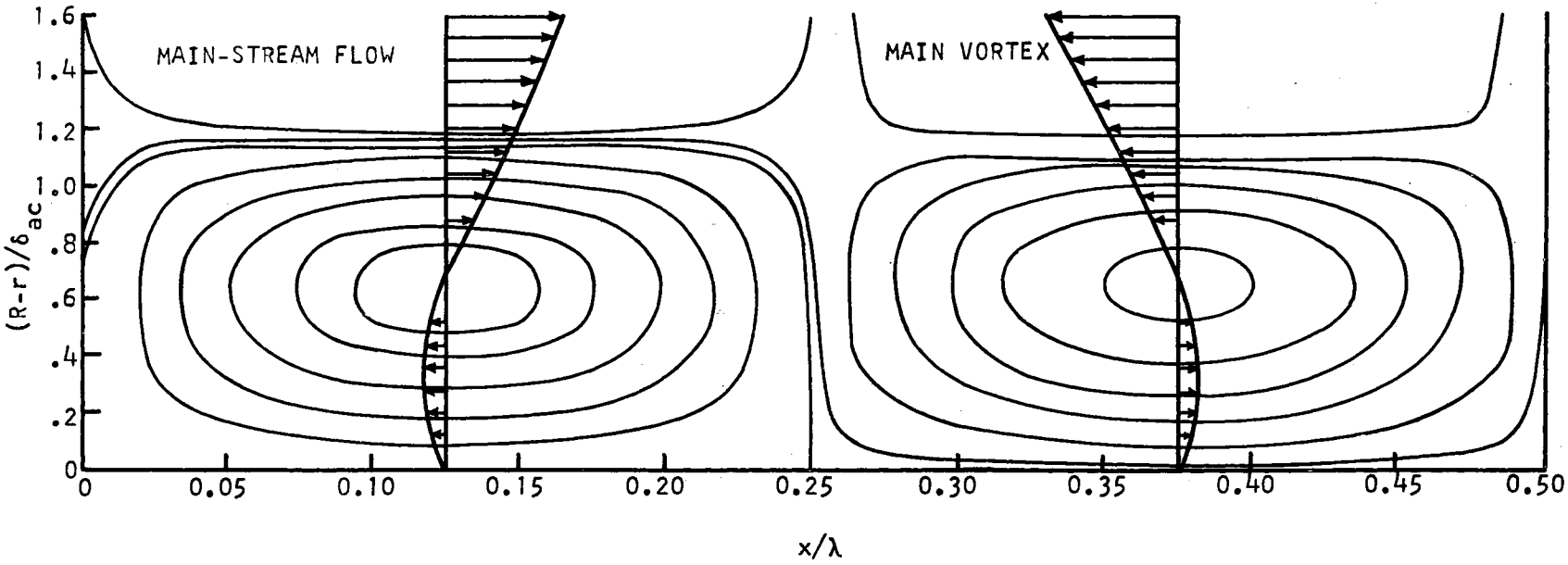

Figure 11. Dimensionless Time-Mean Stream Function for $M/M_o^2 = 0.3$, Showing Details of the Wall Vortices. (Ref. 43)

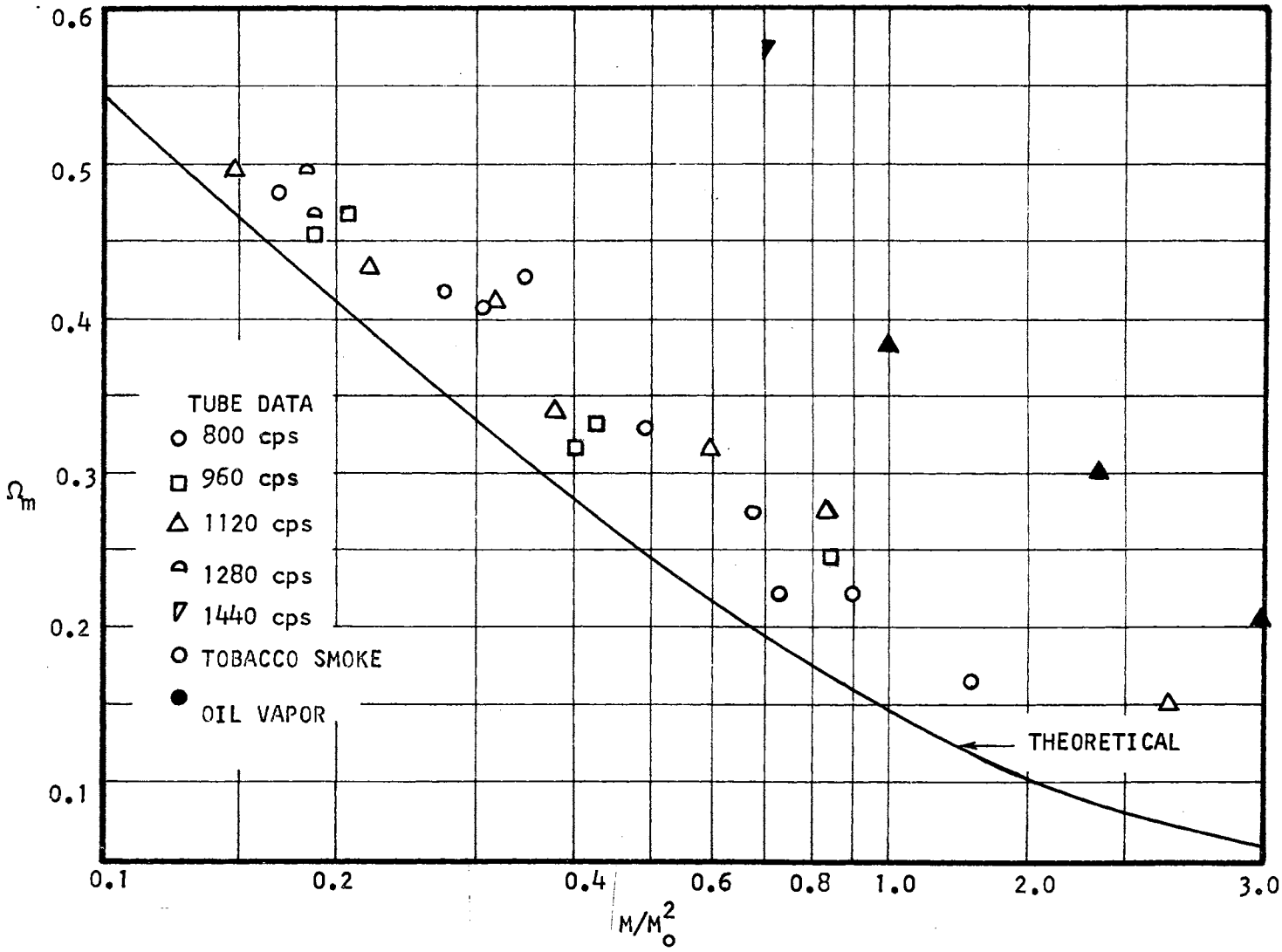

Figure 12. Comparison of Experimental and Theoretical Ω_m for a Tube. (Ref. 43)

sound field on a horizontal thin liquid layer. He proposed a qualitative sketch of the time-mean stream lines in which only one large vortex in each 1/4 wavelength existed, instead of the two predicted by Purdy (Figure 9). However, the difficult task of obtaining a mathematical model for the deformable liquid boundary and its coupling effect with the resonant sound field has not been accomplished.

The effect of a standing sound field on a slow stream discharged from a porous wall was reported by Kestin and Persen (25). The flow field was obtained as a simple superposition of the uniform flow field on the flow field about an oscillating cylinder determined by Schlichting (49). The solution requires that the discharge velocity $v_o << u_o$, where u_o is the maximum velocity value of the oscillating stream. Additionally $\frac{2\pi u_o}{\omega\lambda} << 1$ (which is equivalent to $M_o << 1$) is required. The solution formulated for the stream function (ψ) was given in dimensionless form as:

$$\frac{a}{u_o}\left[\frac{\psi}{\frac{1}{2}u_o\delta_{ac}}\right] = -\left[Ka\xi + \sin(2\pi\xi)\cdot h(\eta')\right]$$

where by definition:

$$K = 4\,\frac{\lambda}{\delta_{ac}}\,\frac{a}{u_o}\,\frac{v_o}{u_o}$$

$$\eta' = y/\delta_{ac}$$

$$\xi = 2x/\lambda$$

$$\lambda = \text{wavelength} = a/f\ ,$$

with $h(\eta')$ given as

$$h(\eta') = \frac{2}{3}\eta' + \eta'\exp(-\eta')\sin\eta' - \frac{1}{4}\left[1 - \exp(-2\eta')\right] + \exp(-\eta')\,(2\sin\eta' + 3\cos\eta') - 3\ .$$

These results are of interest if the condensation process is considered to provide a uniform suction superimposed on a sound field, because the above solution can be employed with v_o taking on a negative value as dictated by the condensation rate.

The Effect of Sound on Heat Transfer

A considerable amount of work has been reported in recent years concerning the effect of sound or vibration of surfaces on free convection, forced convection and boiling heat transfer. An excellent literature survey and bibliography on the effect of sound and vibrations on heat transfer phenomena is presented by Larson (33) and by Soehngen and Holman (52). Therefore, it would be superfluous to present a complete survey here. It should be noted that the interest in this area, as reflected by publications, has dropped significantly in the last 3 years. Consequently, little additional information is available above that covered in the reviews mentioned.

Some general observations regarding the results of the investigations of the effect of sound on heat transfer can be made. Most of the work has been experimental due to the complexities involved in attempting analytical solutions. The results of these investigations cover a range of slight decrease to several hundred percent increase in heat transfer coefficients due to imposing sound or vibrations on the heat transfer situation. In most cases, the results have been explained by a change in the flow field in the region of heat transfer.

This literature survey discovered one article concerning the effect of sonic pulsations on condensation. Mathewson and Smith (38) reported some experimental results for the effect of strong sonic pulsations on

condensation heat transfer rates with isopropanol. The vapor was condensed on the inside walls of a vertical 1 1/8 inch BWG copper tubing jacketed for 6 feet with 1 5/8 inch BWG copper tubing. The sonic pressure pulses were generated by a motor-driven flat plate siren installed at the inlet to the condensing section. The pulse frequencies ranged from 50Hz to 330Hz and the pulsed pressure amplitude ranged from 20 lbf/ft^2 to 250 lbt/ft^2. The graphical results presented by Matthewson and Smith (38) are shown in Figures 13, 14, 15 and 16.

The experimental average heat transfer coefficient with no sonic pulsation ($\bar{h}_o$) is shown in Figure 7, along with the predicted coefficients calculated by Matthewson and Smith from the methods of Nusselt (35) and Carpenter and Colburn (9). The average heat transfer coefficient with sonic pulsation is represented as $\bar{h}_p$. No information was available to determine the amplitudes corresponding to the data shown in Figures 14 and 15. Matthewson and Smith employed a simplified model based on penetration theory in an attempt to correlate the heat transfer data. Although they were successful in correlating their results when considering air forced convection results, the model does not enable a correlation of the condensation heat transfer data. Their predicted curve is shown in Figure 14. In summary, Matthewson and Smith reported: (a) for a highly turbulent vapor stream, a critical pulse amplitude was required before any increase in the heat transfer rate was observed; (b) for pressure amplitudes larger than the critical value, heat transfer rates increased rapidly with pressure amplitude; (c) at very high amplitudes the heat transfer rate was almost independent of the pressure amplitudes; (d) the heat transfer rate is only moderately affected by the frequency. They also noted that the effect of sonic pulsation

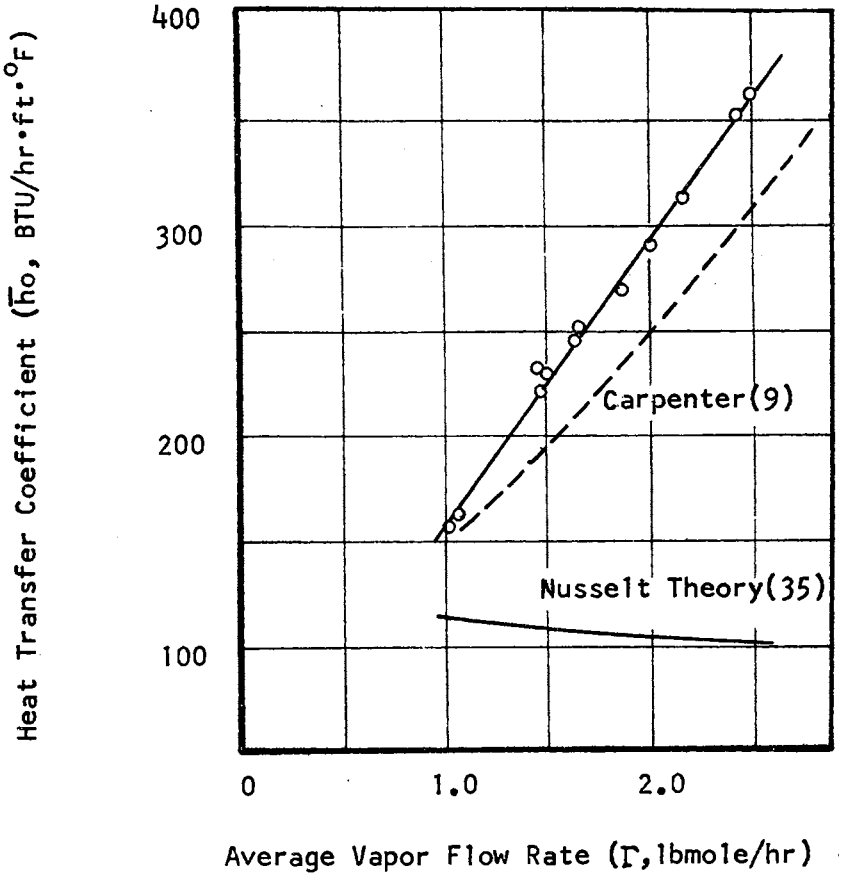

Figure 13. The Effect of Vapor Flow Rate on Film Heat Transfer Coefficient. (Ref. 38)

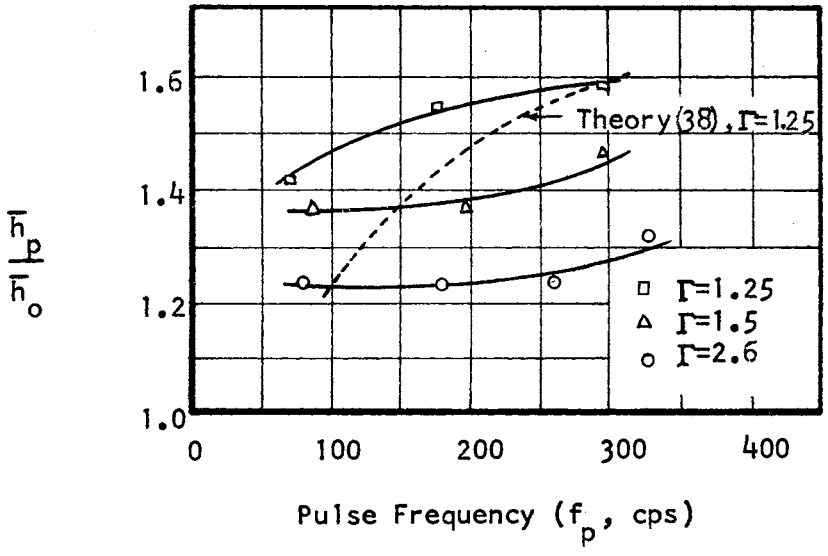

Figure 14. The Effect of Pulse Frequency on Film Heat Transfer Coefficient at Various Vapor Flow Rates. (Ref. 38)

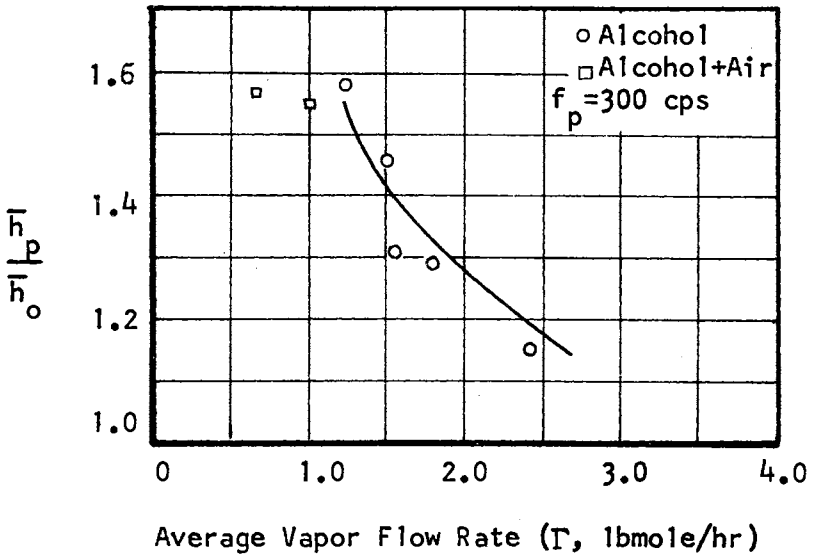

Figure 15. The Effect of Vapor Flow Rate on Heat Transfer Coefficient with Pulsed Alcohol vapor. (Ref. 38)

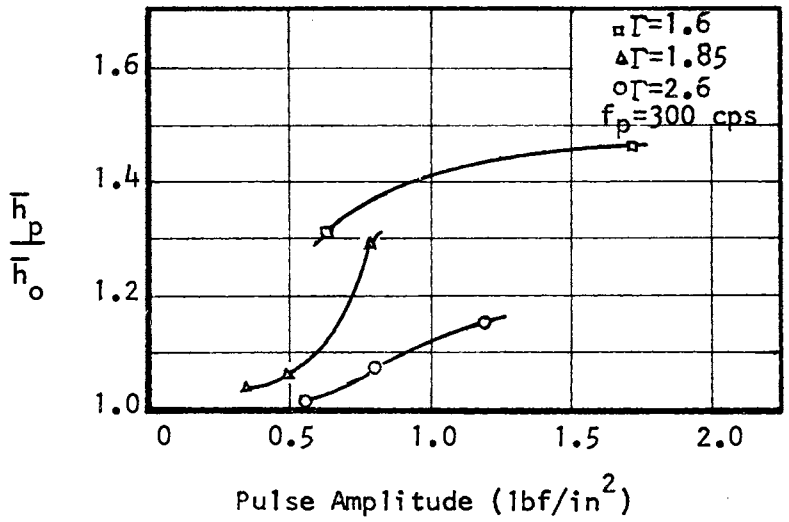

Figure 16. The Effect of Pulse Amplitude on Film Heat Transfer Coefficient at Various Vapor Flow Rates. (Ref. 38)

decreased sharply as the natural turbulence of the stream increased.

Matthewson and Smith attempted to explain the effects of sonic pulsation on condensation heat transfer rates in terms of eddies being generated in the condensate film which penetrate to some depth. They noted that their simplified model and resulting equations were inadequate to explain the results and suggested that the mechanism of heat transferdiffers from the model proposed. It should be noted that their flow situation was such that turbulent film flow was expected, and apparently obtained. They reported that no measurable attenuation of the pulse from top to bottom of the exchanger tube was observed. It was not clear whether this included the isopropanol condensation tests or not, since they were also investigating sonic pulsation effects on forced convective heat transfer to air. Matthewson and Smith were able to show that sonic pulsations could increase the turbulent film condensation heat transfer rate; however, the mechanism was not established.

CHAPTER III

THEORETICAL MODELS

The physical situation considered is the condensation of saturated vapor on the inside walls of a constant temperature vertical tube, with a resonant sound field along the tube axis imposed upon the vapor. This model is shown schematically in Figure 17.

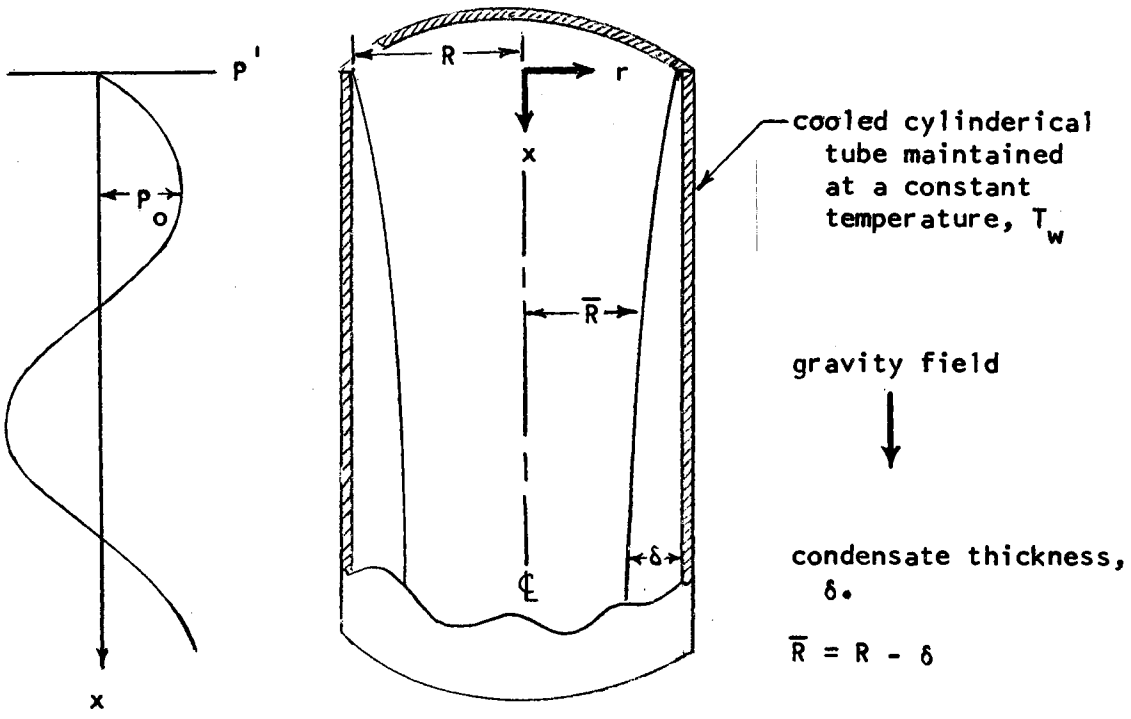

$$P' = P_o \sin(\omega t) \sin\left(\frac{2\pi x}{\lambda}\right)$$

Figure 17. Physical Model for the Effect of Vapor Borne Sound on Filmwise Condensation Heat Transfer.

The saturated vapor is assumed to have a temperature (T_v) greater than the wall temperature (T_w). The condensate film is assumed to behave in a Newtonian manner and to possess constant properties. The condensate film flows under the influence of the gravity field and the forces imposed upon the condensate layer by the vapor. Additionally, it is assumed that the rate of condensation is controlled by the condensate layer and not by the kinetics of the condensation process.

With the above assumptions, the following boundary-layer type equations govern the laminar condensate film for axially symmetric flow.

Continuity equation:

$$\frac{\partial \rho}{\partial t} + \frac{\partial}{\partial x}(\rho u) + \frac{1}{r}\frac{\partial}{\partial r}(r\rho v) = 0 \tag{3.1}$$

Momentum equations:

$$\rho\left(\frac{\partial u}{\partial t} + u\frac{\partial u}{\partial x} + v\frac{\partial u}{\partial r}\right) = F_x - \frac{\partial P}{\partial x} + \mu\left(\frac{1}{3}\frac{\partial^2 v}{\partial r \partial x} + \frac{1}{3}\frac{1}{r}\frac{\partial v}{\partial x} + \frac{4}{3}\frac{\partial^2 u}{\partial x^2} + \frac{\partial^2 u}{\partial r^2} + \frac{1}{r}\frac{\partial u}{\partial r}\right) \tag{3.2}$$

and

$$\rho\left(\frac{\partial v}{\partial t} + u\frac{\partial v}{\partial x} + v\frac{\partial v}{\partial r}\right) = F_r - \frac{\partial P}{\partial r} + \mu\left(\frac{4}{3}\frac{\partial^2 v}{\partial r^2} + \frac{4}{3}\frac{1}{r}\frac{\partial v}{\partial r} - \frac{4}{3}\frac{\partial^2 v}{\partial r^2} + \frac{1}{3}\frac{\partial^2 u}{\partial r \partial x}\right) \tag{3.3}$$

Energy equation (neglecting viscous dissipation):

$$\frac{\partial T}{\partial t} + u\frac{\partial T}{\partial x} + v\frac{\partial T}{\partial r} = \frac{k}{\rho c_p}\left(\frac{\partial^2 T}{\partial x^2} + \frac{\partial^2 T}{\partial r^2} + \frac{1}{r}\frac{\partial T}{\partial r}\right) \tag{3.4}$$

These equations are applicable for $\bar{R} \leq r \leq R$. Properties and dependent variables applying to the condensate are without subscripts; whereas those applying to the vapor are subscripted with a v.

The boundary conditions which apply for the condensate are given:

$$\text{for } r = R;\ u = 0 \tag{3.5}$$

$$v = 0 \tag{3.6}$$

$$T = T_w \tag{3.7}$$

$$\text{for } r = \bar{R};\ \mu\left(\frac{\partial u}{\partial r}\right)_{\bar{R}} = \mu_v\left(\frac{\partial u_v}{\partial r}\right)_{\bar{R}} + \frac{\frac{d\Gamma}{dx}\left[\bar{u}_{v,\infty} - u(\bar{R})\right]}{\pi\,\bar{R}} \tag{3.8}$$

$$T = T_s \tag{3.9}$$

$$\rho\left(\frac{\partial \delta}{\partial t} + u\frac{\partial \delta}{\partial x} - v\right) h_{fg} = k\left(\frac{\partial T}{\partial r}\right)_{\bar{R}} \tag{3.10}$$

Equation 3.5 asserts that there is no slip between the condensate film and the wall. Equation 3.6 reflects the fact that the solid tube allows no radial throughflow. Equation 3.7 implies that a good thermal contact exists at the tube wall-liquid interface. The assumptions involved in Equation 3.8 are that the shearing stress exerted on the liquid is composed of the frictional effect of the vapor on the surface, plus the average momentum change resulting from condensing the vapor. The importance of the momentum term has been noted by Shekriladze and Gomelauri (50). Equation 3.9 appears to be a valid assumption for a pure vapor, whenever ΔT is not too large. Equation 3.10 results from the consideration that the thermal energy released by condensation at the liquid vapor interface is conducted through the cooled wall.

The assumption of a resonant sound field in the axial direction imposed upon the vapor allows the pressure imposed upon the condensate by the vapor to be written as

$$P = \bar{P} + P_o \sin\left(\frac{2\pi x}{\lambda}\right) \sin(\omega t)\ . \tag{3.11}$$

The super bar represents a time-average value. The time-average pressure, $\bar{P}$, of Equation 3.11 is assumed to be equal to the saturation pressure. The next term of Equation 3.11 is sound pressure, where P_o represents the maximum pressure variation from $\bar{P}$. The circular frequency of the sound field is ω, and the wavelength is λ. This pressure description assumes that P is independent of r.

Other reasonable assumptions are that the liquid condensate behaves incompressibly, F_r is negligible, and $F_x = \rho g$.

The problem can be envisioned as a superimposition of the time-dependent effects on a time-average situation, with the time-dependent variation much less than the time-average value. Following this reasoning, one might then assume that the variables can be written as the sum of the time-dependent and time-average values:

$$u(x, r, t) = u'(x, r, t) + \bar{u}(x, r) \tag{3.12}$$

$$v(x, r, t) = v'(x, r, t) + \bar{v}(x, r) \tag{3.13}$$

$$T(x, r, t) = T'(x, r, t) + \bar{T}(x, r) \tag{3.14}$$

Substitution of these expressions (Equations 3.11, 3.12, 3.13 and 3.14) and the previous assumptions into Equations 3.1, 3.2, 3.3 and 3.4 would allow a separation of the time-dependent governing equations and the time-average governing equations. Performing an order of magnitude analysis would allow a reduction in the complexity of the problem, if higher order terms are neglected. Ultimately, one might be able to justify the further assumptions required to linearize the equations or one might attempt a computer solution of the complete set of equations. However, the considerations thus far do not yield a complete problem statement.

A set of equations like Equations 3.1, 3.2 and 3.3 can be written to describe the vapor behavior for $0 \leq r \leq \bar{R}$.

Continuity equation:

$$\frac{\partial \rho_v}{\partial t} + \frac{\partial}{\partial x}(\rho_v u_v) + \frac{1}{r}\frac{\partial}{\partial r}(r\rho_v v_v) = 0 \tag{3.15}$$

Momentum equations:

$$\rho\left(\frac{\partial u_v}{\partial t} + u_v \frac{\partial u_v}{\partial x} + v_v \frac{\partial u_v}{\partial r}\right) = F_x - \frac{\partial P}{\partial x} +$$

$$\mu_v\left(\frac{1}{3}\frac{\partial^2 v_v}{\partial r \partial x} + \frac{1}{3}\frac{1}{r}\frac{\partial v_v}{\partial x} + \frac{4}{3}\frac{\partial^2 u_v}{\partial x^2} + \frac{\partial^2 u_v}{\partial r^2} + \frac{1}{r}\frac{\partial u_v}{\partial r}\right), \tag{3.16}$$

and

$$\left(\frac{\partial v_v}{\partial t} + u_v \frac{\partial v_v}{\partial x} + v_v \frac{\partial v_v}{\partial r}\right) = F_r - \frac{\partial P}{\partial r} +$$

$$\mu_v\left(\frac{4}{3}\frac{\partial^2 v_v}{\partial r^2} + \frac{4}{3}\frac{1}{r}\frac{\partial v_v}{\partial r} - \frac{4}{3}\frac{v_v}{r^2} + \frac{1}{3}\frac{\partial^2 u_v}{\partial r \partial x}\right) \quad . \tag{3.17}$$

The energy is released by the vapor at the liquid-vapor interface due to the condensation process, without the requirement of a temperature gradient in the vapor to transfer the thermal energy. Consequently the energy equation does not appear, but rather the condensation process yields a boundary condition. That is, the effect of the condensation process on the vapor flow field can be considered as a suction process at $\bar{R}$. (Equation 3.18 below). The boundary conditions for the vapor equations can be written:

for $r = \bar{R}$;

$$\mu\left(\frac{\partial u}{\partial r}\right)_{\bar{R}} = \mu_v\left(\frac{\partial u_v}{\partial r}\right)_{\bar{R}} + \frac{\frac{d\Gamma}{dx}\left[\bar{u}_{v,m} - u(\bar{R})\right]}{\pi \bar{R}} \tag{3.8}$$

$$(v_v)_{\bar{R}} = \frac{\frac{d\Gamma}{dx}}{\pi \bar{R} \rho_v} \tag{3.18}$$

$$\text{for } r = 0;\ \left(\frac{\partial u_v}{\partial r}\right)_o = 0 \tag{3.19}$$

$$\left(v_v\right)_o = 0 \tag{3.20}$$

The condition of axially symmetrical flow is given by Equations 3.19 and 3.20.

The mass flow rate can be expressed as a function of the independent variables x and t[$\Gamma = \Gamma(x, t)$], and the liquid and vapor equations are coupled by satisfying boundary conditions which involve $\frac{d\Gamma}{dx}$. Consequently, the solution of each set of equations must satisfy boundary conditions which are dependent upon x and t. It is not difficult to envision the complexity involved in attempting to solve this problem. A logical approach is to simplify the problem much further in order to obtain approximate solutions which may yield valid qualitative results.

Simplified Liquid Condensate Model

The time-average pressure axial distribution resulting from a resonant acoustic field has been described by Barfield (2) as appearing to be sinusoidal, with a maximum pressure difference between the velocity antinode and velocity node of

$$\Delta P = \overline{P_n - P_a} = \frac{1}{2}\rho_v U_o^2$$

as predicted by Howartson (18). The relation between the maximum sound velocity (U_o) and the maximum sound pressure (P_o) can be expressed as $U_o = \frac{P_o}{\rho_v a}$. Therefore, ΔP can be expressed as

$$\Delta P = \frac{1}{2\rho_v}\left(\frac{P_o}{a}\right)^2 \tag{3.21}$$

The time-average pressure distribution which the vapor imposes upon the liquid condensate can be approximated as

$$P = \frac{\Delta P}{2} \sin\frac{2\pi x}{\lambda} + \bar{P} \quad . \tag{3.22}$$

Although these results are for an ideal gas media with no through flow, it is assumed that the time-average effect of a resonant sound field imposed on the condensing vapor can be represented by this simple pressure distribution.

If this is assumed to be the only time-average effect the vapor imposes upon the liquid condensate, then the problem can be reduced to that of considering the Nusselt problem with a sinusoidal pressure distribution superimposed. This is shown schematically in Figure 18, as a two-dimensional model.

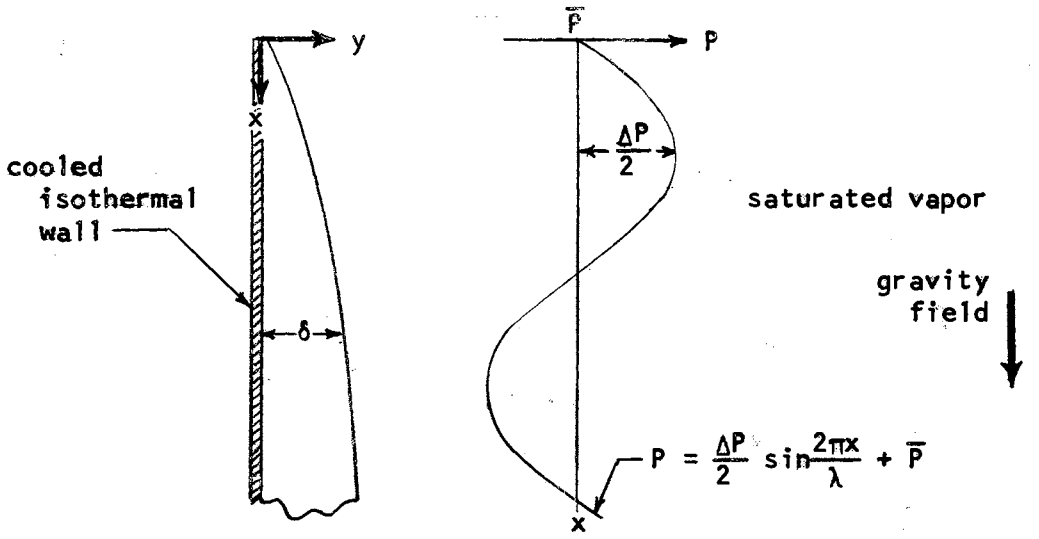

Figure 18. Simplified Liquid Condensate Model of the Effect of a Resonant Acoustic Field on Condensation.

The two-dimensional model has the simplified governing equations:

Continuity equation:

$$\frac{\partial u}{\partial x} + \frac{\partial v}{\partial y} = 0 \tag{3.23}$$

Momentum equation:

$$\mu\left(\frac{\partial^2 u}{\partial y}\right) = \frac{\partial P}{\partial x} - \rho g \tag{3.24}$$

With the boundary conditions:

$$\text{for } y = 0;\ u = 0 \tag{3.25}$$

$$v = 0 \tag{3.26}$$

$$\text{for } y = \delta(x);\ \left(\frac{\partial u}{\partial y}\right)_{\delta} = 0 \ . \tag{3.27}$$

The momentum equation is linear and can be integrated with the given boundary conditions (Equations 3.25 and 3.27) to obtain the results

$$\frac{\partial u}{\partial y} = \frac{\rho g}{\mu}\left(1 - \frac{1}{\rho g}\frac{\partial P}{\partial x}\right)(\delta - y)\ , \tag{3.28}$$

$$\text{and}\quad u = \frac{\rho g}{\mu}\left(1 - \frac{1}{\rho g}\frac{\partial P}{\partial x}\right)\left(y\delta - \frac{y^2}{2}\right)\ . \tag{3.29}$$

By use of the usual assumptions for a steady state laminar condensation process, an energy analysis of an element of condensate flow δ by dx by unity yields:

$$h'_{fg}\frac{d}{dx}\left[\int_0^{\delta(x)} \rho u dy\right] = k\frac{\Delta T}{\delta(x)}\ . \tag{3.30}$$

Substitution of Equation 3.29 for u, performance of the indicated operations and rearrangement yields:

$$4\delta^3\frac{d\delta}{dx} + \frac{4}{3}\frac{\frac{d}{dx}\left(1 - \frac{1}{\rho g}\frac{\partial P}{\partial x}\right)}{\left(1 - \frac{1}{\rho g}\frac{\partial P}{\partial x}\right)}\delta^4 = \frac{4k\mu\Delta T}{\rho^2 g\, h'_{fg}\left(1 - \frac{1}{\rho g}\frac{\partial P}{\partial x}\right)}\ . \tag{3.31}$$

A solution for this equation can be written as

$$\delta^4 = \left(1 - \frac{1}{\rho g}\frac{\partial P}{\partial x}\right)^{-\frac{4}{3}}\left\{\frac{4k\mu\Delta T}{\rho^2 g\, h'_{fg}}\int\left(1 - \frac{1}{g}\frac{\partial P}{\partial x}\right)^{\frac{1}{3}} dx + C\right\} \tag{3.32}$$

C is a constant of integration which must be determined with the boundary condition:

$$\text{at } x = 0;\ \delta = 0 \quad . \tag{3.33}$$

The pressure is given by Equation 3.22 as

$$P = \frac{\Delta P}{2} \sin\frac{2\pi x}{\lambda} + \bar{P} \quad .$$

Using Equation 3.21 for ΔP and defining

$$\zeta \equiv \frac{\pi}{2\rho g \lambda \rho_v} \left(\frac{P_o}{a}\right)^2 \tag{3.34}$$

$$\text{and} \quad \tilde{x} = \frac{2\pi x}{\lambda} \tag{3.35}$$

allows $\frac{1}{\rho g}\frac{\partial P}{\partial x}$ to be written as

$$\frac{1}{\rho g}\frac{\partial P}{\partial x} = \zeta \cos \tilde{x} \quad . \tag{3.36}$$

The magnitude of ζ will be considered before attempting the integral portion of Equation 3.32.

Assuming saturated steam at atmospheric pressure is being condensed, then from Keenan and Keyes (22): $\frac{1}{\rho} = 0.01672$ ft^3/lbm and $1/\rho_v = 26.80$ ft^3/lbm. The speed of sound as given by Beranek (3) is 1328 ft/sec. Assuming the maximum sound pressure deviation (P_o) is 1 psi for an acoustic wavelength (λ) of ½ ft, and g = 32.174 ft/sec^2, then the value for ζ obtained using these values represents the maximum ζ value to be considered.

$$\zeta_{max} = 0.537$$

Therefore, a reasonable approximation of the cube root term in Equation 3.32 is

$$\left(1 - \frac{1}{\rho g}\frac{\partial P}{\partial x}\right)^{\frac{1}{3}} \approx 1 - \frac{1}{3}\left(\frac{1}{\rho g}\frac{\partial P}{\partial x}\right) - \frac{1\cdot 2}{3\cdot 6}\left(\frac{1}{\rho g}\frac{\partial P}{\partial x}\right)^2 - \frac{1\cdot 2\cdot 5}{3\cdot 6\cdot 9}\left(\frac{1}{\rho g}\frac{\partial P}{\partial x}\right)^3$$

$$- \frac{1\cdot 2\cdot 5\cdot 8}{3\cdot 6\cdot 9\cdot 12}\left(\frac{1}{\rho g}\frac{\partial P}{\partial x}\right)^4 \quad . \tag{3.37}$$

Using this approximation of $\left(1 - \frac{1}{\rho g}\frac{\partial P}{\partial x}\right)^{\frac{1}{3}}$, and neglecting terms involving ζ^m with $m > 4$ allows an approximate solution for Equation 3.31 to be written as

$$\delta = \left\{\frac{4k\mu\Delta Tx}{\rho^2 g\, h_{fg}'}\right\}^{\frac{1}{4}} \left\{1 - \zeta\cos\tilde{x}\right\}^{-\frac{1}{3}} \left\{1 - \frac{\zeta^2}{18} - \frac{5\zeta^4}{324}\right.$$

$$- \frac{1}{\tilde{x}}\left[\left(\frac{\zeta}{3} \frac{3}{1292}\zeta^2 + \frac{5\zeta^3}{81}\right)\sin\tilde{x} + \left(\frac{\zeta^2}{36} + \frac{5\zeta^4}{486}\right)\sin 2\tilde{x}\right.$$

$$\left.\left. - \frac{\zeta^2}{1292}\sin 3\tilde{x} + \frac{\zeta^4}{388}\sin 4\tilde{x}\right]\right\}^{\frac{1}{4}} \quad . \tag{3.38}$$

The first bracketed term raised to the ¼ power on the right hand side of Equation 3.38 is the Nusselt expression for film thickness (δ_{Nu}) with vapor density neglected. Dividing both sides of Equation 3.38 by δ_{Nu} will allow a dimensionless film thickness ($\tilde{\delta}$) to be defined:

$$\tilde{\delta} \equiv \frac{\delta}{\delta_{Nu}} = \left\{1 - \zeta\cos\tilde{x}\right\}^{-\frac{1}{3}} \left\{1 - \frac{\zeta^2}{18} - \frac{5\zeta^4}{324}\right.$$

$$- \frac{1}{\tilde{x}}\left[\left(\frac{\zeta}{3} + \frac{3\zeta^2}{1292} + \frac{5\zeta^3}{81}\right)\sin\tilde{x} + \left(\frac{\zeta^2}{36} + \frac{5\zeta^4}{486}\right)\sin 2\tilde{x}\right.$$

$$\left.\left. - \frac{\zeta^2}{1292}\sin 3\tilde{x} + \frac{\zeta^4}{388}\sin 4\tilde{x}\right]\right\}^{\frac{1}{4}} \quad . \tag{3.39}$$

The average heat transfer coefficient ($\bar{h}$) for a plate length L can be written as

$$\bar{h} = \frac{1}{L}\int_0^L \frac{k}{\delta(x)}\,dx \quad .$$

Substitution of Equation 3.38 for $\delta(x)$ and utilizing the approximation given by Equation 3.37 in the above equation yields:

$$\bar{h} = \frac{4}{3}\left\{\frac{\rho^2 g\, h_{fg}' k^3}{4\mu\Delta T L}\right\}^{\frac{1}{4}}\left\{1 - \frac{\zeta^2}{18} - \frac{5\zeta^4}{324} - \frac{1}{\tilde{x}}\left[\left(\frac{\zeta}{3} + \frac{3\zeta^2}{1292} + \frac{5\zeta^3}{81}\right)\sin\tilde{x}\right.\right.$$

$$\left.\left. + \left(\frac{\zeta^2}{36} + \frac{5\zeta^4}{486}\right)\sin 2\tilde{x} - \frac{\zeta^2}{1292}\sin 3\tilde{x} + \frac{\zeta^4}{388}\sin 4\tilde{x}\right]\right\}^{\frac{3}{4}}. \qquad (3.40)$$

A dimensionless average heat transfer coefficient can be defined:

$$\tilde{h} \equiv \frac{\bar{h}}{\bar{h}_{Nu}} = \left\{1 - \frac{\zeta^2}{18} - \frac{5\zeta^4}{324} - \frac{1}{\tilde{x}}\left[\left(\frac{\zeta}{3} + \frac{3\zeta^2}{1292} + \frac{5\zeta^3}{81}\right)\sin\tilde{x}\right.\right.$$

$$\left.\left. + \left(\frac{\zeta^2}{36} + \frac{5\zeta^4}{486}\right)\sin 2\tilde{x} - \frac{\zeta^2}{1292}\sin 3\tilde{x} + \frac{\zeta^4}{388}\sin 4\tilde{x}\right]\right\}^{\frac{3}{4}}. \qquad (3.41)$$

Calculated results for $\tilde{\delta}$ and $\tilde{h}$ with $\zeta = 0.5$ are shown in Figure 19. As may be observed from Equation 3.39 and Figure 19, the term $(1 - \zeta\cos\tilde{x})^{-1/3}$ dominates the film thickness deviation. As $\tilde{x}$ becomes large, $\tilde{h}$ approaches a value of $(1 - \zeta^2/18 - 5\zeta^4/324)$, indicating a slight decrease in the average heat transfer coefficient for large values of $\tilde{x}$.

The simplified liquid condensate model for determining the effect of sound on laminar condensation heat transfer rate indicates only slight deviation from Nusselt's average heat transfer coefficient. The simplified liquid condensate model resulted from assuming a time-average solution for the vapor equations, which provided boundary conditions for the liquid condensate problem. Another approach to the

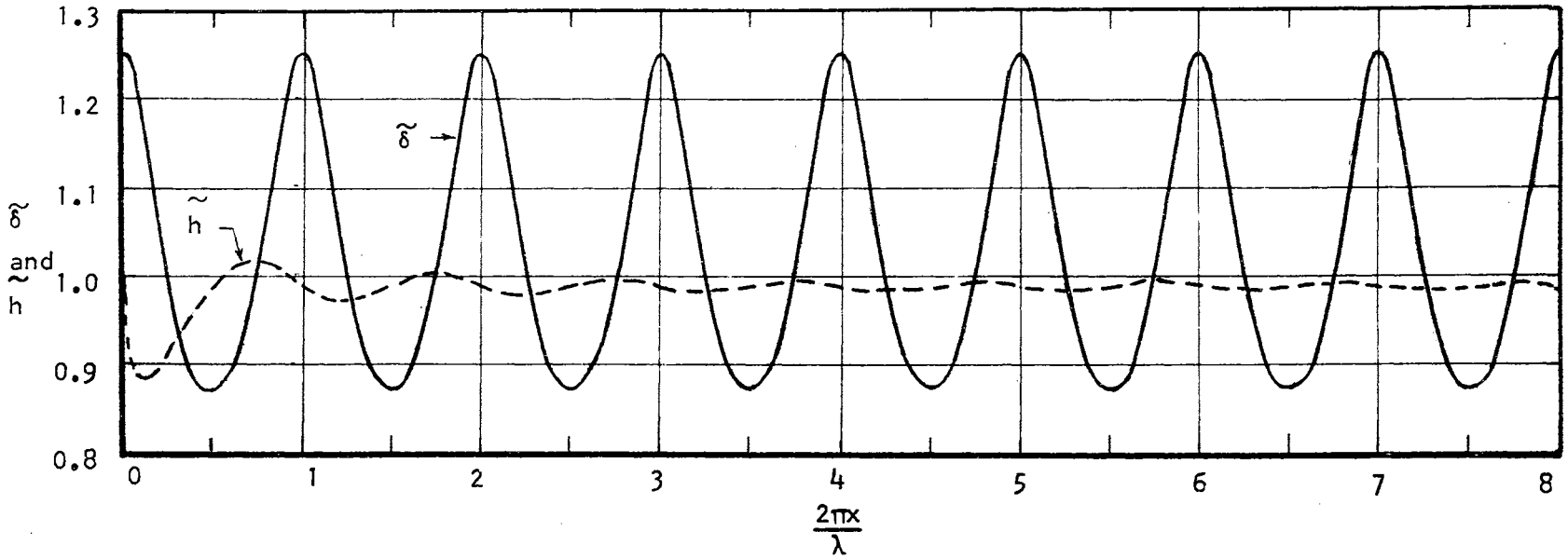

Figure 19. Dimensionless Film Thickness and Average Heat Transfer Coefficient for the Simplified Liquid Condensate Model with $\zeta = 0.5$.

problem is to assume a time-average solution for the laminar condensate film equations, thereby extablishing workable boundary conditions for the vapor equations.

Simplified Condensing Vapor Model

The time-average solution for the condensate film is assumed to be the results given by Nusselt's expressions. It is assumed that the effect of condensation on the vapor can be treated mathematically as though a suction process occurs at the tube walls. Additionally, the film thickness is assumed to be much less than the tube radius; and consequently the "suction" boundary conditions can be applied at the tube wall. That is, the radial boundary of the vapor is assumed to be at the tube radius R. The vapor is assumed to behave as an ideal gas with constant viscosity. The vapor flow is assumed to be laminar, axially symmetric, time-dependent and compressible--with a resonant acoustic field superimposed. The pressure node is assumed to be at $x = 0$. This model should provide a qualitative description of the vapor flow field, and perhaps an insight into the coupling that may exist between the condensate liquid film and the vapor at the liquid-vapor interface.

Purdy et al. (43) have considered the problem of a resonant acoustic field superimposed upon laminar flow of an ideal gas in the circular tube. Their governing equations are the same as those given by Equations 3.15, 3.16 and 3.17. Assuming that the variables of interest could be represented as the sum of a time average component and a time dependent component (like Equations 3.11, 3.12 and 3.13), they expressed the governing equations as time-average and time-dependent equations.

The pressure variations were assumed to be the same as for an inviscid gas, and the compression-rarefaction process was assumed to be isentropic to eliminate the time-dependent density term in favor of the pressure term. Additionally they neglected time-mean density and pressure variations, and assumed that the average through flow velocity ($\bar{U}$) was small in comparison with the maximum amplitude of the time-dependent velocity, U_o.

With these assumptions, Purdy et al. performed an order of magnitude analysis to reduce and linearize the governing equations. Their reduced time-dependent and time-average equations, expressed as vapor quantities, are shown below.

Time-dependent continuity equation:

$$\frac{\partial \rho_v'}{\partial t} + \bar{\rho}_v\left(\frac{\partial u_v'}{\partial x}\right) + \frac{1}{r}\frac{\partial}{\partial r}\left(r v_v'\right) = 0 \quad . \tag{3.42}$$

Time-dependent momentum equations:

$$\frac{\partial p_v'}{\partial r} = 0 \tag{3.43}$$

$$\frac{\partial u_v'}{\partial t} + \frac{1}{\bar{\rho}_v}\frac{\partial p'}{\partial x} = \frac{\mu_v}{\bar{\rho}_v}\frac{1}{r}\frac{\partial}{\partial r}\left(r\frac{\partial u_v'}{\partial r}\right) \tag{3.44}$$

Time-average continuity equation:

$$\frac{1}{r}\frac{\partial}{\partial r}\left(r\bar{v}_v\right) = -\frac{\partial \bar{u}_v}{\partial x} - \frac{1}{\bar{\rho}_v}\left[\frac{1}{r}\frac{\partial}{\partial r}\left(r\overline{\rho_v' v_v'}\right) + \frac{\partial}{\partial x}\left(\overline{\rho_v' u_v'}\right)\right] . \tag{3.45}$$

Time-average momentum equation:

$$\mu_v\frac{\partial}{\partial r}\left[\frac{1}{r}\frac{\partial}{\partial r}\left(r\frac{\partial \bar{u}_v}{\partial r}\right)\right] = \bar{\rho}_v\frac{\partial}{\partial r}\left[\overline{\frac{\rho_v'}{\bar{\rho}_v}\left(\frac{\partial u_v'}{\partial t}\right) + v_v'\left(\frac{\partial u_v'}{\partial r}\right) + u_v'\left(\frac{\partial u_v'}{\partial x}\right)}\right] . \tag{3.46}$$

They obtained solutions to these equations for the boundary conditions:

$$\text{at } r = 0;\ v_v' = 0,\ \frac{\partial u_v'}{\partial r} = 0,\ \bar{v}_v = 0, \text{ and } \frac{\partial \bar{u}_v}{\partial r} = 0$$

$$\text{at } r = R;\ v_v' = 0,\ u_v' = 0,\ \bar{v}_v = 0 \text{ and } \bar{u}_v = 0$$

$$\text{for all } x;\ \int_0^R 2\pi\, \bar{\rho}_v \bar{u}_v r dr = \text{constant}$$

Employing the assumptions made by Purdy et al, Equation 3.42, 3.43, 3.44, 3.45 and 3.46 are applicable for the simplified condensing vapor model. The appropriate boundary conditions for the simplified condensing vapor model are as follows:

$$\text{At } r = 0;\ v_v' = 0,\ \frac{\partial u_v'}{\partial r} = 0 \tag{3.47}$$

$$\bar{v}_v = 0, \text{ and } \frac{\partial \bar{u}_v}{\partial r} = 0 \tag{3.48}$$

$$\text{At } r = R;\ v_v' = 0, u_v' = 0 \tag{3.49}$$

$$\bar{v}_v = \frac{1}{2\pi \bar{\rho}_v R}\left(\frac{d\Gamma}{dx}\right) \text{ and } \bar{u}_v = B_\ell x^{\frac{1}{2}} \tag{3.50}$$

$$\text{For all } x: \int_0^R 2\pi\, r \bar{\rho}_v \bar{u}_v dr = \Gamma_o - \Gamma(x)\ . \tag{3.51}$$

Where by definition:

$$\Gamma(x) \equiv 2\pi R A_\ell x^{\frac{3}{4}} \tag{3.52}$$

$$A_\ell \equiv \frac{1}{3}\left[\frac{g\rho(\rho - \bar{\rho}_v)}{\mu}\right]^{\frac{1}{4}}\left[\frac{4k\Delta T}{h_{fg}}\right]^{\frac{3}{4}} \tag{3.53}$$

$$B_\ell \equiv \left[\frac{k\Delta T g(\rho - \rho_v)}{\rho \mu h_{fg}}\right]^{\frac{1}{2}}, \tag{3.54}$$

and $\Gamma_o \equiv$ Vapor Mass Flow rate at x = 0.

The boundary conditions given by Equations 3.47 and 3.48 are required by symmetry. The conditions given by Equation 3.49 imply that there is no slip at the liquid vapor boundary. The conditions given by Equation 3.50 result from assuming the radial "suction" velocity and the interface surface velocity in the axial direction is specified by Nusselt's solution for the liquid condensate equations.

The problem as stated is essentially the same as that considered by Purdy et al., with the exception of the time-average boundary conditions. Since the time-dependent equations and boundary conditions are the same as those of Purdy et al., their time-dependent solutions are valid for the simplified condensing vapor model. These solutions are expressed as a function of Bessel functions of argument $\tilde{r}\, i\sqrt{i}$ of the first kind, where $i = +\sqrt{-1}$.

Time-dependent axial velocity:

$$u_v'(\tilde{r}, x, t) = -\frac{U_o}{M_o^2(\tilde{R})} \cos\left(\frac{2\pi x}{\lambda}\right) *$$

$$\left\{ \left[M_o^2(\tilde{R}) - ber_o(\tilde{R})ber_o(\tilde{r}) - bei_o(\tilde{R})bei_o(\tilde{r}) \right] \cos(\omega t) \right.$$

$$\left. + \left[ber_o(\tilde{R})bei_o(\tilde{r}) - bei_o(\tilde{R})ber_o(\tilde{r}) \right] \sin(\omega t) \right\} \qquad (3.55)$$

Time-dependent radial velocity:

$$v_v'(\tilde{r}, x, t) = \frac{2\pi U_o \sqrt{\mu_v \sqrt{\omega \bar{\rho}_v}}}{M_o^2(\bar{R})} \sin\left(\frac{2\pi x}{\lambda}\right) *$$

$$\left\{ \left[ber_o(\tilde{R})bei_o'(\tilde{r}) - bei_o(\tilde{R})ber_o'(\tilde{r}) \right] \cos(\omega t) \right.$$

$$\left. + \left[ber_o(\tilde{R})ber_o'(\tilde{r}) + bei_o(\tilde{R})bei_o'(\tilde{r}) \right] \sin(\omega t) \right.$$

$$- \gamma M_1(\tilde{R}) M_o(\tilde{R}) \sin\left[\omega t + \theta_1(\tilde{R}) - \theta_o(\tilde{R}) - \pi/4\right]\Big\} \tag{3.56}$$

Where by definition:

$$M_o^2(\tilde{R}) \equiv ber_o^2(\tilde{R}) + bei_o^2(\tilde{R}), \tag{3.57}$$

$$M_1^2(\tilde{R}) \equiv ber_1^2(\tilde{R}) + bei_1^2(\tilde{R}), \tag{3.58}$$

$$\theta_o(\tilde{R}) \equiv \tan^{-1} \frac{bei_o(\tilde{R})}{ber_o(\tilde{R})} \quad , \tag{3.59}$$

$$\theta_1(\tilde{R}) \equiv \tan^{-1} \frac{bei_1(\tilde{R})}{ber_1(\tilde{R})} \quad , \tag{3.60}$$

$$\tilde{r} \equiv \frac{r}{\sqrt{\mu_v/\omega\bar{\rho}_v}} \tag{3.61}$$

and $$\gamma \equiv \tilde{r}/\tilde{R} = r/R \quad . \tag{3.62}$$

It should be noted that the boundary conditions at r = 0 and r = R can not be satisfied simultaneously. To alleviate this difficulty, Purdy replaced $1/\tilde{r}$ by $\tilde{r}/\tilde{R}^2$. This permitted both boundary conditions to be satisfied, and the approximation in the A.C. boundary layer was excellent--according to Purdy et al. A detailed account of the order of magnitude analysis, assumptions and method of solution are presented by Purdy et al. (43); consequently, the interested reader should consult this reference for details.

Solutions for the time-average equations (3.45 and 3.46) with the boundary conditions given by Equations 3.48 3,50 and 3.51 can be obtained by employing the same techniques as used by Purdy et al. Utilization of these techniques, information on Bessel Functions as presented by Dwight (14) and McLachlan (36), and perserverance yielded

the time-average results which follow. The time-average axial velocity is determined from Equation 3.46 and the specified boundary conditions.

Time-average axial velocity:

$$\bar{u}_v(\tilde{r}, x) = (2\gamma^2 - 1)B_\ell x^{\frac{1}{2}} + \frac{2}{\pi\bar{\rho}_v R^2}(1 - \gamma^2)(\Gamma_o - 2\pi R A_\ell x^{\frac{3}{4}})$$

$$- \frac{U_o^2}{4a}\sin\left(\frac{4\pi x}{\lambda}\right) * \left\{ \frac{2}{\tilde{R}^2}(\gamma^2 - 1) + (\gamma^2 - \tfrac{1}{2})\frac{M_1^2(\tilde{R})}{M_o^2(\tilde{R})}\right.$$

$$+ \frac{1}{2}\frac{M_1^2(\tilde{r})}{M_o^2(\tilde{R})} - 3\frac{M_o(\tilde{r})}{M_o(\tilde{R})}\sin[\theta_o(\tilde{r}) - \theta_o(\tilde{R})]$$

$$- \gamma\frac{M_1(\tilde{r})M_1(\tilde{R})}{M_o^2(\tilde{R})}\cos[\theta_1(\tilde{r}) - \theta_1(\tilde{R})] +$$

$$+ \frac{\gamma}{\tilde{R}}\frac{M_1(\tilde{r})M_o(\tilde{r})}{M_o^2(\tilde{R})}\cos[\theta_1(\tilde{r}) - \theta_o(\tilde{r}) - \pi/4]$$

$$+ \frac{2}{\tilde{R}}\frac{M_o(\tilde{r})M_1(\tilde{R})}{M_o^2(\tilde{R})}\cos[\theta_1(\tilde{R}) - \theta_o(\tilde{r}) - \pi/4]$$

$$+ \frac{4}{\tilde{R}}\left[\gamma^2 - \frac{7}{4}\right]\frac{M_1(\tilde{R})}{M_o(\tilde{R})}\cos[\theta_1(\tilde{R}) - \theta_o(\tilde{R}) - \pi/4]$$

$$+ \frac{4}{\tilde{R}}\left[\gamma^2 - 1\right]\frac{M_1(\tilde{R})}{M_o(\tilde{R})}\sin\left[\theta_1(\tilde{R}) - \theta_o(\tilde{R}) - \pi/4\right]. \qquad (3.63)$$

The time-average radial velocity can be determined from Equation 3.45.

Time-average Radial Velocity:

$$\bar{v}_v(\tilde{r}, x) = -\frac{r}{4}\left(\gamma^2 - 1\right)B_\ell x^{-\frac{1}{2}} + \frac{3}{4}\frac{A_\ell\gamma}{\bar{\rho}_v}(2 - \gamma^2)x^{-\frac{1}{4}} +$$

$$+ \pi \frac{U_o^2}{a} \frac{R}{\lambda} \cos\left(\frac{4\pi x}{\lambda}\right) * \left\{ \frac{\gamma}{2\tilde{R}^2} (\gamma^2 - 2) + \frac{\gamma}{4} (\gamma^2 - 1) \frac{M_1^2(\tilde{R})}{M_o^2(\tilde{R})} \right.$$

$$+ \frac{1}{2\tilde{R}} \frac{M_o(\tilde{r})M_1(\tilde{r})}{M_o^2(\tilde{R})} \cos\left[\theta_1(\tilde{r}) - \theta_o(\tilde{r}) - \pi/4\right] + \frac{3}{\tilde{R}} \frac{M_o(\tilde{r})}{M_o(\tilde{R})} *$$

$$\cos\left[\theta_1(\tilde{r}) - \theta_o(\tilde{R}) - \pi/4\right]$$

$$- \frac{\gamma}{\tilde{R}} \frac{M_o(\tilde{r})M_1(\tilde{R})}{M_o^2(\tilde{R})} \cos\left[\theta_1(\tilde{R}) - \theta_o(\tilde{r}) - \pi/4\right] - \frac{4}{\tilde{R}^2} \frac{M_1(\tilde{r})M_1(\tilde{R})}{M_o^2(\tilde{R})} *$$

$$\sin\left[\theta_1(\tilde{R}) - \theta_1(\tilde{r})\right]$$

$$+ \frac{\gamma}{\tilde{R}^2} \frac{M_o^2(\tilde{r})}{M_o^2(\tilde{R})} - \frac{2}{\tilde{R}^3} \frac{M_o(\tilde{r})M_1(\tilde{r})}{M_o^2(\tilde{R})} \sin\left[\theta_1(\tilde{r}) - \theta_o(\tilde{r}) - \pi/4\right]$$

$$+ \frac{\gamma}{\tilde{R}} \left[\gamma^2 - \frac{7}{2}\right] \frac{M_1(\tilde{R})}{M_o(\tilde{R})} \cos\left[\theta_1(\tilde{R}) - \theta_o(\tilde{R}) - \pi/4\right]$$

$$+ \frac{\gamma}{\tilde{R}} \left(\gamma^2 - 2\right) \frac{M_1(\tilde{R})}{M_o(\tilde{R})} \sin\left[\theta_1(\tilde{R}) - \theta_o(\tilde{R}) - \pi/4\right]$$

$$- \frac{\pi U_o^2}{a} \epsilon \left\{ \cos\left(\frac{4\pi x}{\lambda}\right) \frac{M_1(\tilde{r})}{M_o(\tilde{R})} \cos\left[\theta_1(\tilde{r}) - \theta_o(\tilde{R}) - \pi/4\right] \right.$$

$$- \left[1 - \cos\left(\frac{4\pi x}{\lambda}\right)\right] \left[\frac{M_1(\tilde{r})}{M_o(\tilde{R})} \cos\left[\theta_1(\tilde{r}) - \theta_o(\tilde{R}) - \pi/4\right] \right.$$

$$\left. \left. - \gamma \frac{M_1(\tilde{R})}{M_o(\tilde{R})} \cos\left[\theta_1(\tilde{R}) - \theta_o(\tilde{R}) - 4/\pi\right] \right] \right\} + \frac{f(x)}{\tilde{r}} \qquad (3.64)$$

where: $\epsilon \equiv \dfrac{\sqrt{\mu_v / \omega \bar{\rho}_v}}{\lambda}$, (3.65)

and, $f(x)/\tilde{r}$ = a function to be determined from boundary conditions.

It is of interest to note that $\epsilon << 1$ and the terms multiplied by ϵ represent the contribution of

$$-\frac{1}{\bar{\rho}_v}\left[\frac{1}{r}\frac{\partial}{\partial r}\left(r\,\overline{\rho_v' v_v'}\right) + \frac{\partial}{\partial x}\left(\overline{\rho_v' u_v'}\right)\right]$$

from the time-average continuity equation (3.45). Since all other terms multiplied by ϵ are less than 1, then the contribution of this term is of the order of magnitude ϵ, in comparison with the term resulting from $-\left(\frac{\partial \bar{u}_v}{\partial x}\right)$. Consequently, the time-average continuity equation (3.45) can be reduced to

$$\frac{1}{r}\frac{\partial}{\partial r}\left[r\,\bar{v}_v\right] + \frac{\partial \bar{u}_v}{\partial x} = 0\,, \tag{3.66}$$

and the time-average radial velocity as determined from Equation 3.66 is as follows.

Time-average Radial Velocity:

$$\bar{v}_v(\tilde{r}, x) = -\frac{\tilde{r}}{4}(\gamma^2 - 1)B_\ell x^{-1/2} + \frac{3}{4}\frac{A_\ell}{\bar{\rho}_v}\gamma(2 - \gamma^2)x^{-1/4}$$

$$+ \pi\frac{U_o^2}{a}\frac{R}{\lambda}\cos\left(\frac{4\pi x}{\lambda}\right) * \left\{\frac{\gamma}{2\tilde{R}^2}(\gamma^2 - 3) + \frac{\gamma}{4}(\gamma^2 - 1)\frac{M_1^2(\tilde{R})}{M_o^2(\tilde{R})}\right.$$

$$+ \frac{1}{2\tilde{R}}\frac{M_o(\tilde{r})M_1(\tilde{r})}{M_o^2(\tilde{R})}\cos\left[\theta_1(\tilde{r}) - \theta_o(\tilde{r}) - \pi/4\right] + \frac{3}{\tilde{R}}\frac{M_1(\tilde{r})}{M_o(\tilde{R})} *$$

$$\cos\left[\theta_1(\tilde{r}) - \theta_o(\tilde{R}) - \pi/4\right]$$

$$\left. - \frac{\gamma}{\tilde{R}}\frac{M_o(\tilde{r})M_1(\tilde{R})}{M_o^2(\tilde{R})}\cos\left[\theta_1(\tilde{R}) - \theta_o(\tilde{r}) - \pi/4\right] - \frac{4}{\tilde{R}^2}\frac{M_1(\tilde{r})M_1(\tilde{R})}{M_o^2(\tilde{R})} *\right.$$

$$\left.\sin\left[\theta_1(\tilde{R}) - \theta_1(\tilde{r})\right]\right\}$$

$$+ \frac{\gamma}{\tilde{R}^2} \frac{M_o^{2(\tilde{r})}}{M_o^2(\tilde{R})} - \frac{2}{\tilde{R}^3} \frac{M_o(\tilde{r})M_1(\tilde{r})}{M_o^2(\tilde{R})} \sin [\theta_1(\tilde{r}) - \theta_o(\tilde{r}) - \pi/4]$$

$$+ \frac{\gamma}{\tilde{R}} \left(\gamma^2 - \frac{7}{2}\right) \frac{M_1(\tilde{R})}{M_o(\tilde{R})} \cos [\theta_1(\tilde{R}) - \theta_1(\tilde{R}) - \pi/4]$$

$$+ \frac{\gamma}{\tilde{R}} \left(\gamma^2 - 1 - \frac{2}{\tilde{R}^2}\right) \frac{M_1(\tilde{R})}{M_o(\tilde{R})} \sin [\theta_1(\tilde{R}) - \theta_o(\tilde{R}) - \pi/4] \Big\} \qquad (3.67)$$

The reduced time-average continuity equation (3.66) allows a time-average stream function (Ψ) to be defined by the following equations:

$$\bar{v}_v = - \frac{1}{r} \frac{\partial \Psi}{\partial x} \qquad (3.68)$$

$$\bar{u}_v = \frac{1}{r} \frac{\partial \Psi}{\partial r} \qquad (3.69)$$

Note that $\Psi(0,x) = 0$ and define a dimensionless stream function ($\tilde{\Psi}$) as

$$\tilde{\Psi} \equiv \frac{\Psi}{(\bar{U}_o R^2/2)}, \qquad (3.70)$$

where $\bar{U}_o$ is the time-average vapor velocity at $x = 0$. (i.e., $\bar{U}_o = \Gamma_o / \bar{\rho}_v \pi R^2$). Then $\tilde{\Psi}(R, 0) = 1$ and for $0 \leq \tilde{r} \leq \tilde{R}$, $0 \leq \tilde{\Psi} \leq 1$ for all x values. The dimensionless stream function can be written in polar form as shown below.

$$\tilde{\Psi}(\tilde{r},x) = \frac{\gamma^2}{\bar{U}_o} (\gamma^2 - 1) B_\ell x^{\frac{1}{2}} + \gamma^2(2 - \gamma^2)\left(1 - \frac{2\pi R A_\ell}{\Gamma_o} x^{3/4}\right)$$

$$- \frac{U_o^2}{4\bar{U}_o a} \sin\left(\frac{4\pi x}{\lambda}\right) \cdot \left\{ \frac{\gamma^2}{\tilde{R}^2} \left[\frac{2M_o^2(\tilde{r})}{M_o^2(\tilde{R})} + \gamma^2 - 3 \right] + \frac{\gamma^2}{2}(\gamma^2 - 1) \frac{M_1^2(\tilde{R})}{M_o^2(\tilde{R})} \right.$$

$$+ \frac{\gamma}{\tilde{R}} \frac{M_1(\tilde{r})}{M_o(\tilde{R})} \left[6 \cos [\theta_1(\tilde{r}) - \theta_o(\tilde{R}) - \pi/4] + \frac{M_o(\tilde{r})}{M_o(\tilde{R})} \cos[\theta_1(\tilde{r}) \right.$$

$$\left. \left. - \theta_o(\tilde{r}) - \pi/4] - 2 \frac{M_o(\tilde{r})}{M_o(\tilde{R})} \cos [\theta_1(\tilde{R}) - \theta_o(\tilde{r}) - \pi/4] - \frac{8}{\tilde{R}} \frac{M_1(\tilde{R})}{M_o(\tilde{R})} \right.\right.^*$$

$$\sin[\theta_1(\tilde{R}) - \theta_1(\tilde{r})] - \frac{4}{\tilde{R}^2}\frac{M_o(\tilde{r})}{M_o(\tilde{R})}\sin[\theta_1(\tilde{r}) - \theta_o(\tilde{r}) - \pi/4]\Big]$$

$$+ \frac{2\gamma^2}{\tilde{R}}\left(\gamma^2 - \frac{7}{2}\right)\frac{M_1(\tilde{R})}{M_o(\tilde{R})}\cos[\theta_1(\tilde{R}) - \theta_o(\tilde{R}) - \pi/4]$$

$$+ \frac{2\gamma^2}{\tilde{R}}\left(\gamma^2 - 1 - \frac{2}{\tilde{R}^2}\right)\frac{M_1(\tilde{R})}{M_o(\tilde{R})}[\theta_1(\tilde{R}) - \theta_o(\tilde{R}) - \pi/4]\Big\} \qquad (3.71)$$

In the following discussion of the equations developed for the simplified condensing vapor model, secondary flow induced by the resonant sound field is considered to be the mechanism whereby the sound can affect the condensate liquid layer--and the condensation rate. Significant effects should be demonstrated to warrant further analytical considerations directed toward the determination of the liquid-vapor interface boundary conditions and the solution of the complete problem statement.

The third term of Equation 3.71,

$$\frac{U_o^2}{2a\bar{U}_o}\sin\left(\frac{4\pi x}{\lambda}\right)\cdot\left\{F(\tilde{r})\right\}, \qquad (3.72)$$

is the contribution of the superimposed sound field to the time-average stream function. Some observations about this term will serve to emphasize its salient features.

The bracketed portion of the third term is a function of $\tilde{r}$ and is less than one for the range of $\tilde{r}$ considered. That is, $\left\{F(\tilde{r})\right\} < 1$, for $0 \leq \tilde{r} \leq \tilde{R}$. Since $\tilde{r} \equiv r/\sqrt{\mu_v/\omega\bar{\rho}_v}$, then the order of magnitude of $\tilde{r}$ being considered is 10^2 to 10^3. The term, $\sin(4\pi x/\lambda)$, indicates that the

influence of the superimposed sound field on the time-average stream function is repetitive each half wavelength axial distance.

The magnitude of Equation 3.72 can be expressed as

$$\frac{U_o^2}{2a\bar{U}_o} = \frac{U_o^2 R^2}{\Gamma_o} \frac{\pi}{2} \frac{\bar{\rho}_v}{a} \quad . \tag{3.73}$$

The vapor properties which enhance the effect are obviously the ratio of density to acoustic velocity. If the vapor can be approximated as an ideal gas (as assumed for this development), then $a = \sqrt{k_v g_c p/\bar{\rho}_v}$. The results indicate that a high density of the vapor increases the effect of sound on the time-average stream function. The parameters which can be controlled--once a condensing vapor and condensate rate (which establishes Γ_o) is specified--are U_o and R. The maximum sound velocity (U_o) is determined by the sound intensity imposed upon the vapor. Increasing the sound intensity and/or the flow area increases the effect of sound on the vapor flow field.

The size of the region affected by secondary flow for a non-condensing vapor through-flow situation was shown by Purdy et al. to decrease as the through flow increased. This is shown in Figure 12. Qualitatively, the same result is observed for the simplified condensing vapor model; in that, as the axial through flow decreases, the relative magnitude of the term represented by Equation (3.72) increases.

To demonstate the time-average stream function for a physical situation similar to the experiments which were conducted, the following set of property and parameter values are considered:

$\omega = 2\pi \cdot 500$ ft/ft.sec $\qquad \rho = 60.1$ lbm/ft^3

R = 0.200 in $\qquad \bar{\rho}_v = .0372$ lbm/ft^3

$P_o = 1.0$ lbm/in^2 $\qquad \mu = 2.1 \times 10^{-4}$ lbm/ft-sec

$\Gamma_o = 8.0$ lbm/hr $\qquad \mu_v = 8.72 \times 10^{-6}$ lbm/ft-sec

$\Delta T = 5.0^oF$ $\qquad k = 0.394$ BTU/hr.ft.^oF

$a = 1328$ ft/sec $\qquad h_{fg} = 970$ BTU/lbm

Quantities calculated from the given values are:

$$\frac{B_\ell}{\bar{U}_o} = \frac{\rho_v \pi R^2}{\Gamma_o} \cdot \left[\frac{k\Delta T g(\rho - \bar{\rho}_v)}{\rho \mu h_{fg}} \right]^{\frac{1}{2}} = 0.0086 \text{ ft}^{-\frac{1}{2}}$$

$$\frac{2\pi R A_\ell}{\Gamma_o} = \frac{2\pi R}{3\Gamma_o} \left[\frac{g\rho(\rho - \bar{\rho}_v)}{\mu} \right]^{\frac{1}{4}} \left[\frac{4k\Delta T}{h_{fg}} \right]^{3/4} = 0.282 \text{ ft}^{-3/4}$$

$$\frac{U_o^2}{4a\bar{U}_o} = \frac{\pi P_o^2 R^2}{4\bar{\rho}_v a^3 \Gamma_o} = 0.0485$$

$$\tilde{R} = \frac{R}{\sqrt{\mu_v / \omega \bar{\rho}_v}} = 60.92$$

$$Re = \bar{\rho}_v \bar{U}_o 2R/\mu_v = 1951 \ .$$

The time-average stream function for this particular case can be written in the following manner:

$$\tilde{\psi}(\tilde{r}, x) = 0.0086\, \gamma^2(\gamma^2 - 1)\, x^{\frac{1}{2}} + \gamma^2(2 - \gamma^2)(1 - 0.282\, x^{3/4}) - 0.0485 \sin \frac{4\pi x}{\lambda} \cdot F(\tilde{r}) \ .$$

The dimensionless time-average stream function was calculated for this combination of values, and the results are shown in Figure 20. This combination of parameters and variables is considered to be the most favorable to demonstrate any induced secondary flow for the experiments conducted. As evidenced by Figure 20, the condensation process dominates the flow situation and no significant regions of sound induced

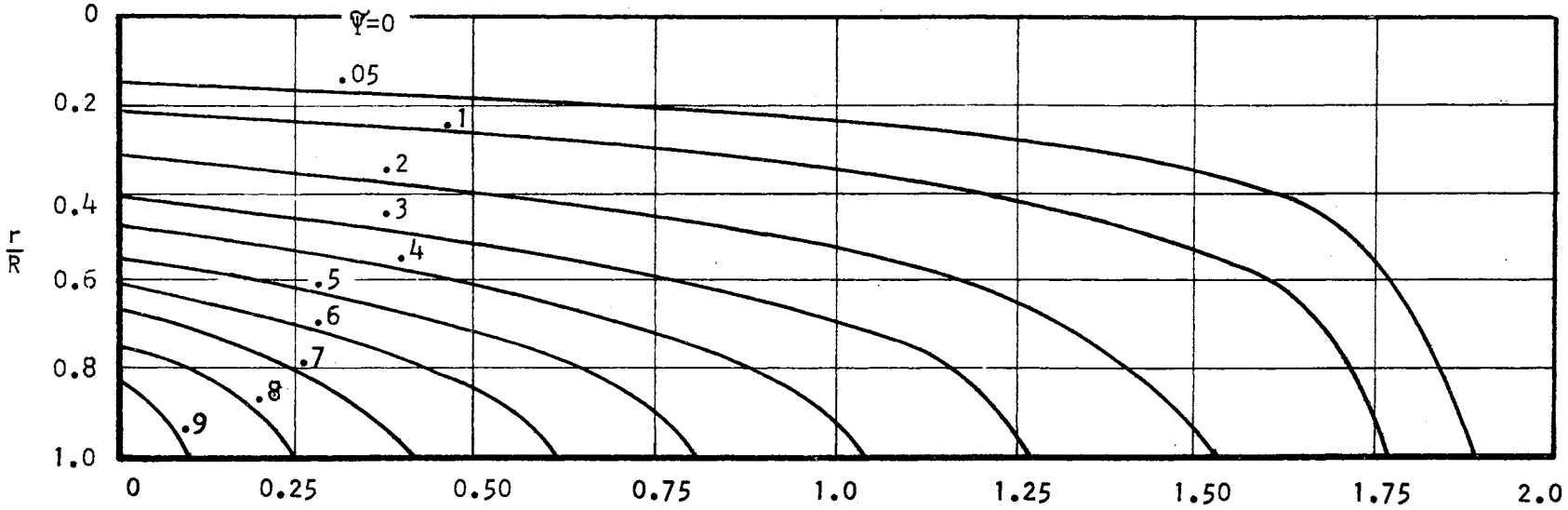

Figure 20. Dimensionless Time-Average Stream Function for a Resonant Sound Field Superimposed on a Condensing Vapor, as Predicted by Equation 3.71.

secondary flow exist. The value of M/M_o^2 for the case under consideration is 5.16 at the inlet and comparison of the results depicted by Figure 20 with the results of Purdy et al. (43), as shown in Figures 10 and 12, reveals the overriding effect of the condensation process.

The primary mechanism whereby the resonant sound field can alter the condensation rate has been assumed to be an alteration in the liquid condensate thickness resulting from induced secondary flow in the vapor. This simplified condensing vapor model was proposed to determine the conditions which would favor sound induced secondary vapor flow. These have been noted. If a back-flow vortex pattern similar to that shown in Figure 10 did exist in the vapor, then the possibility of increasing the heat transfer rate would depend upon the liquid condensate becoming turbulent up-stream of the transition point without sound.

The results from the two simplified models proposed indicate that the effect of a resonant sound field on condensation heat transfer is not significant for the conditions considered. The simplified liquid condensate model predicts a decrease in the heat transfer coefficient for tube lengths greater than 2λ. The simplified condensing vapor model shows that the through flow vapor velocity and the sound intensity are the most significant parameters influencing the region of sound induced secondary flow. The most significant fluid properties which would favor an effect are low values of h_{fg} and a. No significant effect was evident for the case considered.

The approach with the two simplified models which have been proposed has been to assume the solution for either the vapor governing equations or for the liquid condensate governing equations, thereby

establishing the liquid-vapor interface boundary conditions for the other set of equations. The results of these simplified models have not demonstrated that significant effects would be expected from superimposing a resonant sound field on the condensing vapor flow. Consequently, attempts to solve both sets of equations simultaneously with the time and position dependent liquid-vapor interface coupling boundary condition were not pursued.

One aspect of this problem which has not been explored is the possible effect of the condensing process on the sound field. The time dependent sound pressure fluctuations are assumed to be imposed upon the incoming vapor and propagated by the vapor in the axial direction. If the molecules which condense are considered to possess sound energy, then the removal of these particles by the condensation process should reduce the amount of sound energy (and intensity) propagated. If this is a correct assessment of the physical situation, then the effect of imposing a sound field on condensing vapor would be even less than that predicted by the proposed models.

CHAPTER IV

EXPERIMENTAL INVESTIGATIONS

Theoretical and experimental results reported in the literature indicate that condensation heat transfer rate is governed predominantly by the ratio of the condensate thermal conductivity to film thickness, when the film flow is laminar. If the condensate film flow is turbulent, the condensation heat transfer rate is related to the thickness of the laminar sublayer. Improvement in the rate of condensation heat transfer can generally be traced to a decreased thickness of condensate which experiences laminar flow. The experiments which have been conducted were designed to determine the parameters which are required to determine the effect of a vapor-borne resonant sound field on condensation heat transfer rate.

Several of the experiments conducted were exploratory in nature and yielded only qualitative results. These exploratory type experiments are presented solely as background information with some discussion of the qualitative results obtained.

Exploratory Experiments

Experiment to Determine the Feasibility of Coupling a Sound System with a Condensing System.

A flat-plate siren was used as a sound generating device in the experiments reported by Matthewson and Smith (38). Although the siren has the capability of generating high intensity sound, the intensity is dependent upon the vapor flow rate and the frequency range is somewhat limited. The use of commercially available electronically generated sound system was considered advantageous for the following reasons: (1) A wide frequency range capability. (2) A wide intensity range capability. (3) A capability of generating various pressure waveforms. (4) In event of a component failure, replacement parts would be readily obtainable. (5) The horn driver units were the only components which would need to be bought.

Water was selected as the condensing fluid due to the wealth of information available on its properties and results from various condensing situations. The saturation temperature ($212^{\circ}F$) of water at normal atmospheric pressure is considerably above the design conditions for commercially available horn-driver units. One problem encountered is that the driving coils located on the horn diaphragm dissipates, as heat, about 80 percent of the energy required to drive the horn unit; consequently, the coils will reach temperatures well above $212^{\circ}F$ when coupled with steam at atmospheric pressure. Another problem is that the characteristic acoustical impedance (ρa) of saturated steam at 1 atmosphere pressure is about 0.67 times ρa of air at standard

temperature ($70^{o}F$) and pressure (1 atm.). This impedance difference from that of the driver unit design condition could appreciably alter the amount of acoustical power transmitted to the vapor. In order to determine the magnitude of the difficulties noted above, an experiment was conducted.

The apparatus arrangement for this experiment is shown schematically in Figure 21. The boiler was electrically heated by a 3.75 KW heater composed of three elements. The power supplied to the boiler was controlled by a powerstat. Due to the physical size and shape of the boiler, the vapor which was generated emerged with time-dependent pressure pulsation. Since the experiment was undertaken to study the effect of sound on condensation, the pulsation of the vapor flow from the boiler was an undesirable characteristic. To correct this situation a baffled pulsation damping tank was constructed and installed between the boiler and test condenser. The pulsations in flow of the vapor to the test condenser were negligible after this modification.

The vertical test section was constructed from 3/4 galvanized steel pipe with a 1/4 inch stainless steel tube positioned in the center. A stainless steel annulus plug with a 0.339 inch diameter hole in the center was press fitted in the 3/4 inch pipe at the lower end of the test section. The purpose of the plug was to serve as a surface to partially reflect the sound waves, and yet allow the condensate to flow out of the condenser to be collected. This arrangement left an annular space immediately below the test condenser in which the condensate could accumulate and flow out into a condensate

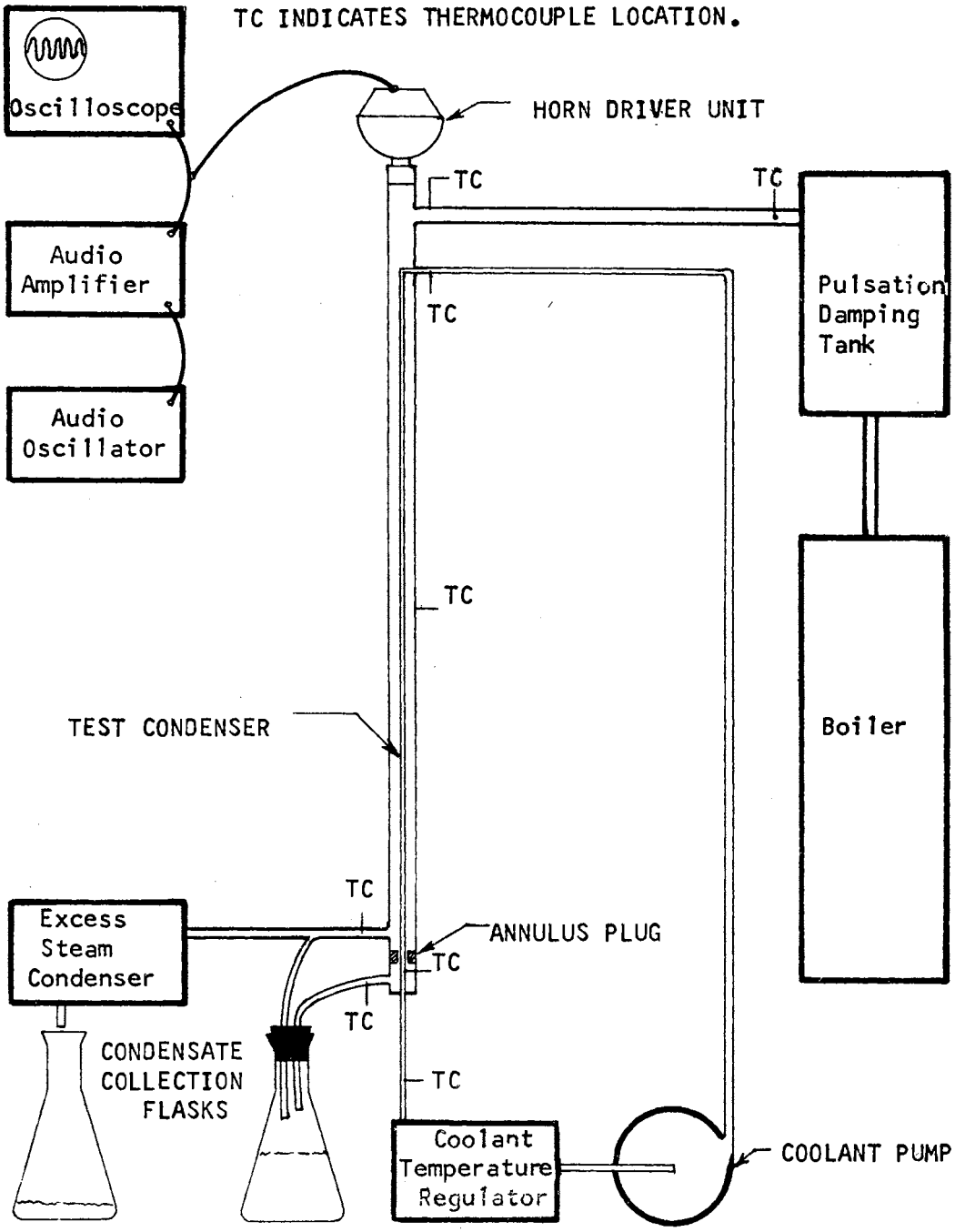

Figure 21. Schematic Diagram of Experiment to Determine the Feasibility of Coupling a Sound System with a Condensing System.

collection flask. The boiler, pulsation damping tank and test condenser were covered with 1 inch thick fiber glass insulation.

The excess steam which was not condensed in the test condenser flowed out through a tee connection 3 inches above the top of the annulus plug. This excess steam was piped to an auxiliary condenser, condensed, and collected in a flask.

The temperature of the coolant water was controlled by circulating the coolant water, with a pump, through a coolant temperature regulator. This regulator was equipped with a variable (0 - 2KW) electric heater to bring the coolant up to the desired operating temperature, then the heater was turned off and a flow of city water was mixed with the coolant water to hold the coolant temperature at the specified level. The total water level was maintained by an overflow drain. The inlet coolant temperature was maintained at the desired value by regulating the flow of city water which was mixed with the coolant water. This arrangement for controlling the inlet temperature of the coolant worked satisfactorily.

The line connecting the condensation collection flask to the excess steam line was provided in an effort to obtain system pressure in the condensate collection flask. The first arrangement designed to establish system pressure in the condensation collection flask provided for a line connecting the flask to the upper portion of the accumulation section of the test condenser (physically, just below the plug in the annulus). The undesirable result was that whenever the stopper with the condensate line and pressure equalizing line was removed from the condensate collection flask, a sudden flow of condensate occurred.

Several physical arrangements were tried and the final arrangement (as shown in Figure 21) seemed to work best, with no sudden flow of condensate occurring when the stopper was removed.

Copper-constantan thermocouples were clamped to the surface of the coolant tube at entrance and exit from the test condenser. An iron-constantan thermocouple was positioned such that the steam leaving the damping tank flowed across it. Copper-constantan thermocouples were attached to the outer wall of the inlet steam pipe, the condenser test section steam pipe, and the outlet steam pipe. A copper-constantan thermocouple was installed so that the condensate leaving the test condenser flowed over it. The readings from this last thermocouple fluctuated quite a bit, even under steady-state conditions, indicating that the thermocouple was not installed properly.

Knowing the condition of the steam at the inlet to the test section and measuring the amount of condensate that occurs in the test section allows the heat transfer rate (Q) to be estimated as the mass condensation rate Γ_c multiplied by the difference in enthalpy of the incoming steam and the collected condensate $(h_i - h_c)$. Since the average difference in temperature (ΔT) between the vapor and the condensing surface (with area A) can be measured with the thermocouples, then the average condensing heat transfer coefficient ($\bar{h}$) can be calculated:
$\bar{h} = Q/(A\Delta T) = \Gamma_c(h_i - h_c)/(A\Delta T)$.

The sound was imposed upon the vapor in an axial direction by a 60 watt horn driver unit (University Sound, Model 60T). The horn driver unit was connected directly to the 3/4 inch pipe of the test condenser with an adapter. The power to the driver unit was supplied by coupling

an audio oscillator with a 30 watt audio amplifier. The input voltage to the horn driver unit was monitored on an oscilloscope to insure that the sinusoidal wave pattern was not distorted. The apparent resonant condition was noted to yield peak voltage input, so that the approximate point of resonance could be detected from the oscilloscope display of the input to the driver unit.

A number of operating conditions involved in utilizing a horn driver unit in this experiment are detrimental to the driver unit. At atmospheric pressure the saturation temperature of the steam is 212 ^{o}F which is well above the temperature which the driver unit was designed to operate. To alleviate this problem, several 1 inch diameter holes were drilled in the back of the driver unit body so that the unit could be air cooled. A blower continuously forced air through the back side of the driver unit while the test condenser was being used (for tests with and without sound). The driver unit has a phenolic and fiber structure diaphragm, and after approximately 25 hours of use, no detrimental effects on the diaphragm were observed from a visual inspection. The driver unit specifications indicate that the unit is capable of 60 watts continuous duty operation if integrated program material is used. Operation at high intensities, high temperature and constant frequency is suspected as being the reason for a failure of the diaphragm after 30 hours of operation. The particular mode of failure was that the coil support became separated from the diaphragm, apparently due to excessive driving force.

At the time of operation, a suitable pressure transducer was not available to measure the actual sound pressure generated. The horn

driver unit was normally operated at the highest undistorted input available from the oscillator and amplifier, for a given resonant frequency condition.

A complete set of heat transfer and sound data was not obtained from this experiment. Collection of condensate from the test condenser for a measured period of time for steady-state conditions without sound and with the resonant sound field imposed upon the vapor indicated only modest increase in the heat transfer rate. The maximum increase observed was approximately 30 percent. No trend in this limited data was observable, and several considerations (quite unrelated to the effect of a vapor-borne resonant sound field on condensation heat transfer) peculiar to the physical arrangement would account for the observed increase. Among these considerations are: (1) The diaphragm was air-cooled on the back side; consequently, condensation would be expected to occur on the vapor side of the diaphragm. However, when a resonant sound field was imposed on the vapor, the diaphragm then acted as a moving wall on which condensation occurred. (2) The condensate formed in the test section flowed, due to gravitational attraction, through a 1 inch long annular space with 1/4 inch I. D. and 0.339 inch O. D. If the condensate wetted both the inside and outside walls of the annular space, then some condensate might accumulate in the bottom of the test section rather than in the accumulator. This may have caused the fluctuations of the condensate temperature thermocouple readings noted earlier. The effect of the resonant sound field may have been to pump the condensate into the condensate collection flask.

The difficulty with this experimental configuration was that too many unknown parameters existed, which further instrumentation could

not easily overcome. Modifications of this apparatus to achieve a more complete set of data was not judged to be worth the effort required due to a number of deficiencies. The significant positive information obtained from this experiment was that the horn driver unit could be effectively sealed so that air leaks into the system would not occur, and the diaphragms could withstand the adverse operating conditions for a useful period of time. The feasibility of coupling a commercially available sound system with a condensing system was established.

Since the primary objective of this work was to determine the parameters which influence condensation heat transfer when acoustic pressure pulsations are imposed upon the condensing vapor, it was felt that a visual observation of the liquid condensate film would be advantageous. The following experiments reflected this thought, since all permitted visual observation.

Experiment to Determine the Possible Effect of Vapor-Borne Sound on a Vertical Liquid Film Flow.

The works of Howartson (18) and Barfield (2), as reviewed in Chapter II, show that a resonant air-borne sound field can cause liquid to be ejected from a thin horizontal layer of liquid. The purpose of this experiment was to determine if a similar phenomenon occurs for a thin liquid film flowing down a vertical surface.

The apparatus arrangement for this experiment is shown schematically in Figure 22. The sound generating system was composed of two 75 watt horn driver units (University Sound, Model ID-75), a 75 watt audio amplifier (McIntosh 75) and an audio oscillator (Hewlett-Parkard,

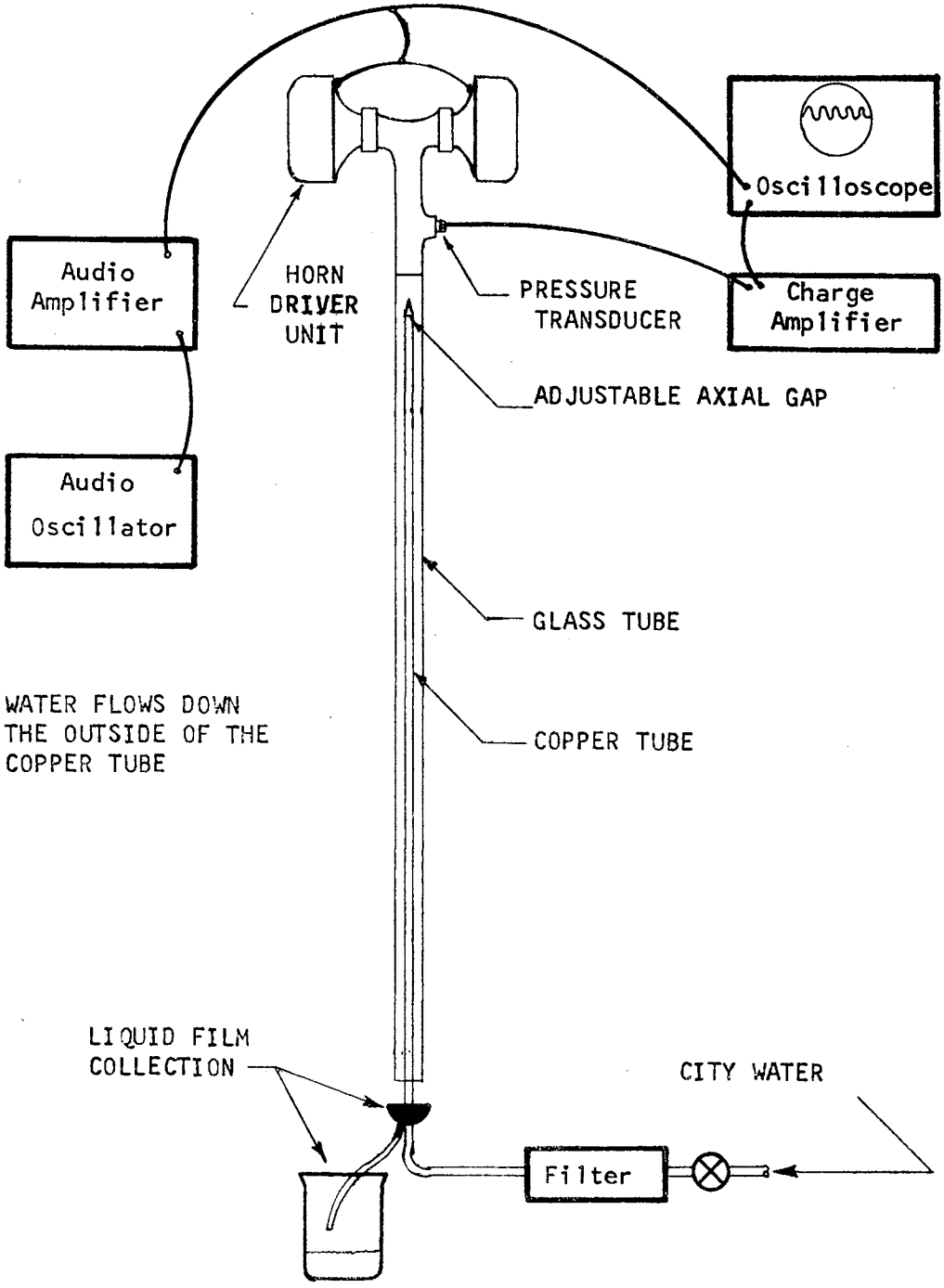

Figure 22. Schematic Diagram of Experiment to Explore the Effect of Vapor-Borne Sound on Vertical Liquid Film Flow.

Model 200-CD). A pressure transducer (Kistler, Model 606L), a Kistler charge amplifier and an oscilloscope (Tektronix, Type 502) were used to determine the amplitude of the sinusoidal pressure wave which was generated. The inside diameter of the glass tube was 1 inch and the outside diameter of the copper tube was ½ inch. Water flowed inside the copper tube to the top where it then flowed out through a small, adjustable, axial gap and down the outside of the copper tube in a thin film.

The experimental procedure was to establish film flow along the length of the copper tube, then decrease the flow rate to obtain a desired film thickness. With a thin film liquid flow established, a resonant sound field was generated in the air in the annulus space. Visual observations revealed that high enough sound intensity could be generated to cause ejection of liquid from the thin film. The ejection sites appeared to occur at half-wavelength locations corresponding to the acoustic pressure nodes (acoustic velocity anti-nodes). The ejection sites were not all simultaneously active. An ejection site would occur close to the first acoustic pressure node when the liquid film was present. This appeared to remain active until the inflow of liquid was insufficient to support the ejection mechanism, at which time the first ejection site would cease and an ejection site 1/2 wavelength further down the tube would be activated. This cessation and activation of sites would proceed in succession of 1/2 wavelength ejection sites all the way down the four foot length of the annular region. After exhausting the last ejection site, the first ejection site would normally be reactivated almost immediately. Occasionally, an ejection site would be skipped in the progression of the ejection phenomena from

one pressure node to the next. A noticeable "blowing" effect was observed when the ejection mechanism occurred at the lower end of the tube, with drops of water being thrown in many directions.

No further attempts were made to obtain quantitative data from this experiment. At this point it appeared that the vapor-borne sound could cause the average film thickness to be decreased. If this ejection effect occurred in a condensing system, then it is reasonable to expect that the heat transfer rate would be appreciably affected.

In addition to the visual observation of a possible mechanism whereby sound might affect the condensation heat transfer rate, the pressure transducer proved to be capable of yielding reliable pressure measurements at the acoustic pressures under consideration. During this series of experiments, the first failure in attempting to utilize a membrane between the sound generating region and the region of interest was experienced. A latex rubber membrane was stretched across the outer tube just below the horn coupler. Considerable vibration from the excited membrane was superimposed on the sinusoidal pressure wave, as was observable from the resulting distorted sinusoidal pressure wave form displayed on the oscilloscope.

The membrane was desirable since it would allow the horn driver unit to operate under favorable conditions, and thereby improve the life of the horn and reduce the effect of the additional surface area in the condensing test section. Further evaluation of the latex rubber membrane revealed that it would not withstand the steam temperature and acoustic pressure requirements. Attempts to use a thin teflon membrane were pursued in the exploratory experiment described in the following section.

Condensation in a Helmholtz Resonator.

An acoustic Helmholtz resonator can be described as a cavity (with volume V_c) with a neck opening of length ℓ_n and radius r_n. If a sinusoidal pressure (time-wise) is exerted on the opening such that the acoustic wavelength is much less than any system dimension, then the acoustic system can be mathematically modeled as lumped parameters. The mass of gas in the neck opening is assumed to move as a unit, with the pressure of the gas in the cavity being alternately compressed and expanded by the influx and efflux of gass through the opening. The gas in the cavity is thus considered to provide the system stiffness. At the opening, sound is radiated into the surrounding medium, and thereby causes a dissipation of the acoustical energy in the cavity. Viscous dissipation is neglected.

A complete presentation of the Helmholtz resonator, derivation of acoustical equations and limitations of the analytical results are presented by Kinsler and Frey (26). One result of interest in this experimental design was the natural frequency of the Helmholtz resonator, which is:

$$f_o = \frac{ar_n}{2}\sqrt{\frac{1}{V_c(\ell_n + 0.85r_n)}} \qquad (4.1)$$

The basic motivation for conducting this experiment was to obtain a uniform acoustic pressure variation throughout the cavity containing the condensing vapor. From this experiment the effect of sound pressure variation on the condensing vapor could be determined without the presence of the ejection of liquid mechanism. The vapor inlet ports to the test section were designed to have a very large acoustical inertiance, and the cavity was then treated as though it behaved acoustically

as a Helmholtz resonator. The neck opening which connected the cavity to the acoustical transmission tube was 0.1 inch radius by 1 inch length. The calculated natural frequency of this assumed Helmholtz resonator is 445 Hz. The system was designed to operate acoustically as though the Helmholtz resonator were a side branch of the tube transmitting acoustic energy.

The cavity was a sight glass modified to allow pressure and temperature measurements to be made. A pressure transducer (Kistler Model 606L) and a film chromel- constantan thermocouple (Heat Technology Lab Model No. TCS - 102 - ChC) were used in an attempt to measure the acoustic pressure and temperature variations in the cavity. Copper-constantan thermocouples were installed to measure the coolant temperature at the condenser section inlet and outlet, the condensate temperature, and the vapor temperature in the cavity. Provisions were made to measure the mass flow rate of the coolant, the mass flow rate of the condensate, and the cavity pressure. A heat exchanger was constructed to allow control of the inlet coolant temperature. A schematic diagram of this experiment is shown in Figure 23.

Any observed difference in the heat transfer rate for steady-state operation with sound and without sound would be attributable to an increase (or decrease) in the time-average condensation driving force. If thermodynamic equilibrum for the states constituting the sound pressure fluctuation process is a valid description, then this effect will be quite small. From Nusselt's theory, the heat transfer coefficient is proportional to the 1/4 power of the difference between the saturated vapor temperature and the wall temperature (i.e., $h \propto (\Delta T)^{1/4}$).

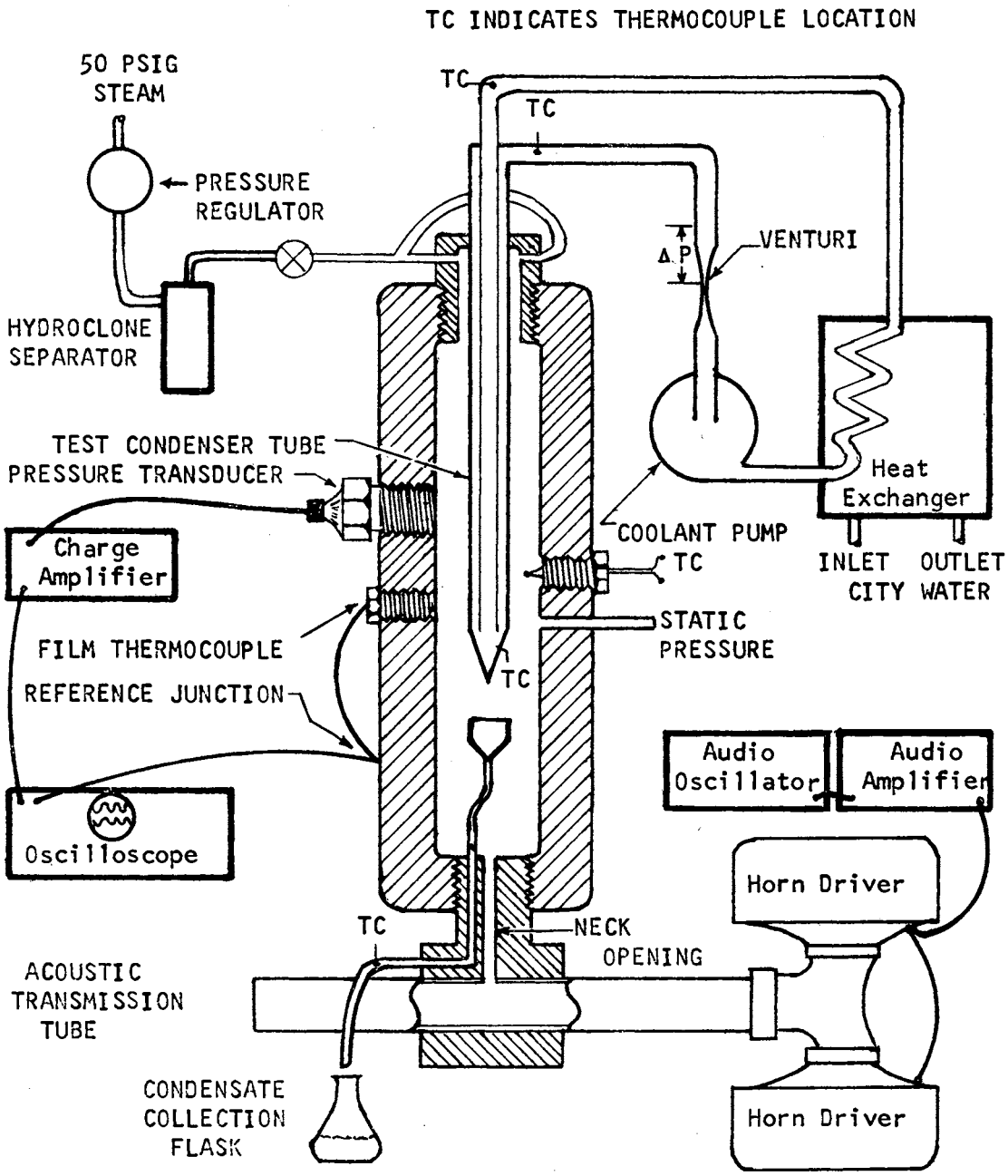

Figure 23. Schematic Representation of Experiment Involving Condensation in a Helmholtz Resonator.

Whether one considers the sound pressure variation to occur isentropically or as a saturated liquid-vapor system (Clausius-Clapeyron Relationship), the time-average temperature difference deviates from a constant value by an extremely small amount. If imposing a uniform pressure variation on the vapor resulted in a time-average change in the condensation heat transfer rate, then one would be led to investigate the rates of the condensation and evaporation processes in more detail.

No results were obtained from this experimental arrangement. Attempts to utilize a teflon membrane (.003 inch thickness) indicated that a significant reduction in the transmission tube sound level resulted. Removal of the membrane still did not allow a measurable sound pressure to be acheived in the cavity. Dropwise condensation occurred on the 1/4 inch condenser tube and persisted for an extended period of time (about 2 hours). The results did not permit an evaluation of the film thermocouple response time. Apparently the high flow rate of vapor into the cavity eliminated the expected Helmholtz resonator type acoustic behavior. Since it was estimated that results from this possible mechanism for sound to affect condensation heat transfer were an order of magnitude less than those of the ejection mode, further attempts to investigate condensation in a Helmholtz resonator were abandoned. The efforts in the later experiments were directed toward obtaining more information about the liquid ejection mechanism.

Experiments to Determine the Effect of a Vapor-Borne Resonant Sound Field on Filmwise Condensation of Steam

Two experimental configurations were used to determine the effect of a vapor-borne resonant sound field on filmwise condensation heat transfer. Both configurations employed a vertically oriented glass tube, with condensation occurring on the inside walls. The configurations were basically the same, with the minor differences between them representing attempts to increase the sound intensity.

A schematic diagram of experimental configuration A is shown in Figure 24. The sound pressure generation system is composed of two horn driver units (University Sound, Model ID 75), two McIntosh 75 Audio amplifiers, and a wide range audio oscillator (Hewlett-Packard, Model 200 CD). The acoustic pressure measurement included a Kistler pressure transducer (Model 606L), a Kistler charge amplifier and a Tektronix Dual-beam Oscilloscope (Type 502). The oscilloscope display of the acoustic pressure trace was recorded with an Oscilloscope Polaroid camera. All thermocouples were copper-constantan, with an ice point reference junction. The vapor pressure was measured with a Statham pressure transducer (Model PA707 TC-15-350), with the input voltage to the strain-gage resistance bridge supplied by a Harrison Laboratories Power Supply (Model 865C). The outputs of the thermocouples and the Statham pressure transducer were read with a digital voltmeter (Non-Linear Systems, Series 2900, Model 29175) to $\pm$.002 millivolts. The coolant mass flow rate was determined with a venturi tube. Calibration curves from the Statham pressure transducer and the venturi

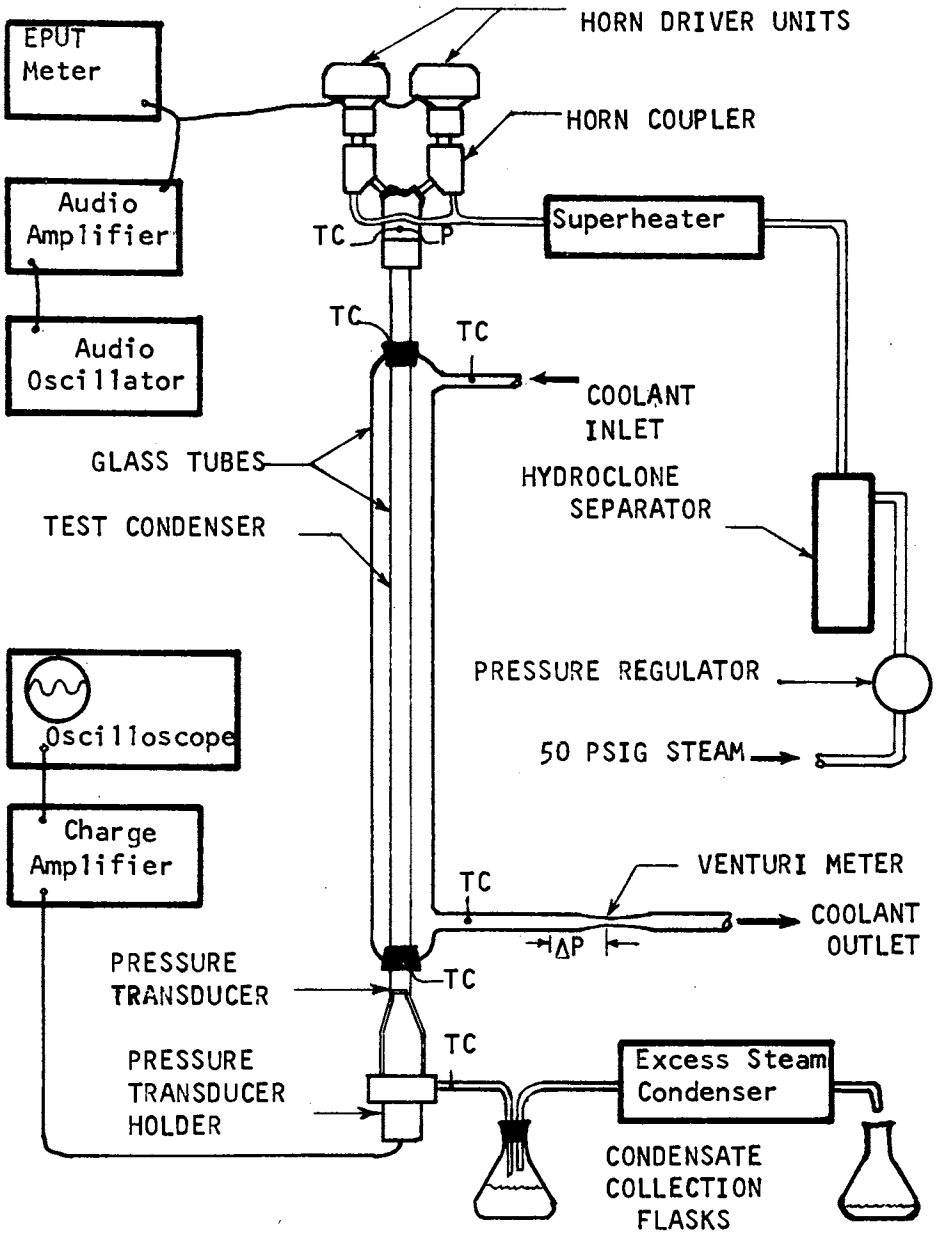

TC INDICATES THERMOCOUPLE LOCATION
P INDICATES STATIC PRESSURE MEASUREMENT LOCATION

Figure 24. Schematic Diagram of Experiment to Determine the Effect of a Vapor-Borne Resonant Sound Field on Condensation.

tube are presented in Appendix C. The test section condensate and the excess vapor condenser condensate was collected in flasks for a measured period of time and weighed. The time period of condensate collection was measured with a Standard Timer which could be read to $\pm$.0002 minutes, and the collected condensate was weighed on a Harvard Trip Balance with an estimated accuracy of $\pm$.025 grams. An EPUT Meter (Beckman/Berkley, Model 5210D) was used to measure the frequency of the audio amplifier output.

The earlier exploratory experiments indicated that significantly better acoustic coupling occurred without a membrane installed to separate the sound generation and condensing sections. Consequently, the horn driver units were modified for exposure to the vapor condensing system. RTV silicone rubber was used to seal around the diaphragm to prevent air leakage into the condensing section, or vapor leakage into the back cavity of the horn driver unit. Water circulating copper coils and forced air cooling lines were installed in the back cavity of the horn driver units to provide some cooling, and thereby prolong the life of the horn palate diaphragm. The cooling became necessary when the average lifetime of the palate diaphragm unit was found to be approximately one hour without the cooling effect. The palate diaphragm failures observed were, in most cases, the result of overheating of the electrical coil insulation.

Since the horn driver units were exposed to steam, a vertical position for the driver units was required to avoid collection of condensate in the driver units. To accomplish this, a horn coupler was constructed. The details are shown in Figure 25. The incoming vapor

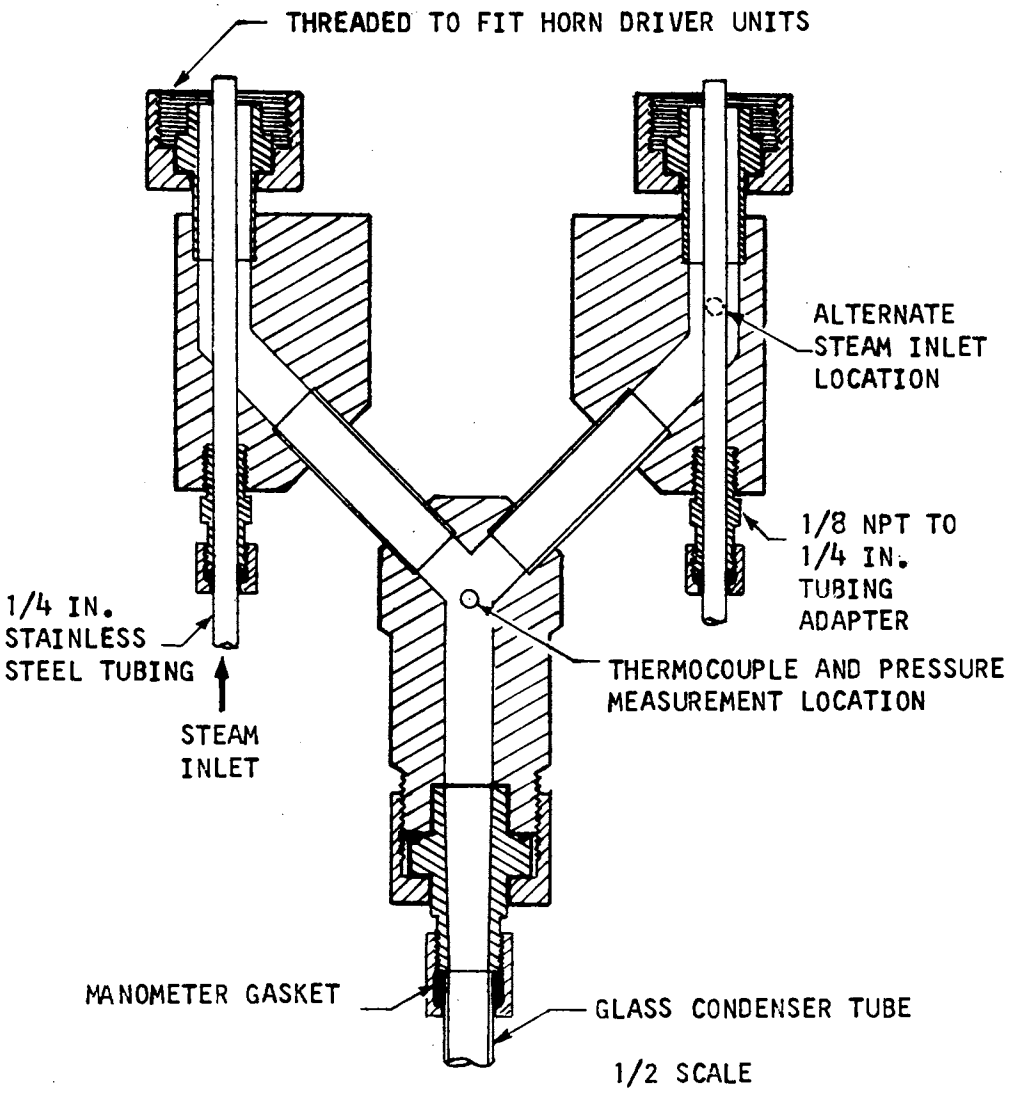

Figure 25. Horn Coupler for Steam Condensation Experiments.

was ported directly into the horn driver compression and expansion region, with the palate diaphragm assembly modified to receive the projecting steam inlet tube. The alternate steam inlet ports were used in experimental configuration B.

The supply steam line, hydroclone separator, superheater, lower portion of the horn driver unit, horn coupler and all connecting lines between the steam line and test condenser were insulated with 1 inch thick fiber glass insulation.

The test condenser for experimental configuration A was a 300MM Sargeant glass condenser. The only modification made to this commercial laboratory-type condenser was to cut the glass condenser tube normal to its axis with a diamond saw, and to fire-polish the cut to achieve a square end. The acoustic pressure transducer holder was machined to have a contour approximately the same as that of the flared end of the glass test condenser. A representation of the lower part of the test condenser, including the acoustic pressure holder and condensate temperature thermocouple, is shown in Figure 24. The advantage of this lower test section design was that the flow of condensate about the transducer could be observed. Particularly interesting was the possible effect of a layer of liquid on the acoustic pressure transducer surface, and the possible effect of acoustic pressure variations on the flow of liquid in this confined region between the pressure transducer holder and the flared portion of the condenser.

The procedure employed with experimental configuration A is outlined below. The power to all electrical units was turned on to allow stabilization to be achieved before a test was begun. The 50 psig

supply steam line was warmed up by allowing steam to flow through the hydroclone separator and auxiliary condenser for about 30 minutes. Steam was then allowed to enter the test condenser. The rate of steam admission to the test condenser was controlled with the pressure regulator adjustment, the test condenser valve, and the auxiliary condenser valve. A moderate throttling process was desired across the steam inlet valve to allow a slightly superheated steam to enter the superheater. However, the inlet vapor temperature, as measured by a thermocouple installed in the horn coupler, never indicated that more than several degrees superheat was attained.

After steady-state operating conditions were established, as determined from periodic readings of the thermocouple and pressure transducer output, a test would be inaugurated. The normal procedure was to collect the condensate from the test condenser and from the excess condenser for a measured time period, and weigh the condensate collected. During the collection period, readings from the instrumentation devices were obtained at approximately 2 minute intervals and averaged for the entire collection period. The interval readings were very consistent over the collection period. Tests were conducted for the same steam admission rate with no sound, and with maximum sound pressure level for several of the harmonic resonant frequencies. The harmonic resonant frequency was determined by operating the sound generation system at a reduced level, and varying the oscillator frequency until a maximum sound pressure level was indicated from observation of the oscilloscope display of the sound pressure transducer output. The maximum sound pressure level was obtained by increasing the power input to the horn driver units to a level just below that causing distortion of the

sinusoidal voltage input wave. This was determined by displaying the voltage from the amplifier output terminals, (along with the pressure trace) on the oscilloscope. The input voltage to the two horn driver units was balanced by use of the oscilloscope dual input feature.

The experimental configuration A employed 16 ohm horn driver units. Even with cooling, the horn palate diaphragm life-time was much shorter than desired. The life-time of the horn palate diaphragm ranged from one minute to approximately 10 hours for the University Sound Model ID 75 horn driver units. Consultation with factory representatives did little to alleviate this problem. One suggestion they offered as the cause of the numerous failures was that the horns were not acoustically coupled. Although the horn driver units coupled well with air in the same physical system, perhaps the characteristic acoustic impedance of steam was low enough (as previously noted) to account for the "non-loading" of the horn driver unit. It was noted that the maximum sound pressure obtained with steam was approximately 1/3 of that for air in the same physical system. Differences in flow field and acoustic impedance for the two media obviously exist, but the expected reduction in maximum sound pressure was approximately half the magnitude observed. No satisfactory method was found to overcome this difficulty, although experimental configuration B was an attempt to increase the maximum attainable sound pressure.

Difficulty in obtaining the standard 16 ohm palate diaphragm assemblies for the horn driver units, and the above mentioned horn driver units led to the decision to use 8 ohm palate diaphragm assemblies. This was of no consequence electronically, since the McIntosh 75

amplifiers are equipped with multiple output impedance terminals to facilitate impedance matching. It was felt that the overall mechanical impedance offered by the steam atmosphere might couple better with the 8 ohm electrical impedance. These 8 ohm palate diaphram assemblies were used in experimental configuration B.

A photograph of the test section used in experimental configuration B is shown in Figure 26. Additional changes between experimental configuration A and B are: (a) The alternate steam admission ports (shown in Figure 25) were used, with the other inlet ports sealed flush with the interior walls of the coupler. (b) The horn driver units were not cooled due to the amount of condensation occurring in the horn section as evidenced from experimental configuration A results. (c) A different condenser tube and lower section were used, since no unusual flow conditions were observed to occur in experimental configuration A. A photograph of the test facility, with experimental configuration B, is shown in Figure 27.

The test procedure for experimental configuration B was essentially the same as that for experimental configuration A, with the exception of the duration of the tests with sound. Due to previous experiences with diaphragm failures, and since cooling of the diaphragm coil was not provided, the duration of the tests with sound were limited to approximately 4 to 10 minutes. The output of the thermocouples which indicated the coolant inlet and outlet temperatures was monitored with a digital voltmeter during the period of operation with a given sound frequency. Any change in the heat transfer rate would cause a change in the coolant temperature rise, with the constant coolant mass flow

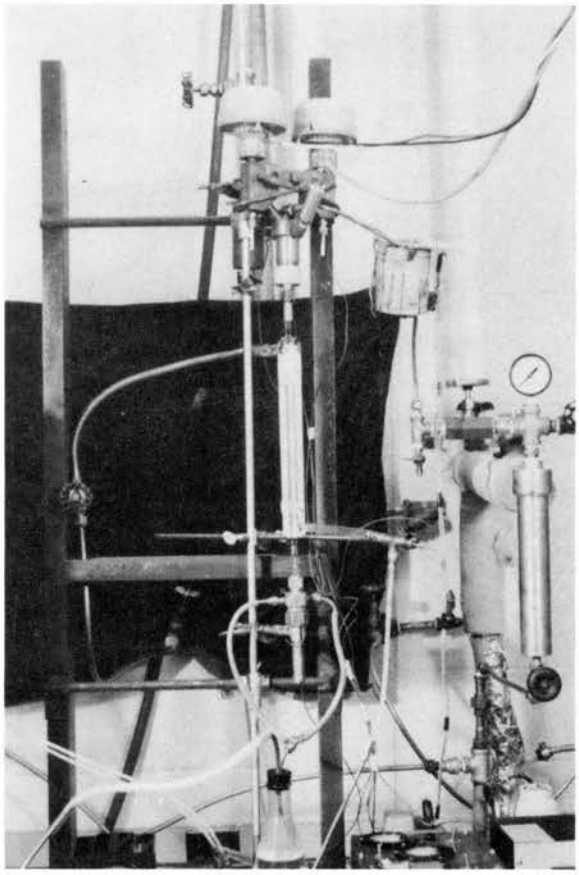

Figure 26. Experimental Configuration B Used in the Effect of Sound on Condensation Heat Transfer Experiments.

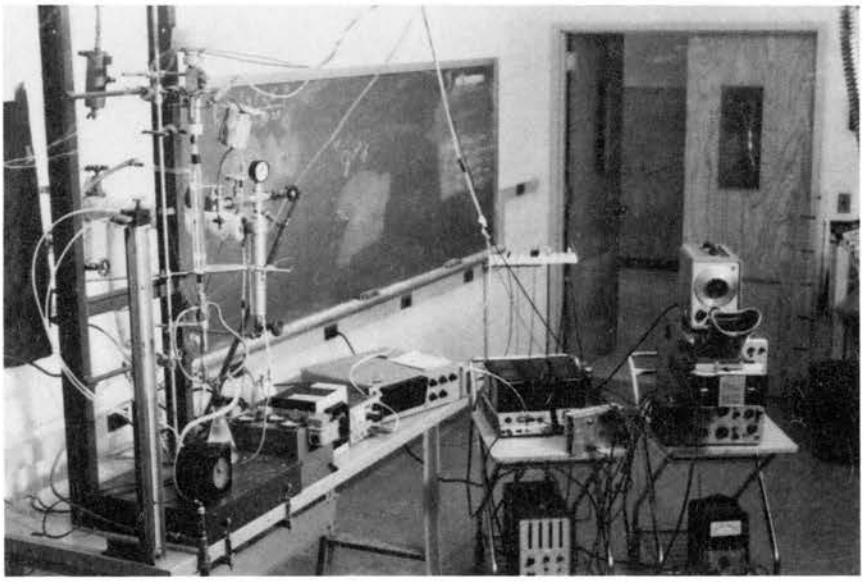

Figure 27. Overall View of the Test Facility with Experimental Configuration B in Place.

rate condition. Using this technique, tests for three different steam admission rates with two or three different frequencies each were conducted in a total time of 1 hour and 7 minutes, which was the lifetime of the diaphragms.

The condensate was collected for the entire duration of a given steam admission rate test. Thus, the condensate heat transfer rate results reflect an average value for a given steam admission rate for all frequencies considered. Results of the experimental determination of the effect of a vapor-borne resonant sound field on filmwise condensation of steam are presented in Chapter V.

Experiments to Determine the Effect of an Air-Borne Resonant Sound Field on Thin-Film Water Flow on the Inside Wall of a Vertical Tube

An experimental investigation was conducted to gain some insight into the mechanism whereby a resonant sound field can cause liquid to be ejected from the surface of a thin-film of flowing liquid. In order to obtain a situation somewhat analogous to the condensation process, tests were conducted with no air through flow and then with different values of air flow rate--with a thin film of water flowing down the inside walls of a vertical glass tube. These tests were conducted with different sound levels and different water film flow rates. A photograph of the test section for this experiment is shown in Figure 28. A cross-section of the upper portion of the test assembly which provides for the inlet of water, the inlet of air, and coupling with the horn driver units, is shown in Figure 29. The lower section of the test assembly is the same section used in experimental configuration B for the condensation tests.

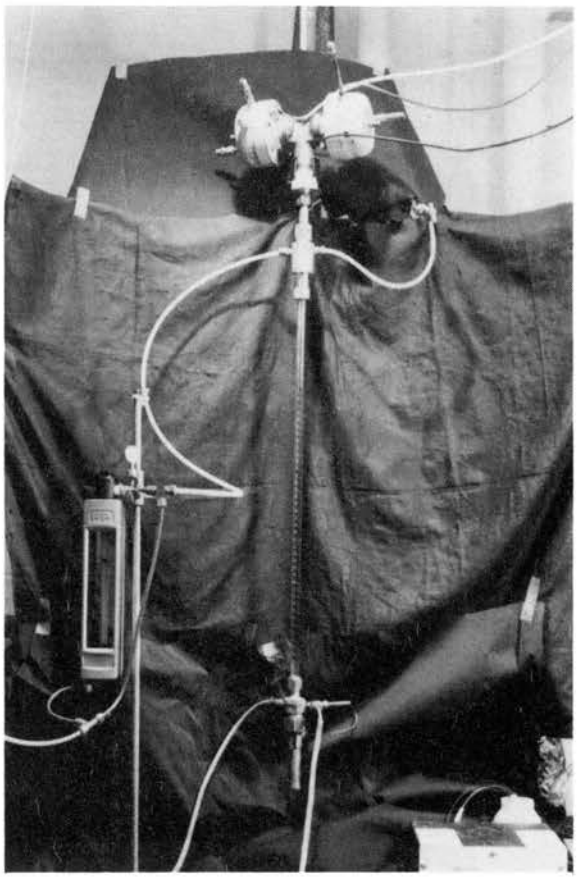

Figure 28. Test Section Used in Experiments to Determine the Effect of an Air-Borne Resonant Sound Field on Thin-Film Water Flow on the Inside Wall of a Vertical Tube.

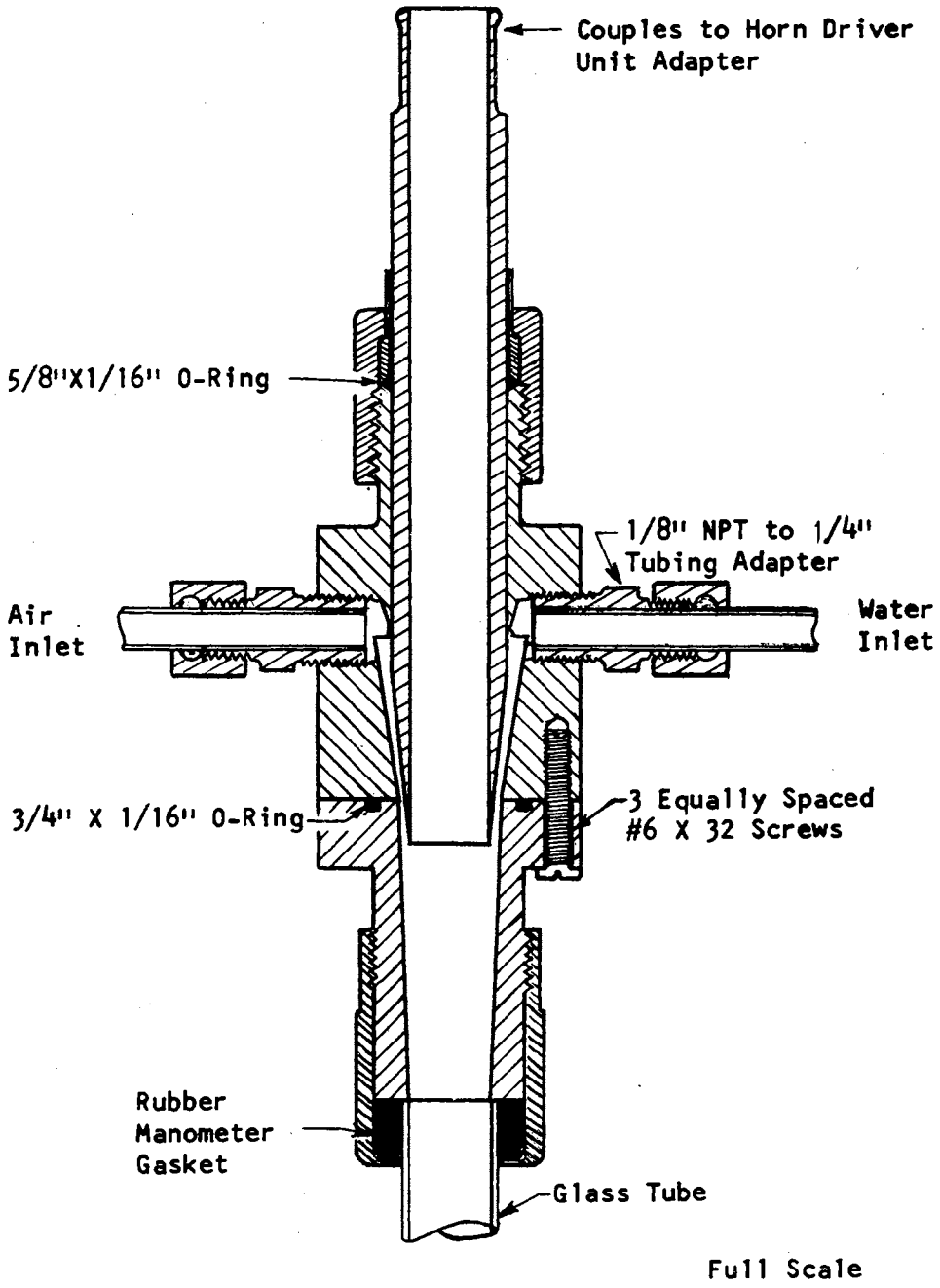

Figure 29. Water, Air and Sound Coupling Part Used in Experiments to Determine the Effect of Air-borne Sound on Thin-Film Water Flow on the Inside Wall of a Vertical Tube.

The water flow rate was regulated with an over-flow arrangement whereby a constant pressure head could be maintained on the inlet water line. The air flow rate was controlled with a pressure regulator on a 100 psig air supply line. The mass flow rate of the water film flow was obtained by collecting the water for a measured time period and weighing it. The air flow rate was measured with a flowrator. A calibration was performed for the flowrator and is presented in Appendix C. The outlet water temperature was measured with a copper-constantan thermocouple and a digital voltmeter. The acoustic pressure measurement was accomplished in the same manner as noted for the condensation tests.

The procedure for conducting this series of experiments was to establish a thin-film flow of water along the length of the inside walls of the vertical glass tube and then to adjust the water flow rate to obtain a desired value. With no air flow, a harmonic resonant frequency was selected. The sound pressure amplitude was then set at a constant value. The data was recorded and photographs (16 mm motion pictures and 35 mm still pictures) were taken of the interesting flow situations. The active ejection sites were noted, and visual observations of the flow situation were obtained. For a given water-film flow rate, air flow rate and resonant frequency--zero, low, moderate and high sound pressure levels were imposed upon the flow situation. These results are also presented in Chapter V.

CHAPTER V

RESULTS OF THE EXPERIMENTAL INVESTIGATIONS

The use of horn driver units as a means of generating a sound field in the vapor did not prove to be as effective nor as versatile as had been anticipated from the exploratory experiments. The maximum sound pressure amplitude (P_o) measured in the condensation heat transfer experiments was 0.5 psi. The range of frequencies for which a useful sound pressure level could be achieved was from 300 Hz to 1300 Hz for the steam vapor system. The maximum sound pressure amplitude experimentally achieved for a given harmonic resonant frequency was the value used in each experiment involving condensation heat transfer; these values are listed in Table 1. One particularly troublesome aspect of using the horn driver units in the condensation experiments was the short life of the horn driver palate diaphragm assemblies which resulted from the adverse operating conditions. The horn driver units were much more servicable and effective in the thin-film liquid vertical flow experiments.

The pressure transducer used to measure the sound pressure amplitude was satisfactory. The sound pressure amplitude measurement was achieved by photographing the oscilloscope display of the sound pressure transducer (coupled through a charge amplifier) output. A photograph of a typical pressure curve is shown in Figure 30. The heavy trace is

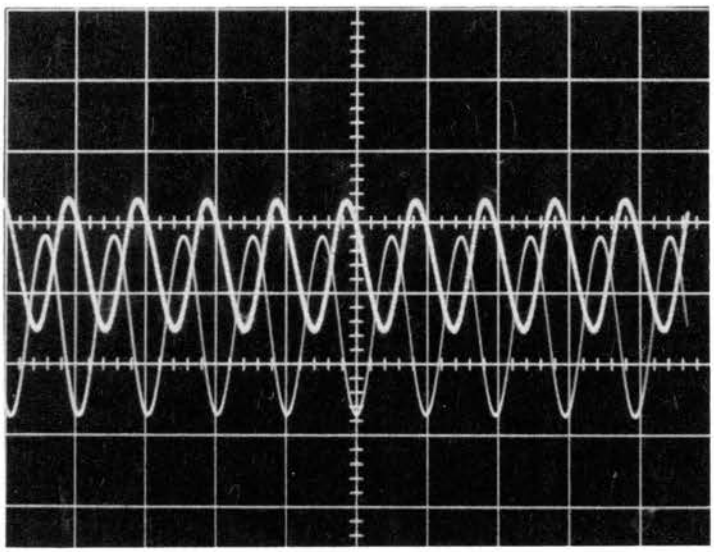

Figure 30. Oscilloscope Display of Acoustic Pressure and Voltage Input to the Horn Driver Units. Recorded During Experiment Number 8; Frequency=739 Hz.

the sound pressure curve. The oscilloscope scale is equal to 20 MV/cm and the pressure transducer output scale is equal to 100 MV/psi. The pressure amplitude (Po) is equal to 1/2 the peak to peak pressure difference represented by the curve and was measured as 0.25 psi for this case. The second trace shown in the photograph is the voltage input to one of the horn driver units. The oscilloscope scale was 20 V/cm for the horn driver voltage input curve. Although this voltage input was not used in calculating results, it was useful in determining the upper operating limit of the horn driver units. The horizontal time scale for the oscilloscope display is 1 Msec/cm. Each major grid division shown in Figure 30 corresponds to 1 cm on the oscilloscope grid.

It was desirable to experimentally determine the axial sound field description in the condensation heat transfer experiments. The physical constraints imposed upon the condensation experiments (and the size of available sound pressure transducers) did not permit a measurement of the axial sound pressure amplitude to be obtained. Future experiments involving the effect of sound on condensation heat transfer should include instrumentation to allow an accurate sound field description. This is required since the condensation process may modify the resonant sound field.

The test condenser was a water cooled cylinderical glass tube with a wall thickness of 0.050 inch and an inside diameter of 0.412 inch. The axis of the tube was vertical with condensation occurring on the inside walls. The glass tube was cooled for a length of 10-5/8 inches by water flowing through annulus region between the outer glass tube

jacket and the condensing tube. Pyrex glass has a thermal conductivity of approximately 0.6 BTU/hr·ft·°F and water has a thermal conductivity which varies monotonically from 0.347 to 0.394 BTU/hr·ft·°F over the temperature range of 70°F to 212°F. The maximum rise of the coolant was 3°F for the experiments conducted. An analysis of this test condenser indicated that the actual test conditions can be considered to closely approach a constant heat transfer coefficient situation rather than a constant wall temperature situation.

A prime consideration involved in the selection of the glass condenser tube and glass tube jacket was the desire to visually observe the condensate film. Since film condensation heat transfer rate is strongly dependent upon the film flow situation, it was felt that any effect of the vapor-borne sound field would be observable as an effect on the condensate film flow situation. The relatively low heat transfer rate was viewed as favorable to yielding an observable effect, since analytical considerations indicated that a low through flow is required to allow sound induced secondary time-average flow to be significant. Water has a very high latent heat of evaporation in comparison with most other organic fluids; consequently, water was not a good fluid choice to yield low vapor flow rates for a given condensing tube size. A complete documentation of all factors considered in selecting the test condenser, flow situation, sound generating equipment and instrumentation would only serve to emphasize that the experiments conducted represent a compromise between desired experiment criteria and economic (time, money and effort) realities.

Data Reduction for Experiments Involving Condensation Heat Transfer

The heat transfer rate for the condensation test section (Q) was considered to be the thermal energy absorbed by the coolant.

$$Q = \Gamma_c c_{p,c} \Delta T_c \tag{5.1}$$

The specific heat of the coolant ($c_{p,c}$) was assumed to have a value of 1.0 BTU/lbm^{o}F. The coolant flow rate Γ_c was determined from the venturi meter flow data and a calibration equation for the venturi meter which is presented in Appendix C. The coolant temperature rise (ΔT_c) was determined from the copper-constantan thermocouple emf output data obtained from the coolant inlet and outlet thermocouples. A least-square method of curve fitting was applied to tabulated standard thermocouple emf values as a function of temperature to obtain an expression for temperature in terms of the thermocouple emf. The resulting least-squares curve fit equation (Appendix C) was used to calculate the temperatures indicated by the thermocouples.

The condensate collected in the test condenser flask included any condensation which might have occurred in the horn driver section, the inlet to the test condenser section, and the connecting flow passages between the test condenser and the collecting flask. The steam side heat transfer rate was calculated as the thermal energy given up by the steam from the vapor inlet condition to the condensate and vapor outlet condition. The steam was assumed to enter as saturated vapor, so that the enthalpy ($h_{g,i}$) of the inlet steam was taken to be the saturated vapor enthalpy evaluated at the temperature indicated by the copper-constantan thermocouple located at the steam inlet section. The

enthalpy of the condensate exiting from the test section was assumed to be the saturated liquid enthalpy $h_{f,e}$ corresponding to the temperature indicated by the thermocouple located in the connecting flow passage between the test condenser and the collection flask. The enthalpy change multiplied by the condensate mass flow rate from the test condenser section (Γ_s) was calculated as the steam-side heat transfer rate (Q_s).

$$Q_s = \Gamma_s(h_{g,i} - h_{f,e}) \tag{5.2}$$

The calculated test condenser and steam-side heat transfer rates are shown in Table I. As evident from the results, a significant amount of condensation heat transfer was occurring outside of the test condenser section. Although the horn section, port of the steam inlet section, and the test section condensation collection flask were insulated with fiberglass type insulation, a portion of the glass tube and lower section of the experimental apparatus was exposed directly to toom temperature air. Since the test section heat transfer rate was considered to be that calculated from the coolant data, the steam-side heat transfer rate served only as a qualitative check of the coolant results. One detrimental factor was the increased vapor flow rate required by the unwanted heat transfer.

In order to provide sufficient vapor flow rate for any increase in heat transfer rate that might result from the effect of sound on condensation heat transfer, a quanity of vapor exceeding the amount condensed in the test section was purposefully admitted. The excess vapor was condensed in the excess steam condenser, and the excess vapor mass flow rate (Γ_x) is tabulated in Table I. Again the increase in vapor

TABLE I

RESULTS FROM EXPERIMENTS TO DETERMINE THE EFFECT OF SOUND ON CONDENSATION HEAT TRANSFER

Exp. No.	f (Hz)	P_o lbf/in^2	Γ_c lbm/min	T_c °F	Q BTU/hr	Γ_s lbm/hr	Q_s BTU/hr	Γ_x lbm/hr	Re_v	Re	M/M_o^2	M_e/M_o^2
1	——	——	12.7	2.25	1715.	2.72	2644.	0.30	3685.	141.	——	——
2	474.	0.25	12.7	2.30	1754.	2.50	2432.	0.35	3486.	130.	82.5	10.2
3	633.	0.21	12.7	2.96	2257.	2.47	2407.	0.44	3562.	129.	119.3	17.9
4	——	——	12.6	3.00	2268.	2.63	2561.	0.94	4370.	137.	——	——
5	562.	0.12	12.7	2.87	2187.	2.54	2469.	0.99	4310.	132.	459.5	128.5
6	1100.	0.125	12.8	2.91	2241.	2.49	2422.	0.95	4202.	130.	410.8	113.1
7	513.	0.495	14.3	2.16	1853.	2.63	2559.	0.76	4150.	137.	25.5	5.7
	990.	0.25									100.1	22.5
8	1047.	0.24	14.2	1.94	1653.	2.58	2514.	0.43	3691.	134.	95.4	13.7
	739.	0.25									88.0	12.6
	529.	0.32									53.7	7.7
9	529.	0.22	14.2	2.21	1883.	2.44	2374.	1.78	5162.	127.	164.7	69.5
	1261.	0.13									471.6	199.0

flow rate which resulted from the admission of excess steam was an unwanted situation, but was required to assure a plentiful supply of vapor.

The inlet vapor velocity ($\bar{U}_o$) was calculated from the total vapor mass flow rate (Γ_{tot}), steam inlet saturate vapor specific volume ($v_{g,i}$) and tube flow area (A_t):

$$\bar{U}_o = \Gamma_{tot} \cdot v_{g,i} / A_t \tag{5.3}$$

where: $\Gamma_{tot} = \Gamma_s + \Gamma_x$.

The maximum acoustic velocity (U_o) was calculated from the sound pressure amplitude (P_o) data, the inlet saturated vapor specific volume ($v_{g,i}$), and the acoustic velocity for saturated steam (a).

$$U_o = \frac{P_o v_{g,i}}{a} \quad . \tag{5.4}$$

The ratio of inlet through flow Mach number (M) to the maximum acoustic Mach number squared (M_o^2) was calculated from the expression

$$\frac{M}{M_o^2} = \frac{\bar{U}_o/a}{U_o^2/a^2} = \frac{\bar{U}_o \cdot a}{U_o^2} \quad . \tag{5.5}$$

The ratio of the vapor through flow Mach number at the test condenser exit (M_e) to the maximum acoustic Mach number was also calculated.

$$\frac{M_e}{M_o^2}_{\text{exit}} = \frac{\Gamma_x v_{g,i} \cdot a}{A_t U_o^2} \tag{5.6}$$

The inlet vapor Reynolds number was calculated from the total steam flow rate (Γ_{tot}) and the inlet vapor viscosity (μ_v) data:

$$Re_v = \frac{4\Gamma_{tot}}{\mu_v} \tag{5.7}$$

The condensate Reynolds number (Re) was calculated, using the test condenser mass flow rate (Γ_s) and the viscosity of the condensate (μ):

$$Re = \frac{4\Gamma_s}{\mu} \tag{5.8}$$

The condensate mass flow rates were calculated from the weight of condensate collected during a measured time interval. These calculated results are presented in Table I.

Discussion of the Results from Experiments to Determine the Effect of Sound on Condensation Heat Transfer

Experiments 1, 2 and 3 were conducted with unchanged valve settings on the inlet steam line and inlet coolant line. The intent was to maintain constant steam inlet flow rate and constant coolant mass flow rate. Experiments 4, 5 and 6 were conducted with the same coolant inlet value setting with an increase in steam flow rate. The coolant mass flow rate for experiments 1 through 6 varied from 12.63 lbm/min to 12.79 lbm/min, indicating that the coolant flow rate was reasonably constant. It is of interest to note that the steam-side heat transfer rate was fairly constant for experiments 1 through 6, while the test condenser heat transfer rates (coolant) for experiments 1 and 2 were markedly different from those for experiments 3 through 6. The steam-side heat transfer rates are from 7 percent to 13 percent larger than the test condenser heat transfer rates. Re-examination of the data revealed no discrepancies or possible physical explanation for the apparantly low test condenser heat transfer rates of experiments 1 and 2.

Visual observation of the condensate film flow revealed that the liquid surface was very smooth for the initial 1.5 to 3 inches of the

cooled test condenser, then ripples began to appear. From about the middle of the test condenser on down, the flow appeared wavy. The calculated liquid Reynolds number for all of the experiments was between 127 and 141. The transition from laminar to turbulent condensate film flow is normally considered to occur for a Reynolds number between 100 and 600. No clear indication of transition to turbulent flow was manifested during the experimental observations.

Experiments 7, 8 and 9 were conducted with a constant coolant inlet valve setting to maintain a constant coolant flow rate, and experimental configuration B was used. The coolant temperature rise did not deviate by more than $0.1^{\circ}F$ for each experiment (7, 8 and 9) with the several frequencies and sound pressure amplitudes imposed upon the condensing vapor. Visual observation of the test condenser section during experiment 7 revealed that with no sound the liquid condensate film flow was very smooth for about 3/4 of the cooled section, with slight waviness occurring in the last quarter length of the condenser. With a frequency of 513 Hz and a sound pressure amplitude of 0.495 psi, waviness was generated near the top of the test condenser, which propagated down the entire length of the tube. Only slight waviness occurred with a frequency of 990 Hz and a sound pressure amplitude of 0.25 psi. No significant change in the heat transfer rate was observed during experiment 7, even with an observed waviness apparently generated by the sound field. This indicates that the time average thickness was not sufficiently affected to cause a change in the heat transfer rate. As noted earlier, the glass condenser tube substantially controls the heat transfer rate. This means that very strong effects would have to

be manifested before an observable change in the test condenser heat transfer rate would be observable.

Visual observation confirmed that large acoustic pressure amplitudes are required to affect the condensate film flow. Experiments 8 and 9 did not reveal any additional information. Initially the 8 horn driver palate diaphragm assemblies were capable of delivering an acoustic pressure amplitude (P_o) of 0.495 psi. During the duration of experiments7, 8 and 9, the maximum achievable acoustic pressure amplitude deteriorated rapidly. It was observed that the achievable P_o decreased with an increase in frequency. Above 2000 Hz, the maximum attainable P_o was less than 0.1 psi.

In order to obtain some qualitative indication of the magnitude of induced secondary flow, the ratio of through flow mach number (at inlet and outlet) to the maximum acoustic Mach number squared was calculated (Equations 5.5 and 5.6). These values are presented in Table I. A qualitative indication of the region of flow affected by the sound field can be gained by considering these Mach numbers ratios and the results of Purdy et al. (43) for air as presented in Figure 12. The obvious inference is that the region of flow affected by the resonant sound field is extremely small. This is the same result predicted by the simplified condensing vapor model presented in Chapter III. The through flow rate must be such that M/M_o^2 is small in order that the region of secondary flow can become significant.

Two out-standing defects in the experimental design are obvious. First, the coupling of the test condenser section and sound generating system did not achieve a good acoustic coupling. Perhaps some

geometry modifications would overcome some of the observed difficulties. A more effective and versatile sound generating system is desirable. Second, the glass test condenser dominated the heat transfer rate such that modest changes in film thickness would not be reflected in the heat transfer rate. This second limitation was recognized, but enough emphasis was placed on achieving visual observation that this defect was over-ruled. Visual observations indicated that a resonant sound field could modestly affect the condensate film flow at high enough sound pressure amplitudes. In turn, the heat transfer rate for a condensate film thickness dominated condensing situation can be expected to be modestly increased.

To obtain a spectacular increase in condensation heat transfer rate, the condensate must be removed from the condensing surface. This was the purpose of maintaining the ability to visually observe the condensate film flow. If the resonant sound field caused an ejection of liquid condensate from the surface (a phenomenon similar to that observed by Howartson (18) and Barfield (2) for air and a horizontal liquid layer), then a mechanism could be clearly established.

To further explore the proposed mechanism of ejecting the liquid condensate film and to determine the effect of vapor through flow, an analogous air and water film flow situation was considered. The geometry, the description of the experimental hardware and the procedure are presented in Chapter IV for the experiments to determine the effect of an air-borne resonant sound field on thin-film vertical water flow.

Data Reduction for Experiments Involving Thin-Film Water Flow

The volume flow rate of air ($\dot{V}$) was measured with a rotameter. The calibration curve and least-squares equation used to determine the volume air flow rate from the rotameter data are presented in Appendix C. The through flow velocity of the air ($\bar{U}_{o,a}$) was calculated as follows:

$$\bar{U}_{o,a} = \frac{\dot{V}}{A_t} \quad . \tag{5.9}$$

The thin-film water flow rate (Γ_f), air Reynolds number (Re_a), thin-film Reynolds number (Re_f) and air Mach numbers ratio, $(M/M_o^2)_{air}$ were calculated for comparison with the condensing experiments. These calculated results are presented in Table II.

Discussion of the Results from Experiments to Determine the Effect of Air-Borne Sound on Thin-Film Vertical Water Flow

The first set of thin-film flow experiments, identified by the TF (thin-film) notation in Table II, were conducted with no air through flow. The thin-film Reynolds number was approximately ten times the condensate Reynolds number calculated for the condensing experiments. In experiment 1 TF, it was found that an occasional thin disc of water was formed momentarily across the tube when the sound pressure amplitude (P_o) was approximately 0.4 psi. Increasing P_o to 0.45 psi resulted in regularly occurring discs at specific axial locations. The later experiments with no air flow revealed that the sound pressure amplitude required to cause an occasional ejection of liquid from the thin-film was approximately 0.4 psi for the thin-film Reynolds numbers of these experiments.

TABLE II

RESULTS FROM EXPERIMENTS TO DETERMINE THE EFFECT OF AIR-BORNE SOUND ON THIN-FILM VERTICAL WATER FLOW

Experiment Identification	f H_z	P_o lbf/in^2	Γ_f lbm/hr	$\bar{U}_{o,a}$ ft/sec	Re_a	Re_f	$\left(M/M_o^2\right)_{air}$
1TF	933.	0.46	68.92	0	0	1195.	0
2TF	941.	0.59	113.50	0	0	1968.	0
3TF	1350.	0.72	119.40	0	0	2071.	0
4TF	1350.	0.56	81.10	0	0	1406.	0
5TF*	1718.	0.48	69.12	0	0	1199.	0
6TF*	658.	0.16	69.12	0	0	1199.	0
1TF&A(a)	—	0	26.03	0	0	451.	0
1TF&A(b)	933.	0.11	25.59	0	0	443.	0
1TF&A(c)	933.	0.315	25.44	0	0	441.	0
1TF&A(d)	933.	0.55	26.20	0	0	454.	0
1TF&A(e)	933.	0.57	25.63	7.46	1637.	444.	8.8
1TF&A(f)	933.	0.49	25.29	16.42	3604.	438.	26.3
1TF&A(g)	933.	0.60	25.84	0	0	448.	0
2TF&A(a)	—	0	3.90	0	0	67.7	0
2TF&A(b)	933.	0.185	3.90	0	0	67.7	0
2TF&A(c)	933.	0.71	3.90	0	0	67.7	0
3TF&A(a)	—	0	86.16	0	0	1494.	0
3TF&A(b)	933.	0.19	84.74	0	0	1469.	0
3TF&A(c)	933.	0.35	86.20	0	0	1495.	0
3TF&A(d)	933.	0.42	87.54	0	0	1518.	0
3TF&A(e)	933.	0.36	84.18	6.82	1497.	1460.	20.2
3TF&A(f)	933.	0.275	83.50	14.08	3090.	1448.	71.5
3TF&A(g)	933.	0.80	81.56	23.51	5160.	1414.	14.1
4TF&A(a)	—	0	12.86	0	0	223.	0
4TF&A(b)	933.	0.18	12.97	0	0	225.	0
4TF&A(c)	933.	0.36	12.71	0	0	220.	0
4TF&A(d)	933.	0.60	12.74	0	0	221.	0
4TF&A(e)	933.	0.57	12.93	6.41	1407.	224.	7.6
4TF&A(f)	933.	0.63	12.69	12.29	2698.	220.	11.9
4TF&A(g)	933.	0.585	12.46	23.51	5160.	216.	26.4

* Non-resonant frequencies

An acoustic velocity antinode was expected to occur reasonably close to the horn driver throat, and a velocity node (acoustic pressure antinode) was assumed to occur at the pressure transducer location for resonant sound field conditions. The pressure transducer did not completely fill the lower tube and the pressure transducer has a finite complex acoustic impedance; however, it was assumed that the acoustic impedance offered by the pressure transducer was large enough to allow the transducer end of the tube to be treated as a solid termination. Consequently, the sound pressure amplitude as indicated by the pressure transducer was assumed to be equal to P_o. The fundamental resonant frequency (f_o) for the tube was calculated from the apparent resonant conditions observed in the experiments. The frequency of 933 Hz was assumed to be the third odd harmonic frequency ($f_3 = 9f_o/3 = 933$ Hz) and the frequency of 1350 Hz was assumed to be the fifth odd harmonic frequency ($f_5 = 13f_o/3 = 1350$ Hz). The fundamental frequency (f_o) was calculated to be 311 Hz and the velocity antinode location near the horn driver throat was calculated to be 32.9 inches above the pressure transducer location.

The axial location of the range of ejection sites is shown in Figure 31. Also shown in Figure 31 is the water inlet location and the pressure transducer location. As evident from Figure 31, the ejection sites range about the acoustic pressure nodes. A similar sketch for experiments 3TF and 4TF is also shown in Figure 31, for the fifth odd harmonic frequency (1350 Hz).

The time-average pressure distribution for a resonant sound field with no through flow can be written as $P = \frac{\Delta P}{2} \cos \frac{2\pi x}{\lambda} + \bar{P}$, with $x = 0$

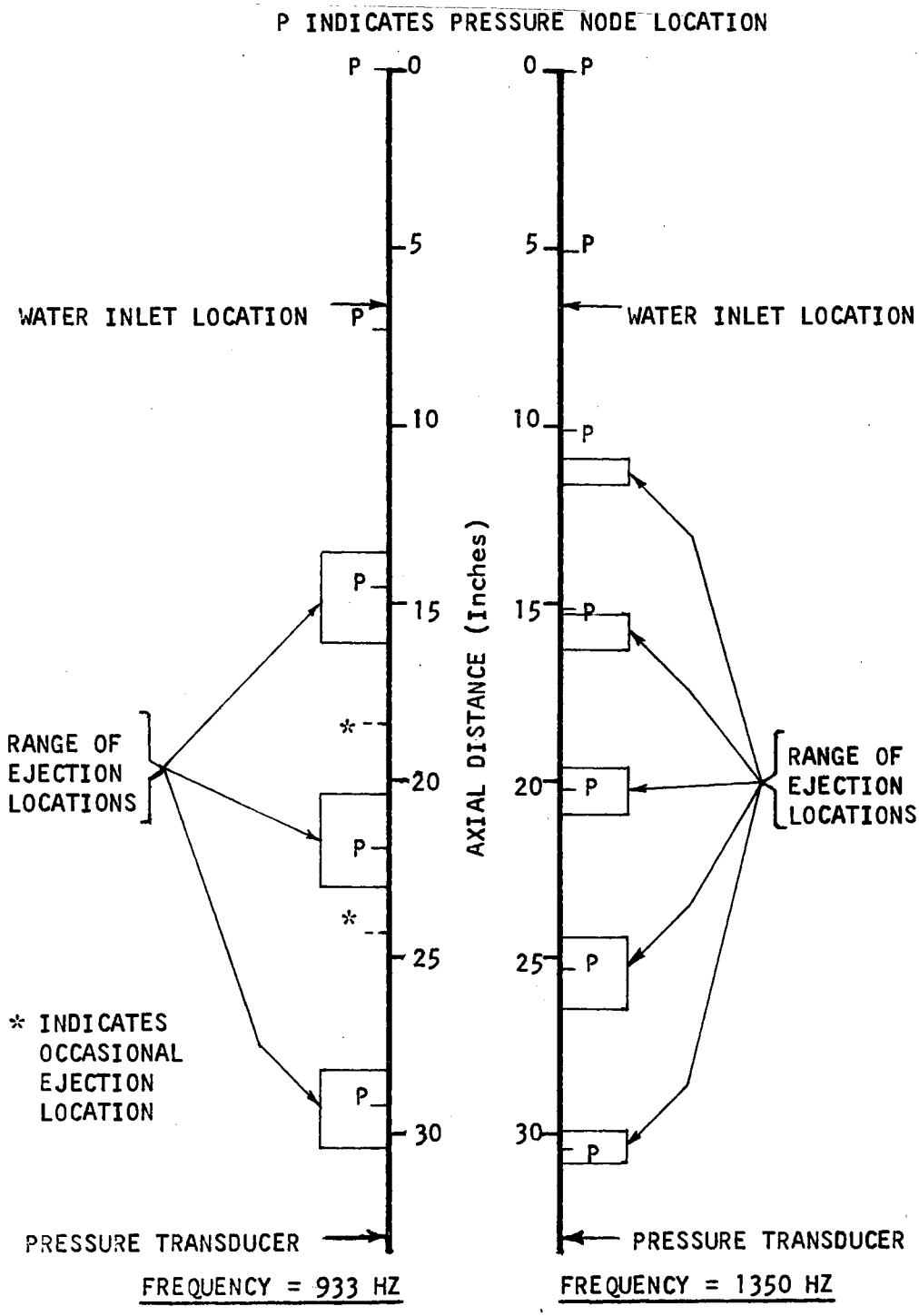

Figure 31. Sketch Illustrating the Range of Liquid Ejection Locations Observed in the Effect of Resonant Air-Borne Sound on Vertical Thin-Film Water Flow Experiments.

at the acoustic velocity antinode nearest the horn driver units, in accordance with Equation 3.22. This time-average pressure distribution is such that any resultant flow of the thin-film liquid would be toward the acoustic pressure nodes. Purdy et al. (43) considered a constant time-average axial pressure in a rigid tube with resonant sound conditions and obtained a description of the sound induced flow. These sound induced flow stream-lines are shown in Figure 9. Consideration of the viscous effect of air on the thin-film liquid indicates that thin-film flow, which resulted from the sound induced air flow, would be toward the pressure nodes. Both simplified models indicate that the effect of an air-borne resonant sound field upon a thin-film of liquid is to cause the liquid to flow toward the pressure node locations.

Photographs of the liquid ejection process are shown in Figure 32. The liquid is ejected from the tube wall toward the center of the tube, and has the appearance of a disc, normal to the tube axis. The disc appeared to break up into droplets as liquid continued to be ejected. Some of the smaller droplets in the center of the tube in the region above the disc moved upward slowly. Other droplets in this region appeared to float. This droplet behavior is interpreted as a qualitative confirmation of the sound induced air flow pattern predicted by Purdy et al. (43). Many droplets of varying size and degrees of activity were seen above and below the ejection site. These droplets are visible in Figure 32.

In the following descriptions of experimental observations, the locations are expressed as distance from the calculated acoustic velocity antinode location as shown in Figure 31.

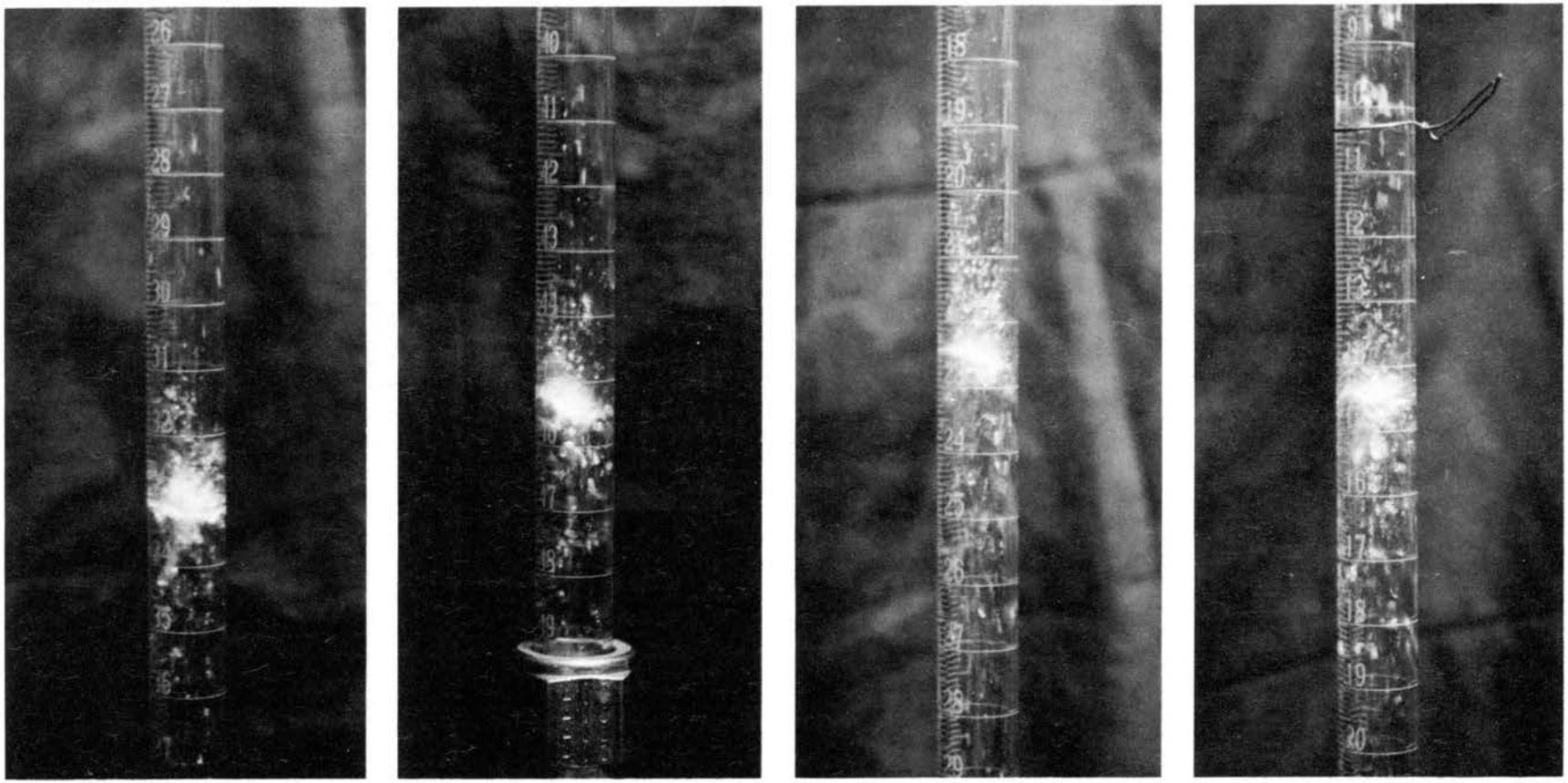

(a) Experiment Number 2TF Disc at 24.4 inches. (b) Experiment Number 2TF Disc at 30.0 inches. (c) Experiment Number 3TF Disc at 19.9 inches. (d) Experiment Number 4TF Disc at 16.3 inches.

Figure 32. The Liquid Ejection Process Observed in the Experiments to Determine the Effect of Air-Borne Sound on Thin-Film Vertical Water Flow.

The discs would normally form near the highest acoustic pressure nodes location. In experiments 1TF and 2TF an ejected liquid disc would form at 14.9 inches, remain continuously active as it drifted down to about 16.2 inches, then disappear. Almost immediately, a disc would be formed at 21 inches, which then drifted down to 24.4 inches and disappeared. Another disc would form at 28.2 inches, drift down to 30.4 inches and disappear. This sequence of events would repeat itself, with the time elapsed between formation and disappearance of each disc varying from a fraction of a second to several seconds. The downstream ejection sites generally were of shorter duration than the first active ejection site. Movie film of some experiments show that the disc disappearance and appearance from one location to the next is almost instantaneous. Very seldom did two discs occur simultaneously, and in no case did simultaneous ejection sites persist. The location of each disc formation was not fixed, but rather occurred normally in the location ranges noted above. Occasionally, an ejection of liquid would occur outside the above noted ranges. It is believed that these off pressure node ejection locations resulted from large disturbances caused by droplets impinging upon the film-flow.

The sound pressure amplitude as indicated by the pressure transducer reflected the fact that sound energy was being absorbed by the ejection process. Several individual traces of the acoustic pressure were recorded on a single polaroid film to obtain an estimate of the sound pressure amplitude. A photograph of 5 traces of the sound pressure transducer output from experiment 4TF and A(d), as displayed on an oscilloscope screen, are shown in Figure 33a. The maximum amplitude

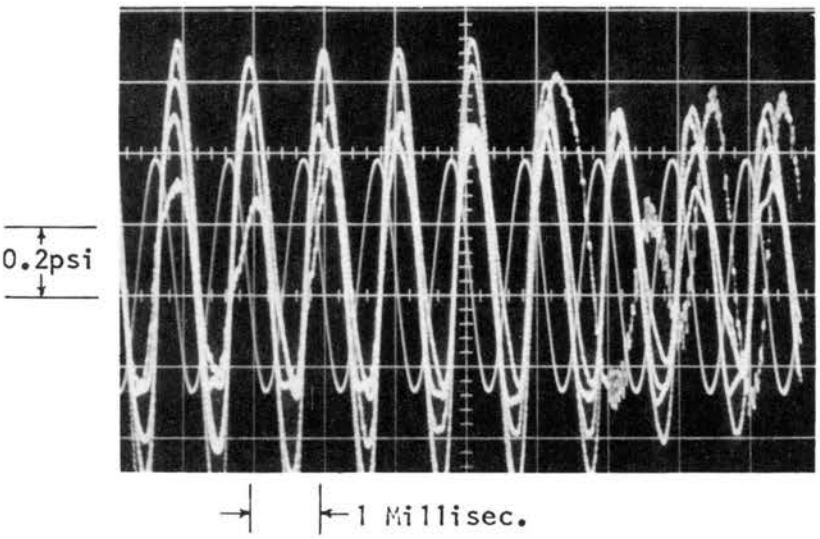

(a) Five Individual Acoustic Pressure Transducer Output Traces and a Single Trace of Voltage Input to a Horn Driver Unit.

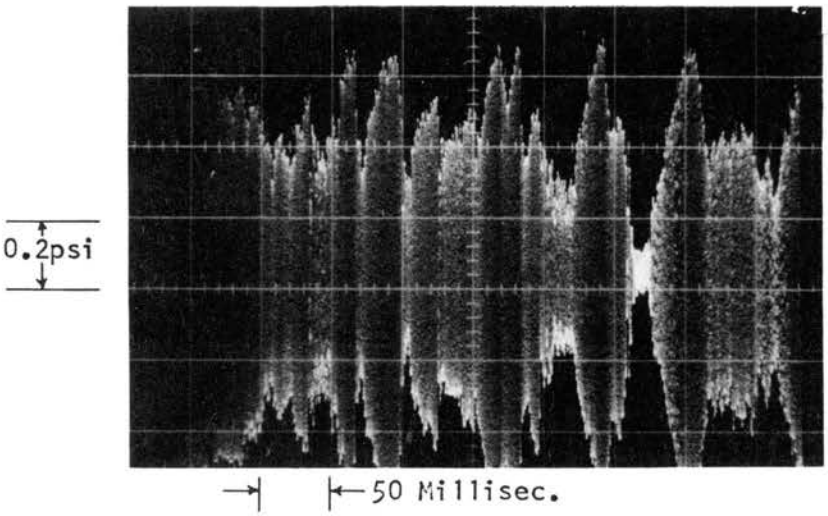

(b) A Single Sweep of the Acoustic Pressure Transducer Output.

Figure 33. Sound Pressure Amplitude Variation with Time, Resulting from the Liquid Ejection Process in Experiment 4TF&A(d).

of the 5 traces was recorded as the sound pressure amplitude (TableII). Since the variation of sound pressure amplitude at the transducer location is a function of time, an increase in the time scale yielded a better indication of this timewise variation, as shown in Figure 33b.

The visual observation of experiments 3TF and 4TF was qualitatively the same as those for experiment 1TF. The regular ejection sites occurred at approximately 11 to 11.4 inches, 15.3 to 16.3 inches, 19.6 to 20.9 inches, 24.4 to 26.5 inches and 30 to 30.9 inches. The calculated acoustic pressure node locations for the fifth odd harmonic frequency (1350 Hz) were 0, 5.06, 10.12, 15.19, 20.25, 25.31 and 30.37 inches. The water inlet location (6.75 inches) was below the location of the first two acoustic pressure nodes. In these experiments, ejection seldom occurred at the 11 to 11.4 inch location, but a thin-film disturbance was evident at this location. Occasionally, the downstream ejection sites were not sequentially excited, with one or more sites being skipped before the following downstream ejection sites were activated.

The seventh odd harmonic frequency was calculated to be 1762.3 Hz. With a slightly off resonance frequency of 1718 Hz, an interesting situation presented itself. The liquid ejection process was quite active, with a disc forming at 13.6 inches drifting down to 15.3 inches, disappearing, then reforming almost immediately at 13.6 inches again. A photograph of the ejection activity occurring in experiment 5TF is shown in Figure 34 with the disc located at 14.3 inches. This cyclic action continued until the sound pressure amplitude was intentionally lowered 30 minutes later. Movie film of the ejection region was

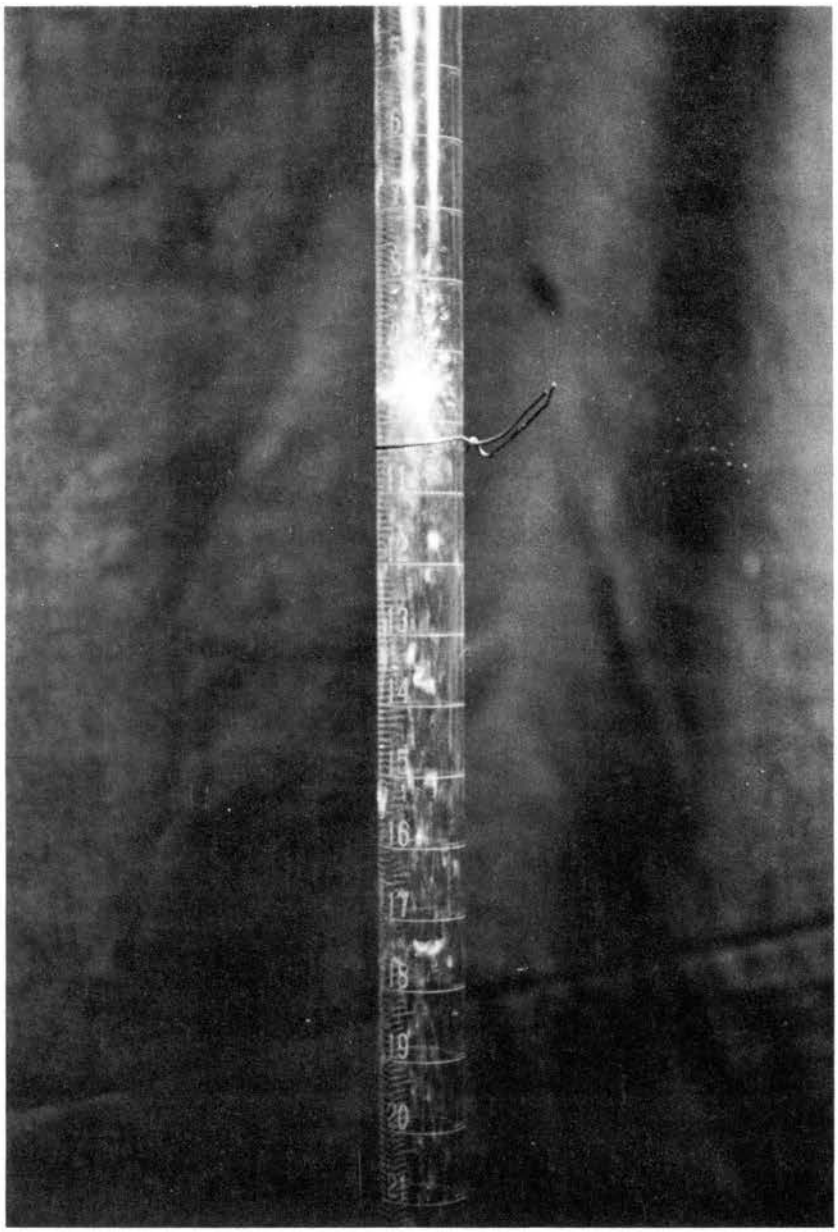

Figure 34. Liquid Ejection Process Observed at a Slightly Off-Resonance Frequency in Experiment 5TF. Disc at 13.6 Inches.

obtained. The movie film was taken at a speed of approximately 500 frames per second. Some of the previously noted observations were confirmed, and the action of the ejection process is quite interesting; however, very little additional quantitative data were obtained from viewing this film.

The experimental conditions associated with experiment 5TF were obtained by holding a high input to the horn driver units and varying the frequency. Later attempts to obtain the situation again proved futile.

Another interesting phenomena occurred at a non-resonance frequency of 658 Hz with the same thin-film water flow rate as in experiment 5TF. In experiment 6TF, the liquid was ejected from the thin-film surface at such a rate that plug flow could occur. As the ejection process began, it would appear to form a disc as in the previous experiments; but instead of a shower of droplets, a plug of liquid would suddenly form across the tube. This plug grew in length until it was approximately 6 to 8 inches long, then the plug of liquid flowed down the tube. The top of the plug flow remained at about the same location during the plug growth period. A photograph of the plug flow observed in experiment 6TF is shown in Figure 35. The upper and lower end of the plug appear frothy, since small bubbles appeared in the liquid near the upper and lower liquid plug surfaces, and small droplets were emitted from both the upper and the lower liquid air interface.

The experiments identified by TF&A (Thin-Film and Air) in Table II denotes that air through-flow was incorporated as a parameter in the thin-film experiments. All of the experiments with TF&A included in

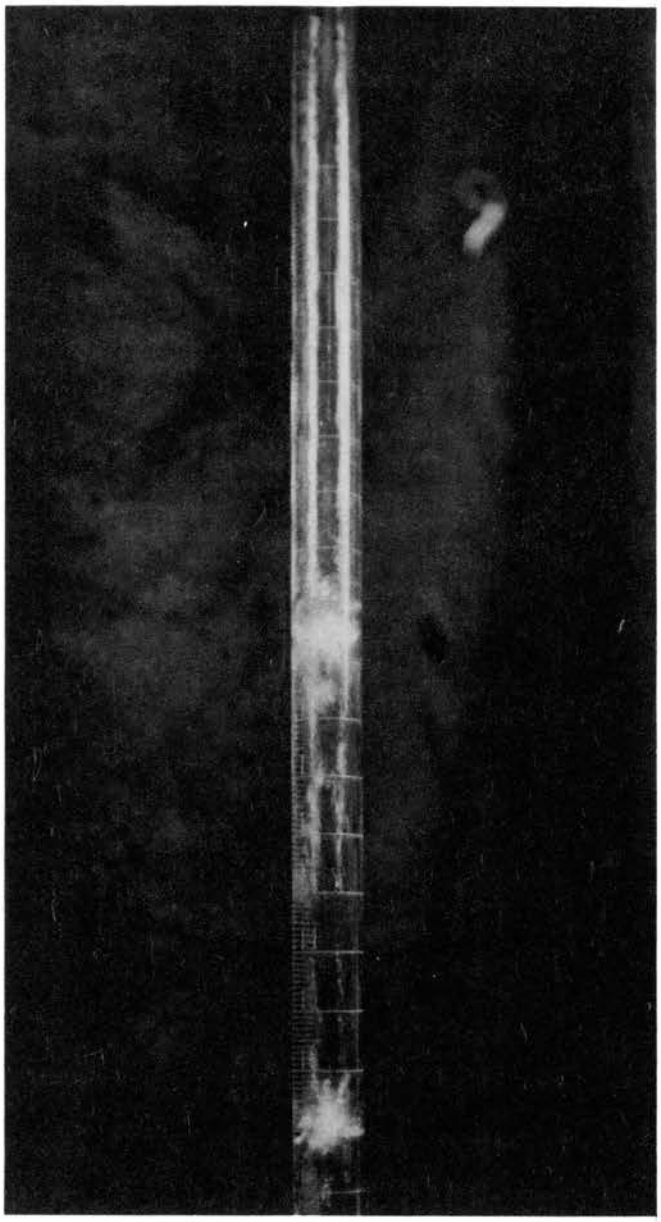

Figure 35. Plug Flow Caused by Imposing Sound on Thin-Film Vertical Water Flow, as Observed in Experiment 6TF for a Non-Resonant Frequency.

the identification were conducted with a harmonic resonant frequency of 933 Hz. The experiments were conducted to determine the effect of a resonant sound field and air through-flow on thin-film vertical liquid flow.

Experiment 1TF&A(a) was conducted with no sound and no through flow. The thin-film water flow appeared smooth down to 10.1 inches, slightly wavy from 10.1 to 15.3 inches, and very wavy from 15.3 inches down to the outlet. The film-flow was quite similar for a low sound pressure amplitude [1TF&A(b)], except that occasionally a slight surge in the inlet flow would result in an occasional ejection of liquid from the film as the surge wave passed a pressure node location. Increasing the sound pressure amplitude to 0.315 psi [1TF&A(c)] did not further alter the visually observed flow situation. Increasing the sound pressure level above 0.315 psi resulted in regular ejection of liquid from locations in the range of acoustic pressure nodes. In experiment 1TF&A(d), liquid ejection discs initiated at 20.5 inches, moved to 21.5 inches and remained there for periods of approximately 10 seconds before vanishing. Discs also formed at 13.6 inches, disappeared from 13.6, and reappeared almost instantly at 21.5 inches, disappeared from 21.5, and reappeared at 29.6 inches, ran to 28.3 inches, and then vanished. Two ejection sites were observed to be active simultaneously, but one would quickly disappear. The liquid ejection mechanism occurred about equally in the 13.6 to 16.2 inch location range and in the 20.5 to 23.1 inch location range, with only occasional liquid ejection occurring in the 28.3 to 30.4 inch location range.

With an air through-flow rate of 0.41 cfm superimposed upon the conditions of experiment 1TF&A(d), it was found that the liquid ejection mechanism was suppressed except for an occasional ejection of liquid occurring at 29.6 inches. The thin-film liquid flow was extremely wavy, appearing quite turbulent in experiment 1TF&A(e). Increasing the air through-flow rate to 0.91 cfm [experiment 1TF&A(f)] did not alter the appearance or behavior from that described for 1TF&A(e). Experiment 1TF&A(g) was conducted with essentially the same conditions as occurred in experiment 1TF&A(c), so that movie film of the entire tube could be obtained. Movie film of various aspects of all the thin-film and air experiments were obtained.

The thin-film water flow rate was decreased for the 2TF&A experiments. Considerable difficulty was encountered in obtaining a thin-film flow which would remain attached to the glass tube walls at the desired low flow rates. The thin-film would remain attached down to 10.2 inches and then would run in a trickle-meandering down the remainder of the tube length. High sound pressure amplitude was required to affect this flow. When ejection occurred, all of the inflowing liquid was ejected with the surface becoming dry below the ejection site. Droplets of water resulting from the ejection process were thrown about in many directions and would cling to the glass tube when they struck the walls. When enough particles would collect near the acoustic pressure node, ejection would occur momentarily. The liquid ejection process occurred at the same location ranges as in the 1TF&A experiments. At a location of approximately 30 inches, relatively large drops of water (estimated to be 0.020 to 0.060 inches in diameter) were observed to

be projected upward. A sharp " pip" sound was heard each time one of these large drops was formed and projected upward.

For a short period of time a thin-film of water remained attached to the glass walls over the entire length of the tube. At high acoustic pressure amplitudes ejection would occur instantaneously at the acoustic pressure node locations--each location sequentially activated as the ejection process seemed to run down the tube. Multiple ejection sites also occurred for these conditions. Attempts to reestablish the attached film flow at the low flow rates of experiments 2TF&A were futile.

The liquid flow rates for experiments 3TF&A were large enough to provide sufficient liquid for plug flow conditions to occur. The film-flow appeared wavy for the entire length with no sound [3TF&A(a)], low sound conditions [3TF&A(b)], and medium sound conditions [3TF&A(c)]. When the sound pressure amplitude was increased to the maximum attainable value, liquid ejection occurred at the acoustic pressure node locations. In experiment 3TF&A(d), double ejection sites occurred approximately one inch apart, and led quickly to plug flow conditions. When the length of the plug grew to a sufficient length, the entire plug would flow, as a plug, down the tube. As the top of the liquid plug passed a normal acoustic pressure node location, liquid ejection occurred at upstream acoustic pressure node locations. After the liquid plug had flowed out of the tube, the entire process would repeat itself. With the air through-flow rates of experiments 3TF&A(e), 3TF&A(f) and 3TF&A(g), no liquid ejection was visible; however, the liquid film-flow appeared more wavy and turbulent than that of experiment 3TF&A(a).

The 4TF&A series of experiments were conducted with the lowest liquid film-flow rate which could be maintained for the sequence of sound and air through-flow conditions imposed upon the thin-film flow. The water flow in experiment 4TF&A(a) was smooth down to 13 inches below the calculated acoustic velocity antinode nearest the horn driver unit. Slight waviness was evident on the liquid surface from 13 inches down to 18.8 inches, where the flow appeared very wavy on down to the exit. The visual observation of experiment 4TF&A(b) revealed conditions similar to those of 4TF&A(a). The sound pressure amplitude recorded for experiment 4TF&A(c) was the threshold value for continuous liquid ejection, as judged from the fact that occasional liquid ejection occurred, and further increase in the sound pressure amplitude caused sustained liquid ejection. The range of liquid ejection locations for experiment 4TF&A(d) were the same as those previous noted for this third odd harmonic resonant frequency (933 Hz). The movement from one liquid ejection site to the next occurred much more rapidly than for the TF, 1TF&A and 3TF&A experiments. No single ejection location dominated the activity.

Visual observation of experiment 4TF&A(e) revealed that the air through-flow rate did not completely eliminate the effect of the sound field on the liquid film flow. Some wave generation occurred at the acoustic pressure node locations, and momentary liquid ejection appeared to occur over a distance of approximately one inch--rather than the very localized ejection which occurs with no through-flow. The air flow rates of experiments 4TF&A(f) and 4TF&A(g) were large enough to eliminate the liquid ejection phenomena. It was observed that the

water film flow did appear much more turbulent for the entire tube length in the last two experiments than in experiment 4TF&A(a).

The results of the thin-film water flow experiments demonstrate that air through-flow rate effectively eliminates the liquid ejection phenomena. The inlet and exit values of M/M_o^2 for the condensing steam experiments is larger than comparable values in the air-water film experiments. The observed lack of an effect of vapor-borne sound on condensation heat transfer rate can be explained by the argument that the vapor through-flow rate was large enough to eliminate the possible liquid ejection mechanism. Additionally, the flow of vapor toward the condensing surface, as required by the condensation process, also acts to suppress the secondary flow which might be induced by the sound field.

It was observed that the duration of liquid ejection at a given location was dependent upon the thickness of the film-flow. Qualitatively, as the film-thickness increased, the duration of the liquid ejection process at a given location increased. If enough liquid flow rate is available to supply the ejection process, plug flow can result. The minimum sound pressure amplitude required to cause liquid ejection was found to be approximately 0.315 psi to 0.36 psi for the air-water film-flow experiments conducted. A correlation of flow parameters and minimum sound pressure amplitude required to cause liquid ejection was not obtained from the limited experimental results.

CHAPTER VI

CONCLUSIONS AND RECOMMENDATIONS

The objective of this investigation was to determine the parameters which influence condensation heat transfer when acoustic pressure plusations are imposed on the condensing vapor, and to establish the controlling mechanisms for this process. Due to various reasons, the experimental investigation was limited to the condensation of steam at atmospheric pressure. Experiments with air-borne sound imposed on liquid film flow down the inside wall of a vertical tube aided in the establishment of a possible mechanism for the effect of sound on condensation heat transfer. Theoretical investigation of simplified models of the effect of sound on condensation heat transfer led to a delineation of the pertinent parameters. The objectives have been realized.

Conclusions

The conclusions which have been reached as a result of the theoretical investigation are:

1. The simplified model for the shearing stress at the liquid-vapor interface proposed by Shekriladze and Gomelauri (50) is useful and reasonably accurate for condensation conditions involving body force and/or forced convection forces.

2. Consideration of the effect of temperature dependent viscosity on laminar condensation heat transfer (Appendix A) yielded the conclusions that (a) a linear temperature profile across the condensate film is a very good approximation, even with fluids having strongly temperature dependent viscosities; and (b) the proper temperature (T_f) to use in evaluating the condensate viscosity for use in Nusselt type heat transfer equations is

$$T_f = T_w + \frac{\Delta T}{4} \text{ , if } \left[\frac{T_v}{T_w} \left(1 - \frac{\Delta T}{2T_w} \right) \ln \left(\frac{\mu_w}{\mu_v} \right) \right] \leq 1 \text{ .}$$

3. The effect of an axially resonant sound field on vertical condensing surfaces will be to decrease the heat transfer rate, if rippling or liquid condensate ejection do not occur.

4. The condensation process dominates the vapor flow pattern if $(U_o^2/a\bar{U}_o) < 1$ or, equivalently, if $(M/M_o^2) > 1$.

5. The most significant parameter in determing the effect of vapor-borne sound on condensation heat transfer is M/M_o^2. All parameters which influence the condensation process or describe the sound field--individually--were found to be involved. Low values for h_{fg} and a would favor an effect.

The conclusions which have been reached as a result of the experimental investigations involving the condensation of steam on the inside wall of a vertical galss tube, with an axially resonant sound imposed on the vapor, are:

1. A significant sound pressure amplitude is required to affect the condensate film flow.

2. The sound generating system used in these experiments was

inadequate, due to the detrimental effect of the steam atmosphere on the horn driver units.

3. The imposed sound field had no effect on the condensation heat transfer rates in these experiments. This was due in part to the thermal resistance of the glass condenser tube; however, the primary reason is that the high vapor flow rate eliminated any sound induced secondary flow.

4. The range of experimental conditions was too limited to obtain results which would encompass possible condensing situations which might realize some effect due to superimposing a sound field on the condensing vapor.

The conclusions which have been reached as a result of experimental investigation of liquid film flow down the inside wall of a vertical tube with an air-borne axially resonant (or near-resonant) sound field superimposed are:

1. Liquid can be ejected from the thin liquid-film toward the center of the tube at axial locations near the acoustic pressure nodes, if the acoustic pressure amplitude exceeds an experimentally obserable threshold value.

2. The ejection mechanism threshold value of the acoustic pressure amplitude depends upon the thickness of the film flow, with very thin films; but, appears to have little dependence on thickness for relatively thick films. This is a qualitative observation.

3. The ejection process at a given active site will continue until the supply of liquid from the film flow can no longer meet the ejection flow requirements.

4. The sound induced secondary flow predicted by Purdy et al. (42), as shown in Figure 2.9, is qualitatively correct for the air, with no through-flow. This conclusion was inferred from observing the behavior of small liquid droplets in the region above the ejection sites.

5. The imposed sound field can cause plug flow to occur if the liquid film thickness is large enough.

6. The ejection process and the droplets formed absorb a significant portion of the sound energy, when the ejection mechanism is active.

7. Through-flow of air can eliminate the ejection mechanism. This was observed to occur for $(M/M_o^2) \geq 7.6$, which was the smallest value used in the experiments.

It is proposed that the mechanism whereby a vapor-borne sound field can measurably affect the condensation heat transfer rate, is the ejection of liquid condensate from the condenser walls.

Recommendations for Future Studies

The areas of effort related to this thesis which are worth pursuing include:

1. Further experimental investigation of the effect of a resonant sound field on liquid film flow is needed to quantify the parameters which control the ejection mechanism. Particularly, a correlation of threshold pressure amplitudes, fluid properties (such as density, viscosity and surface tension), acoustic wavelength, and film thickness is desirable and attainable with equipment commercially available.

2. A theoretical investigation of the ejection mechanism should be considered in the light of instability analysis techniques. A solution for the non-condensing case of air-borne sound imposed upon liquid film flow appears to be a realistic first step.

3. An investigation of condensing situations in which a low value of M/M_o^2 can be attained, with sufficient sound intensity to cause the ejection of liquid condensate from the condenser surface, would allow a quanitative evaluation for the effect of sound on condensation heat transfer. These results should also establish the limits of the effect of sound.

4. The development of a sound generating system which would permit a wide range of frequency and acoustic pressure amplitudes and would allow the utilization of several condensing vapors, without detrimental effects on the generator, is highly desirable.

SELECTED BIBLIOGRAPHY

1. Akers, W. W., S. H. Davis, Jr., and J. E. Crawford. "Condensation of a Vapor in the Presence of a Non-Condensing Gas." Chemical Engineering Progress Symposium Series, No. 30, Vol. 56, 1960, pp. 139-144.

2. Barfield, B. F. "A Study of Liquid Behavior in the Kundt's Tube." Ph. D. Dissertation, Georgia Institute of Technology, 1965.

3. Beranek, Leo L. Acoustic Measurements. John Wiley and Sons, Inc., New York, N. Y., 1949.

4. Beranek, Leo L. Acoustics. McGraw-Hill Book Company, Inc., New York, N. Y., 1954.

5. Bornhorst, W. J. and G. N. Hatsopoulos. "Analysis of a Liquid Vapor Phase Change by the Methods of Irreversible Thermodynamics." ASME Paper No. 67-WA/APM-35, 1967.

6. Bromley, L. A. "Effect of Heat Capacity of Condensate." Industrial and Engineering Chemistry, Vol. 44, No. 12, 1952, pp. 2966-2969.

7. Bromley, L. A., R. S. Brookey, and N. Fishman. "Effect of Temperature Variation Around a Horizontal Condenser Tube." Industrial and Engineering Chemistry, Vol. 44, No. 12, 1952, pp. 2962-2966.

8. Bromley, L. A. "Discussion of Heat Transfer and Temperature Distribution in Laminar-Film Condensation by W. M. Rohsenow." Transactions of the ASME, Vol. 78, 1956, pp. 1647-1648.

9. Carpenter, F. G. and A. P. Colburn. "The Effect of Vapor Velocity on Condensation Inside Tubes." Proceedings of General Discussion on Heat Transfer, Institute of Mechanical Engineers, London, England, 1951, pp. 1-7.

10. Chen, M. M. "An Analytical Study of Laminar Film Condensation: Part 1--Flat Plates." Journal of Heat Transfer, Trans. ASME, Series C, Vol. 83, 1961, pp. 48-54.

11. Chen, M. M. "An Analytical Study of Laminar Film Condensation: Part 2--Single and Multiple Horizontal Tubes." Journal of Heat Transfer, Trans. ASME, Series C, Vol. 83, 1961, pp. 55-60.

12. Chung, Paul M. "Unsteady Laminar Film Condensation on Vertical Plate." Journal of Heat Transfer, Trans. ASME, Series C, Vol. 85, 1963, pp. 63-70.

13. Choi, H. Y. "Electrohydrodynamic Condensation Heat Transfer." Journal of Heat Transfer, Trans. ASME, Series C, Vol. 90, 1968, pp. 98-102.

14. Dwight, H. B. Table of Integrals and Other Mathematical Data, 4th Edition, The MacMillan Company, New York, 1961.

15. Fourteenth Annual Heat Transfer Conference on Condensation Heat Transfer. Oklahoma State University, March, 1968.

16. Hampson, H. "The Condensation of Steam on a Tube with Filmwise or Dropwise Condensation and in the Presence of a Non-Condensable Gas." International Developments in Heat Transfer, Proceeding of Heat Transfer Conference, ASME, New York, 1961, pp. 310-318.

17. Hassen, K. E., and Max Jakob. "Laminar Film Condensation of Pure Saturated Vapors on Inclined Circular Cylinders." Transactions of the ASME, Vol. 80., 1958, pp. 887-894.

18. Howartson, A. F. "The Behavior of Liquids in a Vibrating Air Column." Phil. Mag., Ser. 7, Vol. 36, 1944, pp. 20-31.

19. Jacobs, H. R. "An Integral Treatment of Combined Body Force and Forced Convection in Laminar Film Condensation." International Journal of Heat and Mass Transfer, Vol. 9, 1966, pp. 637-648.

20. Jacobs, H. R. "Combined Body Force with Forced Convection in Laminar Film Condensation Heat Transfer of Freon 113." Ph. D. Dissertation in the Department of Mechanical Engineering, Ohio State University, 1965.

21. Karplus, H. B. "Velocity of Sound in Steam." Delivered before the 1959 International Acoustics Congress.

22. Keenan, J. H. and F. G. Keyes. Thermodynamic Properties of Steam. John Wiley and Sons, Inc., New York, 1936.

23. Kern, D. Q. Process Heat Transfer. McGraw-Hill Book Company, Inc. New York, 1950.

24. Kern, D. Q. and H. J. Karakas. "Mechanically Aided Heat Transfer." Chemical Engineering Progress Symposium Series, No. 29, Vol. 55, 1959, pp. 141-148.

25. Kestin, J. and L. N. Persen. "The Effect of a Standing Sound Field on a Slow Stream Discharged From a Porous Wall." Appl. Sci. Res., Sec. A, Vol. 4, 11, pp. 361-375.

26. Kinsler, L. E. and A. R. Frey. Fundamentals of Acoustics. 2nd Edition, John Wiley and Sons, Inc., 1962.

27. Koh, J. C. Y. "An Integral Treatment of Two Phase Boundary Layer in Film Condensation." ASME Paper No. 60-WA-253, 1960.

28. Koh, J. C. Y. "Film Condensation in a Forced-Convection Boundary-Layer Flow." International Journal of Heat and Mass Transfer, Vol. 5, 1962, pp. 941-954.

29. Koh, J. C. Y., E. M. Sparrow and J. P. Hartnett. "The Two-Phase Boundary Layer in Laminar-Film Condensation." International Journal of Heat and Mass Transfer, Vol. 2, 1961, pp. 69-82.

30. Kreith, Frank. Principles of Heat Transfer, 2nd Edition, International Textbook Company, Scranton, Pa., 1965.

31. Kunz, H. R. and S. Yerazunis. "An Analysis of Film Condensation, Film Evaporation, and Single-Phase Heat Transfer." ASME Paper No. 67-HT-1, 1967.

32. Kutateladze, S. S. Fundamentals of Heat Transfer. (Translated by Scripta Technica, Inc., Edited by R. D. Cess), Academic Press Inc., New York, 1963.

33. Larson, M. B. "A Study of the Effects of Ultrasonic Vibrations on Convective Heat Transfer in Liquids." Tech. Report No. 48, Department of Mechanical Engineering, Stanford University, 1960.

34. Lustenader, E. L., R. Richter and F. J. Neugebauer. "The Use of Thin Films for Increasing Evaporation and Condensation Rates in Process Equipment." Journal of Heat Transfer, Trans. ASME, Series C, Vol. 81, 1959, pp. 297-307.

35. McAdams, W. H. Heat Transmission, 3rd Edition, McGraw-Hill Book Company, Inc., New York, 1954.

36. McLachlan, N. W. Bessel Functions for Engineers, Oxford University Press, London, 1934.

37. Matin, S. A. "A Similarity Solution for the Condensate Film on a Vertical Flat Plate in Presence of a Variable Gravity Field." ASME Paper No. 65-AV-42, 1965.

38. Matthewson, W. F. and J. C. Smith. "Effect of Sonic Pulsation on Forced Convective Heat Transfer to Air and on Film Condensation of Isopropanol." Chemical Engineering Progress Symposium Series, No. 41, Vol. 59, 1963, pp. 173-179.

39. Minkowycz, W. J. and E. M. Sparrow. "Condensation Heat Transfer in the Presence of Non-Condensables, Interfacial Resistance, Superheating, Variable Properties, and Diffusion." International Journal of Heat and Mass Transfer, Vol. 9, 1966, pp. 1125-1144.

40. Nusselt, W. "Die Oberflachenkondensation des Wasserdampfes." Zeitschrift des Vereines Deutscher Ingenieure, Vol. 60, 1916, pp. 541-546.

41. Nusselt, W. "Die Oberflachenkondensation des Wasserdampfes." Zeitschrift des Vereines Deutscher Ingenieure, Vol. 60, 1916, pp. 569-575

42. Othmer, D. F. "The Condensation of Steam." Industrial and Engineering Chemistry, Vol. 21, No. 6, 1929, pp. 576-583.

43. Purdy, K. R., T. W. Jackson, D. A. Willoughby, H. Grady Keith, and C. E. Willbanks. "The Effect of a Resonant Acoustic Field on Laminar Flow in a Circular Tube." Report on Contract No. AF 33(616)-8396, Aeronautical Research Laboratories, Office of Aerospace Research, U. S. Air Force, October, 1963.

44. Purdy, K. R., T. W. Jackson, and C. W. Gorton. "Viscous Compressible Fluid Flow Under the Influence of a Resonant Acoustic Field." Journal of Heat Transfer, Tran. ASME, Series C, Vol. 86, 1964, pp. 97-106.

45. Reid, R. R. and T. K. Sherwood. The Properties of Gases and Liquids, 2nd Edition, McGraw-Hill Book Company, Inc., New York, 1966.

46. Rohsenow, W. M. "Heat Transfer and Temperature Distribution in Laminar-Film Condensation ." Transactions of the ASME, Vol. 78, 1956, pp. 1645-1648.

47. Rohsenow, W. M., J. H. Webber, and A. T. Ling. "Effect of Vapor Velocity on Laminar and Turbulent-Film Condensation." Transactions of the ASME, Vol. 78, 1956, pp. 1637-1643.

48. Rohsenow, W. M. and H. Y. Choi. Heat, Mass and Momentum Transfer, Prentice-Hall, Inc., Englewood Cliffs, New Jersey, 1961.

49. Schlichting, H. (Transl. J. Kestin). Boundary Layer Theory, 4th Edition, McGraw-Hill Book Company, Inc., 1960, pp. 224.

50. Shekriladze, I. G. and V. I. Gomelauri. "Theoretical Study of Laminar Film Condensation of Flowing Vapor." International Journal of Heat and Mass Transfer, Vol. 9, 1966, pp. 581-591.

51. Smith, J. C. and H. T. Robson. "Condensation of Benzene in the Presence of Air." Proceedings of the General Discussion on Heat Transfer, Institute of Mechanical Engineers, London, England, 1951, pp. 38-42.

52. Soehngen, E. E. and J. P. Holman. "Experimental Studies on the Interaction of Strong Sound Fields with Free Convection Boundary Layers." Aeronautical Research Laboratory Report 60-323, W. S. Air Force, Wright-Patterson Air Force Base, Ohio, 1960.

53. Soliman, M., J. R. Schuster, and P. J. Berenson. "A General Heat Transfer Correlation for Annular Flow Condensation." Journal of Heat Transfer, Trans. ASME, Series C, Vol. 90, 1968, pp. 267-276.

54. Sparrow, E. M. and E. R. G. Eckert. "Effect of Superheated Vapor and Noncondensable Gases on Laminar Film Condensation." American Institute of Chemical Engineers Journal, Vol. 7, 1961, pp. 473-477.

55. Sparrow, E. M. and J. L. Gregg. "A Boundary Layer Treatment of Laminar Film Condensation." Journal of Heat Transfer, Trans. ASME, Series C, Vol. 81, 1959, pp. 13-18.

56. Sparrow, E. M. and J. L. Gregg. "Laminar Condensation Heat Transfer on a Horizontal Cylinder." Journal of Heat Transfer, Trans. ASME, Series C, Vol. 81, 1959, pp. 291-296.

57. Sparrow, E. M. and S. H. Lin. "Condensation Heat Transfer in the Presence of a Noncondensable Gas." Journal of Heat Transfer, Trans. ASME, Series C, Vol. 86, 1964, pp. 430-436.

58. Sparrow, E. M. and R. Siegel. "Transient Film Condensation." Journal of Applied Mechanics, Trans. ASME, Series E, Vol. 86, 1959, pp. 120-121.

59. Toor, H. L. and J. M. Marchello. "Film Penetration Model for Mass and Heat Transfer." American Institute of Chemical Engineers Journal, Vol. 4, 1958, pp. 97.

60. Votta, F., Jr. and C. A. Walker. "Condensation of Vapor in the Presence of Noncondensing Gas." American Institute of Chemical Engineers Journal, Vol. 4, 1958, pp. 413-417.

61. Wilhelm, D. J. "Condensation of Metal Vapors: Mercury and the Kinetic Theory of Condensation." Ph. D. Dissertation, Ohio State University, 1964.

APPENDIX A

THE EFFECT OF TEMPERATURE DEPENDENT VISCOSITY ON LAMINAR CONDENSATION HEAT TRANSFER

Consideration of the fluid properties involved in laminar condensation heat transfer reveals that the liquid viscosity exhibits the greatest variation with temperature. In order to evaluate the effect of temperature dependent viscosity on condensation, Nusselt's model (shown in Figure 36) and assumptions as listed in Chapter II will be made--with the exception that viscosity is assumed a function of temperature only. The element of condensate considered for a force balance is also shown in Figure 36.

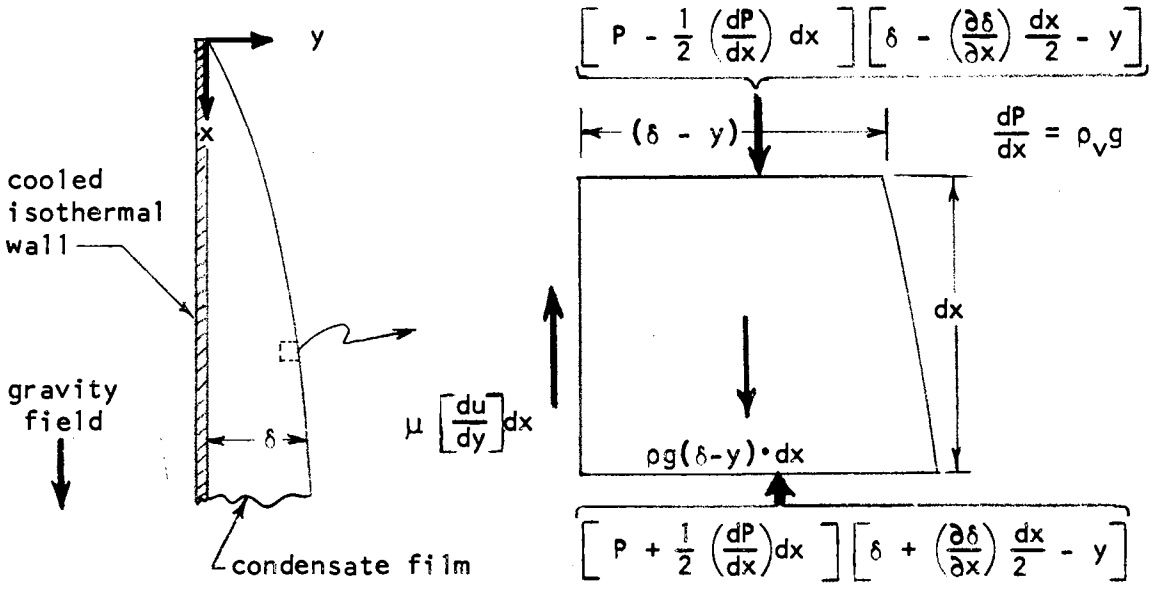

Figure 36. Nusselt's Model and Element Considered for a Force Balance.

Assuming a unit width normal to the plane of the model shown in Figure 36, a force balance can be written as

$$\left(\mu \frac{du}{dy}\right) dx + \rho_v g(\delta - y)\, dx = \rho g(\delta - y)dx, \tag{A.1}$$

when the higher order differential products are neglected.

A dimensionless length is defined by the relationship:

$$z \equiv \frac{y}{\delta(x)} \quad . \tag{A.2}$$

Viscosity can be expressed as a function of z, since temperature is assumed to be a function of z. Employing the definition of z, Equation A.1 can be rearranged and integrated to obtain

$$u = \int_{z=0}^{z} \frac{g\,(\rho - \rho_v)\delta^2}{\mu(z)} (1 - z)dz \tag{A.3}$$

A dimensionless viscosity can be defined in terms of a reference value of viscosity, $\mu_w = \mu(T_w)$:

$$\tilde{\mu}(z) = \frac{\mu_w}{\mu[T(z)]} \tag{A.4}$$

Since all other properties are assumed to be independent of temperature, Equation A.3 can be expressed

$$u(z) = C_u \delta^2(x)\, F_2(z) \tag{A.5}$$

where the terms are defined:

$$C_u \equiv \frac{g(\rho - \rho_v)}{\mu_w} \tag{A.6}$$

$$F_1(z) \equiv \tilde{\mu}(z)(1 - z) \tag{A.7}$$

$$F_2(z) \equiv \int_{z\,=\,0}^{z} F_1(z)\, dz \tag{A.8}$$

At any x distance along the plate, the mass flow rate per unit width can be expressed as

$$\Gamma(x) = \rho\delta \int_{z=0}^{z=1} u\,dz = \rho C_u \delta^3 \int_{z=0}^{z=1} F_2(z)\,dz = \rho C_u C_m \delta^3(x) \qquad (A.9)$$

where: $$C_m \equiv \int_{z=0}^{1} F_2(z)\,dz \qquad (A.10)$$

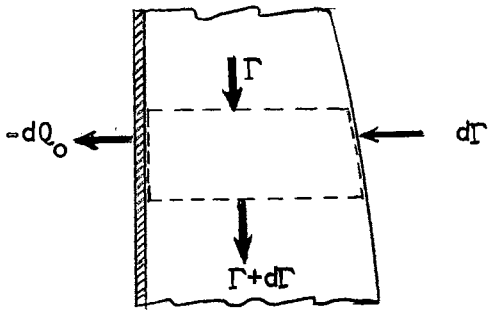

Figure 37. Condensate Element Model for Energy Analysis.

The energy analysis for the unit width element of condensate, enclosed by the dashed lines in Figure 37, yields

$$-dQ_o = k\left(\frac{dT}{dy}\right)_{y=0} dx = -\frac{\partial}{\partial\delta}\left[\int_{y=0}^{\delta} \rho c_p [T(y) - T_v]\, u\,dy\right] d\delta + h_{fg} d\Gamma \,.$$

Enthalpy has an assumed datum ($h = 0$) at $T = T_v$ arbitrarily established by the above expression. With the definition,

$$\Delta T \equiv T_v - T_w \qquad (A.11)$$

and

$$\theta \equiv \frac{T(z) - T_v}{\Delta T} \,, \qquad (A.12)$$

the energy analysis can be written in terms of the dimensionless z coordinate as

$$-dQ_o = \frac{\Delta T k}{\delta(x)}\left(\frac{d\theta}{dz}\right)_{z=0} \cdot dx = -\rho c_p C_u \Delta T \frac{\partial}{\partial\delta}\left[\delta^3 \int_0^1 \theta(z) F_2(z) dz\right] d\delta$$

$$+ h_{fg} d\Gamma(x) \quad . \tag{A.13}$$

The term $d\Gamma(x)$ can be evaluated from equation A.9 as

$$d\Gamma(x) = 3\rho C_u C_m \delta^2(x) d\delta \quad .$$

Define

$$C_T \equiv -\int_0^1 \theta(z) F_2(z)\, dz \quad , \tag{A.14}$$

and note that $\frac{\partial}{\partial\delta}\left[\delta^3(x) C_T\right] = -3C_T\delta^2(x)$.

Substitution of these relationships into Equation A.13 and rearrangement leads to

$$\frac{d\delta}{dx} = \frac{k\Delta T\left(\frac{d\theta}{dz}\right)_o}{3\rho C_u C_m h_{fg} \delta^3(x)\left(1 + \frac{C_T}{C_m}\frac{c_p \Delta T}{h_{fg}}\right)} \quad . \tag{A.15}$$

With the boundary condition of $\delta = 0$ at $x = 0$, the film thickness can be written:

$$\delta(x) = \left[\frac{4\Delta T k \mu_w x}{g\rho(\rho - \rho_v) h_{fg}}\right]^{1/4} \left[\left(\frac{d\theta}{dz}\right) \frac{1}{3C_m\left(1 + \frac{C_T}{C_m}\frac{c_p \Delta T}{h_{fg}}\right)}\right]^{1/4} \tag{A.16}$$

The first bracketed term is recognizable as the Nusselt result for film thickness, with viscosity evaluated at the wall temperature. The second term of Equation A.16 exists due to the viscosity variation with temperature.

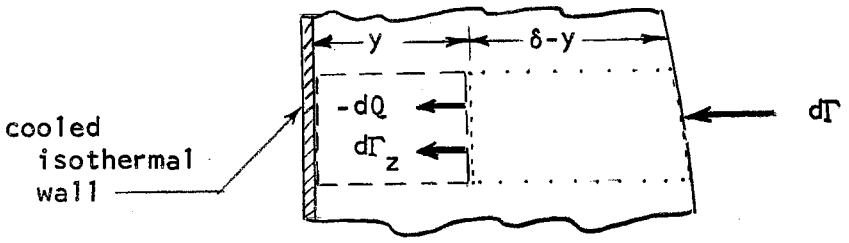

Figure 38. Schematic Model of the Cross-Flow Effect in Laminar Film Condensation.

Conservation of mass for the element enclosed by dashed lines in Figure 38 requires

$$d\Gamma_z = \frac{\partial}{\partial\delta}\left[\int_{y=0}^{y} \rho u dy\right] d\delta = \frac{\partial}{\partial\delta}\left[\rho C_u \delta^3 \int_{z=0}^{z} F_2(z)dz\right] d\delta \quad . \tag{A.17}$$

Define $$F_3(z) \equiv \int_0^z F_2(z)dz \quad , \tag{A.18}$$

and perform the indicated mathematical operation in Equation A.16 to obtain

$$d\Gamma_z = \rho C_u \delta^2(x)\left[3F_3(z) - zF_2(z)\right] d\delta \quad . \tag{A.19}$$

An energy analysis of the element enclosed by the dotted lines in Figure 38 can be shown to give the following equation:

$$-dQ = \frac{\Delta T k}{\delta(x)}\left(\frac{d\theta}{dz}\right) dx = -\frac{\partial}{\partial\delta}\left[\int_z^1 \rho c_p \Delta T \delta(x)\theta(z)u(z)dz\right] d\delta$$

$$-c_p \Delta T \theta(z) d\Gamma_z + h_{fg} d\Gamma \quad . \tag{A.20}$$

Utilization of Equations A.6, A.10, A.17 and A.19, the definition

$$F_4(z) \equiv \int_0^z \theta(z)F_2(z)dz \quad , \tag{A.21}$$

and noting that

$$\int_z^1 \theta(z)F_2(z)dz = \int_0^1 \theta(z)F_2(z)dz - \int_0^z \theta(z)F_2(z)dz$$

$$= -C_t - \int_0^z \theta(z)F_2(z)dz \quad ,$$

allows one to obtain the following expression from Equation A.20:

$$\frac{d\theta}{dz} = 3\frac{\rho C_u C_m h_{fg}\delta^3(x)}{k\,\Delta T}\left\{1 + \frac{C_T}{C_m}\frac{c_p\Delta T}{h_{fg}} + \frac{c_p\Delta T}{h_{fg}}\left[\frac{F_4(z) - \theta(z)F_3(z)}{C_m}\right]\right\}\frac{d\delta}{dx} \, . \tag{A.22}$$

Substituting from Eqaution A.15 for $\frac{d\delta}{dx}$ yields the result

$$\frac{d\theta}{dz} = \left(\frac{d\theta}{dz}\right)_o\left[1 + \frac{F_4(z) - \theta(z)F_3(z)}{C_m\bar{B}}\right], \tag{A.23}$$

where by definition:

$$\bar{B} \equiv \frac{h_{fg}}{c_p\Delta T}\left[1 + \frac{C_T}{C_m}\frac{c_p\Delta T}{h_{fg}}\right] \tag{A.24}$$

Integration of Equation A.23 with the boundary condition of $\theta(z) = 0$ at $z = 0$, yields

$$\theta(z) = \left(\frac{d\theta}{dz}\right)_o\left[z + \frac{F_5(z)}{C_m\bar{B}}\right] = 1 \quad ,$$

with the definition $F_5(z) \equiv \int_0^z [F_4(z) - \theta(z)F_3(z)]\,dz$. (A.25)

Also required is that $\theta(z) = 0$ where $z = 1$, so that

$$\theta(1) = 0 = \left(\frac{d\theta}{dz}\right)_o \left[1 + \frac{F_5(1)}{C_m \bar{B}} \right] - 1 \quad .$$

Consequently: $$\left(\frac{d\theta}{dz}\right)_o = \frac{1}{1 - (C_\theta / C_m \bar{B})} \quad , \tag{A.26}$$

and $$\theta(z) = \frac{1}{1 - \frac{C_\theta}{C_m \bar{B}}} \left[z + \frac{F_5(z)}{C_m \bar{B}} \right] - 1. \tag{A.27}$$

with C_θ defined by the relationship: $C_\theta \equiv -F_5(1)$.

The method of solving the equations for $u(z)$, $\Gamma(z)$, and $\theta(z)$ to determine the appropriate solution involves guessing an initial temperature profile. This assumed temperature profile allows the determination of the following terms:

$$\tilde{\mu}(z) = \frac{\mu_w}{\mu[T(z)]} \quad , \quad F_1(z) = \tilde{\mu}(z)(1 - z) \quad ,$$

$$F_2(z) = \int_0^z F_1(z)dz \quad , \quad F_3(z) = \int_0^z F_2(z)dz \quad ,$$

$$C_m = \int_0^1 F_2(z)dz \quad , \quad F_4(z) = \int_0^z \theta(z)F_2(z)dz \quad ,$$

$$C_T = -\int_0^1 \theta(z)F_2(z)dz \quad , \quad F_5(z) = \int_0^z [F_4(z) - \theta(z)F_3(z)]\, dz \quad ,$$

$$C_\theta = -F_5(1), \text{ and finally } \theta(z) = \frac{1}{1 - \frac{C_\theta}{C_m \bar{B}}} \left[z + \frac{F_5(z)}{C_m \bar{B}} \right] - 1 \quad .$$

If the calculated $\theta(z)$ agrees with the guessed $\theta(z)$, then the solution is completed. If the calculated $\theta(z)$ differs from the guessed $\theta(z)$,

then use of the calculated $\theta(z)$ as the next guessed $\theta(z)$ has been found to "converge" rapidly to an appropriate temperature profile.

This method of solution was used by Rohsenow (46) to obtain the effect of cross-flow in the condensate layer on the heat transfer coefficient. Rohsenow considered the viscosity to be a constant value, evaluated at $T_f = T_w + 1/4\ \Delta T$. Rohsenow attributes this particular value of temperature evaluation to T. B. Drew. It is the value obtained if viscosity is proportional to 1/T. As a check on the solution obtained, a constant viscosity was assumed, and the solution of the above equations gave the same first approximation as Rohsenow (46) obtained.

In order to establish the correction required to use the simpler results of Nusselt's theory, the above results can be rearranged in the following manner:

$$C_\delta \equiv \frac{\delta}{(\delta_w)_{Nu}} = \left[\left(\frac{d\theta}{dz}\right) \frac{1}{3C_m\left(1 + \frac{C_t}{C_m}\frac{c_p \Delta T}{h_{fg}}\right)} \right]^{1/4} \qquad (A.28)$$

$$C_\Gamma \equiv \frac{\Gamma}{(\Gamma_w)_{Nu}} = 3C_m C_\delta^{\,3} \ . \qquad (A.29)$$

The average heat transfer coefficient ($\bar{h}$) can be written as

$$\bar{h} = \frac{1}{L}\int_0^L -\left(\frac{dQ}{dx}\right)dx = \frac{1}{L}\int_0^L \frac{k}{C_\delta(\delta_w)_{Nu}} \cdot \left(\frac{d\theta}{dz}\right)_0 dx \ ,$$

by using Equations A. 13 and A.28. Therefore,

$$\bar{h} = \frac{(\bar{h}_w)_{Nu}\left(\frac{d\theta}{dz}\right)_0}{C_\delta}$$

and by definition, the heat transfer coefficient correction factor is

$$C_h \equiv \frac{\bar{h}}{(\bar{h}_w)_{Nu}} = \frac{\left(\frac{d\theta}{dz}\right)_o}{C_\delta} \quad . \tag{A.30}$$

The Nusselt results to be used in connection with these correction factors (C_δ, C_Γ, and C_h) are based on evaluating the viscosity at the wall temperature, with the other fluid properties evaluated as the average values. These can be expressed:

$$(\delta_w)_{Nu} = \left[\frac{4k\Delta Tx\mu_w}{g\rho(\rho - \rho_v)h_{fg}}\right]^{\frac{1}{4}}$$

$$(\Gamma_w)_{Nu} = \frac{1}{3}\frac{\rho(\rho \quad \rho_v)}{\mu_w}(\delta_w)^3_{Nu} = \frac{1}{3}\left[\frac{\rho(\rho - \rho_v)}{\mu_w}\left(\frac{4k\Delta Tx}{gh_{fg}}\right)^3\right]^{\frac{1}{4}}$$

$$(\bar{h}_w)_{Nu} = \frac{4}{3}\frac{k}{\delta_w(L)_{Nu}} = \frac{4}{3}\left[\frac{g\rho(\rho - \rho_v)k^3h_{fg}}{4\Delta TL\mu_w}\right]^{\frac{1}{4}}$$

The resulting equations can also be rearranged to determine the proper value of viscosity to use in the Nusselt equations to obtain results equivalent to the temperature dependent viscosity analysis.

Film thickness, $\mu_\delta = \mu_w C_\delta$ (A.31a)

Mass flow rate per unit width, $\mu_\Gamma = \frac{\mu_w}{C_\Gamma^4}$ (A.31b)

Heat Transfer coefficient, $\mu_h = \frac{\mu_w}{C_h^4}$ (A.31c)

For a specific viscosity-temperature relationship, the proper temperature for the viscosity determination could be obtained by determing the corresponding temperature for the viscosity term of interest (μ_δ, μ_Γ, or μ_h).

Since the solution was not obtained in closed form, it was necessary to assume some appropriate condensing situations to obtain numerical results. Reid and Sherwood (45) state: "At temperatures near or somewhat below the normal boiling point the behavior is well represented by the relation,

$$\mu = Ae^{B/T} \tag{A.32}$$

where A and B are positive." Absolute temperature (T) is used. Additionally, this relationship is recommended from the freezing point to slightly above the normal boiling point as the best simple temperature-liquid viscosity relationship. The constants A and B are fluid coefficients. This relationship was the one used in the numerical solutions.

The solutions required a relationship for $\tilde{\mu}(T) = \frac{\mu_w}{\mu(T)}$ so that the expression is reduced to:

$$\tilde{\mu}(T) = e^{B\left(\frac{1}{T_w} - \frac{1}{T(Z)}\right)} \quad .$$

The value of B was obtained by using the vapor temperature viscosity and wall temperature viscosity, $B = (T_v T_w/\Delta T)\ell n(\mu_w/\mu_v)$. Seven different fluids were used, with several values of T_w and ΔT, to obtain numerical solutions.

Properties were obtained from Kreith (30) and Reid and Sherwood (45). The equations were numerically integrated by use of the trapezoidal rule, and Simpson's rule. The numerical procedure was programmed in Fortran language for the SDS computer (Sigma 7) at Vanderbilt University. The results are tabulated in Table III. The computer program used for the numerical solution and one set of computer results are presented in Appendix B.

TABLE III

NUMERICAL COMPUTER SOLUTION RESULTS FOR THE EFFECT OF TEMPERATURE DEPENDENT VISCOSITY ON CONDENSATION HEAT TRANSFER

FLUID	T_w °R	ΔT °R	B °R	C_h	C_h ROHSENOW	C_Γ	C_δ	$-\theta_\delta$	$-\theta_\Gamma$	$-\theta_h$	$\frac{d\theta}{dz}_o$	100•MAX θ DEVIATION
	560	50	0	1.00828	1.00828	0.98995	0.99664	—	—	—	1.00489	0.22365
WATER	560	50	3075.2	1.03950	1.03900	1.02105	0.96652	0.715	0.827	0.675	1.00469	0.21680
	560	100	2971.1	1.07796	1.07626	1.04020	0.93622	0.707	0.829	0.664	1.00921	0.42828
COMMERCIAL	560	50	3868.7	1.06045	1.05970	1.01508	0.95375	0.684	0.902	0.608	1.01140	0.52711
ANILINE	560	100	3782.1	1.12168	1.11882	1.03048	0.91081	0.672	0.899	0.591	1.02164	1.00867
AMMONIA	440	70	407.3	1.03279	1.03306	0.98013	0.98168	0.454	1.502	-0.018	1.01387	0.63483
	440	100	406.4	1.05039	1.05084	0.97096	0.97180	0.460	1.445	-0.018	1.02077	0.95017
FREON-12	420	60	1014.3	1.05287	1.05315	0.98363	0.96679	0.585	1.186	0.347	1.01791	0.82159
	420	100	995.9	1.09103	1.09158	0.96829	0.94512	0.558	1.216	0.276	1.03115	1.42958
-BUTYL	560	50	4425.0	1.07082	1.06974	1.01636	0.94653	0.680	0.907	0.598	1.01357	0.62781
ALCHOL	560	100	4459.4	1.15215	1.14771	1.03145	0.89222	0.660	0.812	0.571	1.02797	1.30599
BENZENE	520	40	1968.8	1.03377	1.03380	0.99956	0.97592	0.656	1.006	0.527	1.03377	0.40817
	520	90	2010.9	1.07814	1.07801	0.99933	0.94585	0.647	1.004	0.512	1.01976	0.91165
	530	30	16534.9	1.13956	1.12452	1.12028	0.88126	0.709	0.739	0.699	1.00425	0.20172
GLYCERIN	510	50	14915.9	1.24993	1.20778	1.21801	0.80494	0.688	0.717	0.679	1.00612	0.29829
	510	70	12793.3	1.31532	1.25547	1.26992	0.76642	0.677	0.711	0.667	1.00809	0.39935

For comparison purposes, the equivalent C_h that would be obtained by using Rohsenow's (46) recommended corrections,

$$(C_h)_{\text{Rohsenow}} = \left[\tilde{\mu}\,(T_f) \left(1 + 0.68 \frac{c_p \Delta T}{h_{fg}}\right) \right]^{-\frac{1}{4}} , \qquad (A.34)$$

was also calculated and tabulated. The value of T_f used in Rohsenow's correction factor was $T_f = T_w + (\Delta T/4)$. The ratio of the caluclated velocity to a fictitious maximum Nusselt velocity was obtained by assuming the average velocity across the condensate thickness was the same. This ratio was reduced to the expression

$$\frac{u(z)}{\bar{u}(\delta)_{Nu}} = \frac{2F_2(z)}{3C_m} , \qquad (A.35)$$

where: $$\bar{u}(\delta)_{Nu} \equiv \frac{1}{2} C_u 3 \cdot C_m \delta^2(x) . \qquad (A.36)$$

The results for very viscous flow conditions shows that the velocity profile across the condensate is different from that predicted by Nusselt's theory. Two extreme cases are shown in Figure 39. The behavior of the velocity profile is as expected for the temperature dependent viscosity, although the results were not as pronounced for other less viscous fluids considered.

The results from the numerical computer solution are presented in Table III. It can be seen that Rohsenow's correction factors agrees very well with those calculated. The terms $-\theta_\delta$, $-\theta_\Gamma$ and $-\theta_h$ represent the value of θ that sould be used to determine μ_δ, μ_Γ, and μ_h. The column labeled 100* Max θ deviation represents 100 times the difference between the calculated θ and a linear θ. It was observed that the maximum calculated temperature deviation occurred for $0.6 \leq z \leq 0.66$ for all of the condensing situations considered. Obviously, the

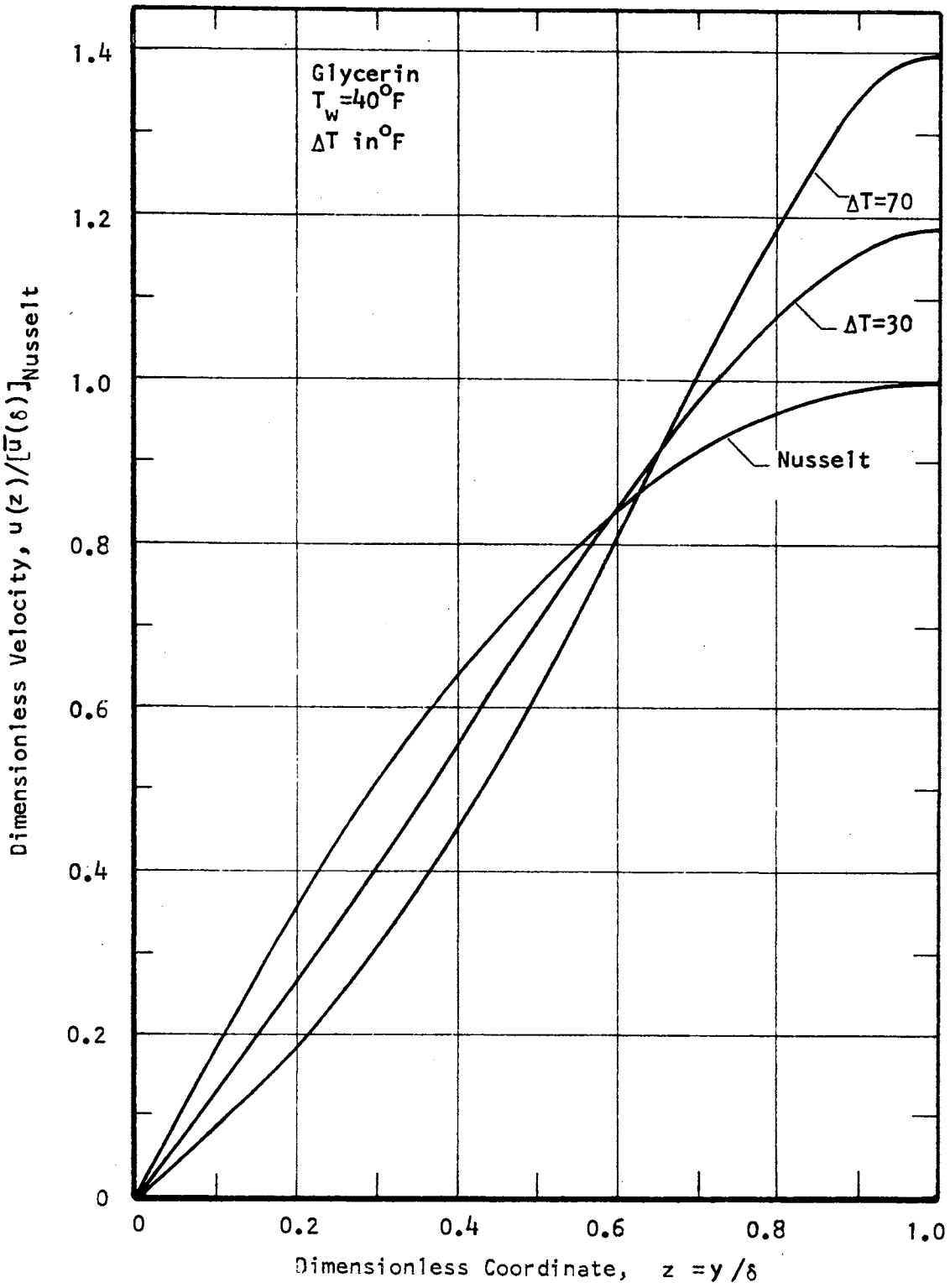

Figure 39. The Effect of Temperature Dependent Viscosity on the Velocity Profile of Laminar Condensate Film.

deviation from a linear profile is very small, even with the large variations of viscosity with temperature which were considered.

The results of the numerical solution indicate that the temperature profile is essentially linear for the condensing situations considered. Therefore, a reasonable approximation for the temperature function is:

$$\theta(z) = z - 1$$

The assumed viscosity temperature relationship is $\mu(T) = Ae^{B/T}$. With these two relations, then the dimensionless viscosity relationship can be written as a function of the dimensionless coordinate z:

$$\tilde{\mu}(z) = \exp\left[\frac{(B\Delta T/T_w^2)z}{1 + (\Delta T/T_w)\, z}\right]$$

This function is not too convenient for illustrating the viscosity temperature dependency effect. Since $\Delta T/T_w < 1$ for most cases, then the expression within the exponential brackets can be approximated as:

$$\frac{B\Delta T}{T_w^2}\, z\left(1 - \frac{\Delta T}{T_w}\, z\right)$$

The expression will yield a solution if the term $\exp\left(\frac{-B\Delta T^2}{T_w^3}\, z^2\right)$ is approximated as $\left(1 - \frac{B\Delta T^2}{T_w^3}\, z^2\right)$. The difficulty with this approximation is simply that a computer solution is again required, and the effect of viscosity is not entirely evident. If the approximation

$$\tilde{\mu}(z) = \exp\left[\left(\frac{B\Delta T}{T_w^2}\right)\left(1 - \frac{\Delta T}{2T_w}\right) z\right]$$

is used, then the resulting approximate solution agrees very well with the results of the numerical computer solution, and the viscosity temperature dependency effect is clarified.

Define:

$$\beta \equiv \frac{B\Delta T}{T_w^2}\left(1 - \frac{\Delta T}{2T_w}\right) \tag{A.37}$$

The results, with these assumptions, are presented below:

$$F_1(z) = \tilde{\mu}(z)(1 - z) = e^{\beta z}(1 - z)$$

$$F_2(z) \equiv \int_0^z F_1(z)dz = \frac{e^{\beta z}}{\beta}\left(1 + \frac{1}{\beta} - z\right) - \frac{1}{\beta}\left(1 + \frac{1}{\beta}\right)$$

$$F_3(z) = \int_0^z F_2(z)dz = -\frac{e^{\beta z}}{\beta^2}\left(1 + \frac{2}{\beta} - z\right) - \frac{1}{\beta}\left(1 + \frac{1}{\beta}\right)z - \frac{1}{\beta^2}\left(1 + \frac{2}{\beta}\right)$$

$$F_4(z) = \int_0^z \theta(z)F_2(z)dz = -\frac{e^{\beta z}}{\beta^2}\left[\left(1 + \frac{3}{\beta} + \frac{3}{\beta^2}\right) - \left(2 + \frac{3}{\beta}\right)z + z^2\right]$$
$$+ \frac{1}{\beta}\left(1 + \frac{1}{\beta}\right)\left(z - \frac{z^2}{2}\right) + \frac{1}{\beta^2}\left(1 + \frac{3}{\beta} + \frac{3}{\beta^2}\right)$$

$$F_5(z) = \int_0^z \left[F_4(z) - \theta(z)F_3(z)\right] dz = -\frac{e^{\beta z}}{\beta^4}\left[\left(1 + \frac{4}{\beta} - z\right)\right]$$
$$+ \frac{1}{6\beta}\left(1 + \frac{1}{\beta}\right)z^3 + \frac{1}{2\beta^2}\left(1 + \frac{2}{\beta}\right)z^2 + \frac{1}{\beta^3}\left(1 + \frac{3}{\beta}\right)z + \frac{1}{\beta^4}\left(1 + \frac{4}{\beta}\right)$$

$$C_m = \int_0^1 F_2(z)dz = F_3(1) = \frac{2}{\beta^3}\left[e^{\beta} - \left(1 + \beta + \frac{\beta^2}{2}\right)\right] \tag{A.38}$$

$$C_T = -\int_0^1 \theta(z)F_2(z) = -F_4(1) = \frac{3}{\beta^4}\left[e^{\beta} - \left(1 + \beta + \frac{\beta^2}{2} + \frac{\beta^3}{6}\right)\right] \tag{A.39}$$

$$C_\theta = -F_5(1) = +\frac{4}{\beta^5}\left[e^{\beta} - \left(1 + \beta + \frac{\beta^2}{2} + \frac{\beta^3}{6} + \frac{\beta^4}{24}\right)\right] \tag{A.40}$$

The quanities C_m, C_T and C_θ are the results which allow the determination of the correction coefficients, C_δ, C_T and C_h, for a given $\frac{c_p \Delta T}{h_{fg}}$. These previous results can be rewritten for reference

purposes:

$$\bar{B} = \frac{h_{fg}}{c_p \Delta T}\left[1 + \frac{C_T}{C_m}\frac{c_p \Delta T}{h_{fg}}\right] \tag{A.24}$$

$$\frac{d\theta}{dz}_0 = \frac{1}{1 - \frac{C_\theta}{C_m \bar{B}}} \tag{A.26}$$

$$C_\delta = \left[\frac{\left(\frac{d\theta}{dz}\right)_0}{3\left[C_m + C_T \frac{c_p \Delta T}{h_{fg}}\right]}\right]^{1/4} \tag{A.28}$$

$$C_T = 3 C_m C_\delta^3 \tag{A.29}$$

$$C_h = \frac{\left(\frac{d\theta}{dz}\right)_0}{C_\delta} \tag{A.30}$$

Thus it becomes evident that a proper determination of C_m, C_T and C_θ will allow an evaluation of the effect of temperature dependent viscosity on condensation heat transfer. Additionally, the results for $\beta < 1$ can be explored by expressing the previous results for C_m, C_T and C_θ, as series:

$$C_m = \frac{2}{\beta^3}\left(\frac{\beta^3}{6} + \frac{\beta^4}{24} + \frac{\beta^5}{120} + \frac{\beta^6}{720} + \cdots\right) = \frac{1}{3}\left(1 + \frac{\beta}{4} + \frac{\beta^2}{20} + \frac{\beta^3}{120} + \cdots\right)$$

$$C_T = \frac{3}{\beta^4}\left(\frac{\beta^4}{24} + \frac{\beta^5}{120} + \frac{\beta^6}{720} + \frac{\beta^7}{5040} + \cdots\right) = \frac{1}{8}\left(1 + \frac{\beta}{5} + \frac{\beta^2}{30} + \frac{\beta^3}{210} + \cdots\right)$$

$$C_\theta = + \frac{4}{\beta^5}\left(\frac{\beta^5}{120} + \frac{\beta^6}{720} + \frac{\beta^7}{5040} + \frac{\beta^8}{40320} + \cdots\right) = + \frac{1}{30}\left(1 + \frac{\beta}{6} + \frac{\beta^2}{42} + \frac{\beta^3}{336} + \cdots\right)$$

If viscosity is considered to be a linear function of inverse temperature ($\mu \propto \frac{1}{T}$), which corresponds to a small β value, then for $\beta << 1$, $\tilde{\mu}(z) = e^{\beta z} \rightarrow 1 + \beta z$.

The results can be approximated:

$$C_m \to \frac{1}{3}\left(1 + \frac{\beta}{4}\right), \quad C_T \to \frac{1}{8}\left(1 + \frac{\beta}{5}\right), \quad C_\theta \to + \frac{1}{30}\left(1 + \frac{\beta}{6}\right)$$

$$\left(\frac{d\theta}{dz}\right)_0 \to 1 + \frac{1}{10}\frac{c_p\Delta T}{h_{fg}}\left[1 - \frac{\beta}{12} - \frac{3}{8}\frac{c_p\Delta T}{h_{fg}}\left(1 - \frac{\beta}{20}\right)\right]$$

If $\frac{c_p\Delta T}{h_{fg}}$ is also assumed to be less than 1, then

$$\left(\frac{d\theta}{dz}\right)_0 \to 1 + \frac{c_p\Delta T}{10\, h_{fg}}$$

$$C_\delta \to 1 - \frac{c_p\Delta T}{4\, h_{fg}}\left(\frac{11}{40} - \frac{\beta}{60}\right)$$

$$C_\Gamma \to \left(1 + \frac{\beta}{4}\right)\left[1 - \frac{3}{4}\frac{c_p\Delta T}{h_{fg}}\left(\frac{11}{40} - \frac{\beta}{60}\right)\right]$$

$$C_h \to \left(1 + \frac{1}{10}\frac{c_p\Delta T}{h_{fg}}\right)\left[1 + \frac{c_p\Delta T}{4h_{fg}}\left(\frac{11}{40} - \frac{\beta}{60}\right)\right]$$

If $\frac{c_p\Delta T}{h_{fg}} = 0$, which corresponds to neglecting the condensate subcooling, then $C_\delta = 1$, $C_h = 1$ and $C_\Gamma = 1 + \frac{\beta}{4}$. This last result corresponds to evaluating the viscosity at $T_f = T_w + \frac{\Delta T}{4}$, which is T. B. Drew's recommendation. If viscosity is assumed constant ($\beta = 0$), the heat transfer correction term (for small $\frac{c_p\Delta T}{h_{fg}}$) becomes:

$$C_h = 1 + \frac{c_p\Delta T}{h_{fg}}\left(\frac{1}{10} + \frac{11}{160}\right) = 1 + 0.16875\,\frac{c_p\Delta T}{h_{fg}}$$

$$C_h = \left[1 + 0.675\,\frac{c_p\Delta T}{h_{fg}}\right]^{1/4}$$

This result agrees with that of Bromley (6) and Rohsenow (46), as it should. The recommendation that h_{fg} be replaced by $h'_{fg} = h_{fg}\left[1 + \frac{3}{8}\frac{c_p\Delta T}{h_{fg}}\right]$ can be accounted for by the assumptions of a linear temperature profile,

constant viscosity, and a finite specific heat. With these assumptions, $\left(\frac{d\theta}{dz}\right)_0 = 1$, $C_m = \frac{1}{3}$ and $C_T = \frac{1}{8}$; consequently,

$$C_\delta = \left[\frac{\left(\frac{d\theta}{dz}\right)_o}{3\left[C_m + C_T \frac{c_p \Delta T}{h_{fg}}\right]}\right]^{1/4} = \left[\frac{1}{1 + \frac{3}{8}\frac{c_p \Delta T}{h_{fg}}}\right]^{1/4} .$$

Thus by considering only the effect of the condensate specific heat having a finite value, the Nusselt results should be multiplied by the correction terms:

$$C_T = 3C_m C_\delta^3 = \left[\frac{1}{1 + \frac{3}{8}\frac{c_p \Delta T}{h_{fg}}}\right]^{\frac{3}{4}}$$

$$C_h = \frac{\left(\frac{d\theta}{dz}\right)_o}{C_\delta} = \left[1 + \frac{3}{8}\frac{c_p \Delta T}{h_{fg}}\right]^{\frac{1}{4}} .$$

These corrections are acheived in the practical manner of simply replacing h_{fg} by $h'_{fg} = h_{fg}\left(1 + \frac{3}{8}\frac{c_p \Delta T}{h_{fg}}\right)$ --Rohsenow's recommendation.

Another consideration that is possible with the approximate model is that of the effect of a large viscosity variation on the temperature profile. The asymptotic values of Equations A.38, A.39 and A.40 for large β are:

for $\beta \to \infty$ $\quad C_m \to \frac{2e^\beta}{\beta^3}$

$$C_T \to \frac{3e^\beta}{\beta^4}$$

$$C_\theta \to \frac{4e^\beta}{\beta^5} .$$

Consequently:

$$\overline{B} \to \frac{h_{fg}}{c_p \Delta T}\left(1 + \frac{3}{2}\beta \frac{c_p \Delta T}{h_{fg}}\right)$$

$$\frac{C_\theta}{C_m \overline{B}} \to 0$$

$$\left(\frac{d\theta}{dz}\right)_o \to 1$$

$$F_5(z) \to -\frac{e^{\beta z}}{\beta^4}\left[1 + \frac{4}{\beta} - z\right] .$$

From Equation A.27:

$$\theta(z) = \frac{1}{1 - \frac{C_\theta}{C_m \overline{B}}}\left[z + \frac{F_5(z)}{C_m \overline{B}}\right] - 1 .$$

Considering the term

$$\frac{F_5(z)}{C_m \overline{B}} = \frac{-\frac{e^{\beta z}}{\beta^4}\left(1 + \frac{4}{\beta} - z\right)\frac{c_p \Delta T}{h_{fg}}}{\frac{2e^{\beta}}{\beta^3}\left(1 + \frac{3}{2}\beta \frac{c_p \Delta T}{h_{fg}}\right)}$$

$$\frac{F_5(z)}{C_m \overline{B}} = -\frac{\frac{e^{\beta(z-1)}}{2\beta}\left(1 + \frac{4}{\beta} - z\right)\frac{c_p \Delta T}{h_{fg}}}{\left(1 + \frac{3}{2}\beta \frac{c_p \Delta T}{h_{fg}}\right)}$$

and since $0 \leq z \leq 1$, $\frac{F_5(z)}{C_m \overline{B}} \to 0$.

Consequently, the asymptotic approximation solution for $\beta \to \infty$ predicts a linear temperature profile.

$$\theta(z) = z - 1$$

A comparison of the results predicted by Equations A.38, A.39 and A.40 with the numerical computer solution is presented in Figure 40. The agreement is quite good, consequently the values for C_m, C_T and C_θ predicted by the approximate solution were used to determine the heat transfer correction factor for a range of the dimensionless viscosity parameter β and for a range of $\frac{c_p \Delta T}{h_{fg}}$. A comparable Rohsenow heat transfer factor was also calculated with $\frac{c_p \Delta T}{h_{fg}} = 0.2$ for comparison purposes. The Rohsenow factor was expressed as

$$\left(C_h\right)_{\text{Rohsenow}} = \left[e^{\beta/4}\left(1 + 0.68 \frac{c_p \Delta T}{h_{fg}}\right) \right]^{1/4} \qquad (A.41)$$

These calculated results are shown in Figure 41.

The range of validity for assuming that viscosity is a linear function of inverse temperature is greater than expected, due primarily to the fact that the condensing heat transfer coefficient is a function of $\left[\frac{1}{\mu}\right]^{1/4}$. For values of $\beta > 1.1$, the effect of considering the viscosity temperature dependency begins to show up. As can seen in Figure 40, most of the fluids and condensing conditions considered involved a value of $\beta < 2$. Consequently, no marked difference between the present solution and earlier predictions is observable. As is obvious from Figure 41, the effect of viscosity can become significant for high values of β.

This analytical investigation of the effect of viscosity on laminar condensation heat transfer has yielded an approximate model which has asymptotic solutions (for $\beta \to 0$) that agree with several previously

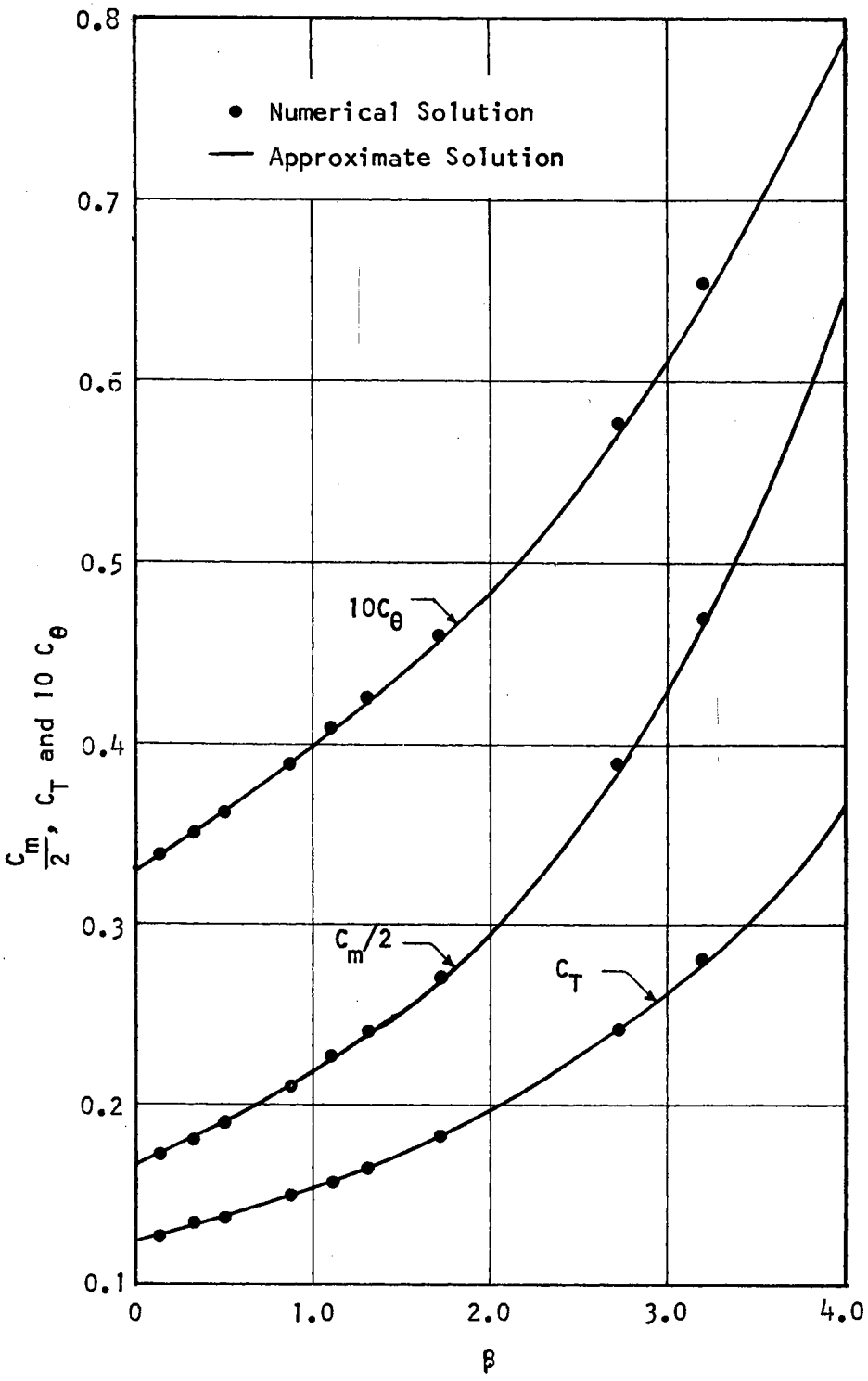

Figure 40. Comparison of Dimensionless Results from the Numerical and Approximate Solutions for the Effect of Temperature Dependent Viscosity on Laminar Condensation Heat Transfer.

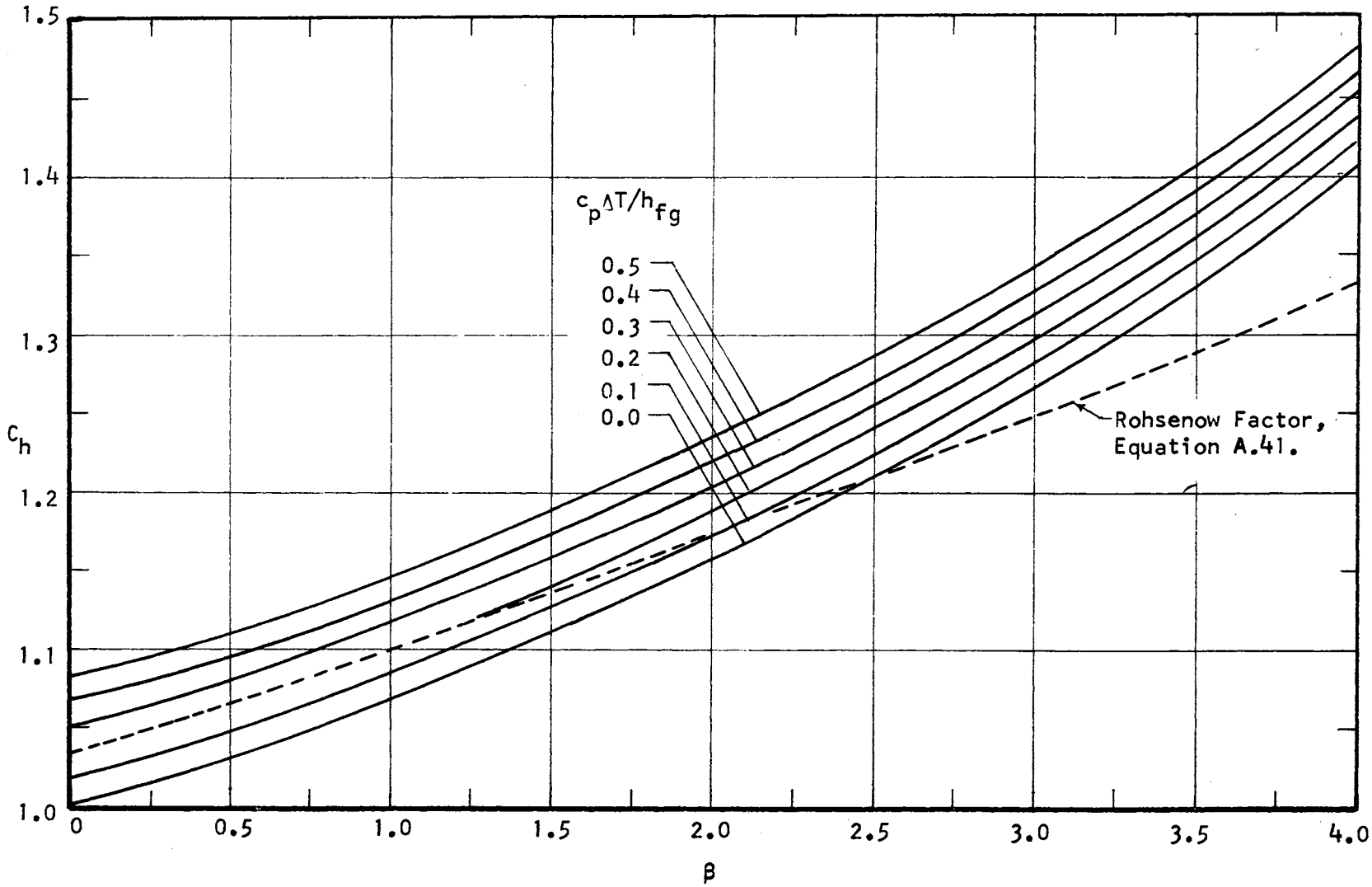

Figure 41. Condensation Heat Transfer Coefficient Correction Factor for Fluids with a Temperature Dependent Viscosity.

proposed models. The approximate solution has reinforced the validity of a linear temperature profile assumption, even under conditions of large viscosity variation with temperature. The range of validity for the simplifying assumption of $\mu \propto \frac{1}{T}$ (which allows an evaluation of viscosity at $T_f = T_w + \Delta T/4$) has been shown. Heat transfer coefficient factors have been presented which allow the use of the simpler Nusselt analysis.

APPENDIX B

SDS SIGMA 7 COMPUTER PROGRAM:: NUMERICAL SOLUTION FOR THE EFFECT OF TEMPERATURE DEPENDENT VISCOSITY ON LAMINAR CONDENSATION HEAT TRANSFER

```
C     NUMERICAL SOLUTION FOR THE EFFECT OF TEMPERATURE DEPENDENT VIS-
      COSITY ON LAMINAR CONDENSATION HEAT TRANSFER
      IMPLICIT REAL*8(A-H), REAL*8(O-Z)
      DIMENSION F(5,501),Z(501),THETA(501),TH(3)
      READ(1,100)MITER,INCR, LOW,MAX,DZ,F(1,1),F(2,1),F(3,1),F(4,1),
     1F(5,1),THETA(1),Z(1)
      DO 10 I=2,501
   10 Z(I)=Z(I-1)+DZ
   11 READ(1,101)NSUBS,NDIV,TS,TW,DLT,VISCS,VISCW,C,HFG
      IF(NSUBS-20)12,12,120
   12 NCOUN=0
      WRITE(5,508)
      B=(TS*TW/DLT)*DLOG(VISCW/VISCS)
      CDTOH=C*DLT/HFG
      BOTW=B/TW
      BDTW1=B*DLT/TW/100.
      BDTW2=B*DLT/(TW*TW)
      TSODT=TS/DLT
      DTDZ0=1.
      ROHSN=((1.+.68*CDTOH)/DEXP(BOTW*.25/(.75-TSODT)))**.25
C     INITIAL TEMPERATURE DISTRIBUTION GUESS
      DO 20 I=2,NDIV
   20 THETA(I)=-1.+1.2*Z(I)*(1.-Z(I))
   21 DO 30 I=2,NDIV
   30 F(1,I)=(1.-Z(I))*DEXP(BOTW*((THETA(I)+1.)/(THETA(I)+TSODT)))
      F(2,2)=(F(1,1)+F(1,2))*DZ/2.
      F(3,2)=F(2,2)*DZ/2.
      F(4,2)=(F(2,2)*THETA(2))*DZ/2.
      F(5,2)=(F(4,2)-THETA(2)*F(3,2))*DZ/2.
      DO 40 I=2,3
      DO 40 J=3,NDIV
   40 F(I,J)=(DZ/3.)*(F(I-1,J-2)+4.*F(I-1,J-1)+F(I-1,J))+F(I,J-2)
      DO 50 J=3,NDIV
      F(4,J)=F(4,J-2)+(THETA(J-2)*F(4,J-1)+F(4,J)-THETA(J-2*F(3,J-2)
     4J)*F(2,J))*DZ/3.
   50 F(5,J)=F(5,J-2)+(F(4,J-2)+4.*F(4,J-1)+F(4,J)-THETA(J-2)*F(3,J-2)-
     54.*THETA(J-1)*F(3,J-1)-THETA(J)*F(3,J))*DZ/3.
      CM=F(3,NDIV)
      CT=-F(4,NDIV)
      CTOCM=CT/CM
      BT=(1./CDTOH)+CTOCM
      CMBT=1./(CM*BT)
      DTDZ1=DTDZ0
      DTDZ0=1./(1.+F(5,NDIV)*CMBT)
      DO 60 I=2,NDIV
   60 THETA(I)=DTDZ0*(Z(I)+CMBT*F(5,I))-1.
      WRITE(5,507)CM,CT,CTOCM,CMBT,DTDZ0
      NCOUN=NCOUN+1
      IF(NCOUN-MITER)61,62,62
   61 THETF=DABS(DTDZ0-DTDZ1)
      IF(THETF-.00001)62,21,21
   62 TMU=1.+CTOCM*CDTOH
```

```
      DLCO=DTDZO/(3.*CM*TMU)
      DLCOF=DLCO**.25
      CMDOT=3.*CM*(DLCOF**3)
      HTCOF=DTDZO/DLCOF
   63 ADEL=DLOG(1./DLCO)/BOTW
      AHTC=4.*DLOG(DTDZO)/BOTW+ADEL
      AMAS=(DLOG(3.*CM)+3.*DLOG(DTDZO/TMU))/BOTW
      TH(1)=(ADEL*TSODT-1.)/(1.-ADEL)
      TH(2)=(AMAS*TSODT-1.)/(1.-AMAS)
      TH(3)=(AHTC*TSODT-1.)/(1.-AHTC)
      LOC=1
      F1MAX=1
   66 DO 68 I=LOW,MAX
      IF(F(1,I)-F1MAX)68,67,67
   67 F1MAX=F(1,I)
      LOC=1
   68 CONTINUE
      IF(LOC-251)72,71,72
   71 LOW=251
      MAX=501
      GO TO 66
   72 LOW=2
      MAX=251
      IF(B-10,)73,73,74
   73 DO 74 I=1,3
      TH(I)=-1.0
   74 CONTINUE
      CVREL=2./(3.*CM)
      WRITE(5,503)
      WRITE(5,504)NSUBS,TS,TW,DLT,VISCS,VISCW,HFG,C,CDTOH,BDTW1,BDTW2,
     4B,BOTW
      WRITE(5,505)LOC
      WRITE(5,506)NCOUN,ROHSN,HTCOF,DTDZO,CMDOT,DLCOF,F1MAX,TH(1),TH(2),
     6TH(3),THETF
      WRITE(5,501)
      DO 80 I=1,NDIV,INCR
      VRENU=F(2,I)*CVREL
      DLINT=L)).*(THETA(I)-Z(I)+1.)
   80 WRITE(5,502)Z(I),THETA(I),F(1,I),F(2,I),F(3,I),F(4,I),F(5,I),
     7DLINT,VRENU
      GO TO 11
  120 CALL EXIT
  100 FORMAT(4I4,F9.0,7F5.0)
  101 FORMAT(2I5,7F10.0)
  501 FORMAT(6H1 Z(I),2X8HTHETA(I),2X6HF(1,I),4X6HF(2,I),4X6HF(3,I),
     14X6HF(4,I),4X6HF(5,I),4X7HDEVLINT,3X10HVEL/VELNUS)
  502 FORMAT(1XF5.2,8(F10.5))
  503 FORMAT(42HOSUBS  TS   TW   DLT   VISS   VISW   HFG  ,38HC  CDTOH
     3 BD/TW B/TW2   B    B/TW   )
  504 FORMAT(I4,6F6.0,4F6.3,F8.1,F7.3)
  505 FORMAT(47H IT ROHSN  HTCOF  DTDZO   CMDOT  DLCOF  F(1,,I3,27H)
     5TH(1) TH(2) TH(3)  THETF)
```

```
  506 FORMAT(I3,6F8.5,3F6.3,F9.6)
  507 FORMAT(4H CM=,F8.5,4H CT=,F8.5,7H CT/CM=,F8.5,7H CM*KT=,F8.5,7H DT
     7DZ0=,E14.8)
  508 FORMAT(1H1)
      END
```

One set of results from the numerical solution corresponding to the condensation of saturated glycerin vapor at 70°F, on a constant temperature wall at 40°F is shown below and in Table IV.

```
CM=0.46212 CT=0.36516 CT/CM=0.79020 CM*KT=0.10612 DTDZ0=0.99896518E+00
CM=0.54420 CT=0.18479 CT/CM=0.33956 CM*KT=0.09215 DTDZ0=0.10042525E+01
CM=0.54562 CT=0.18403 CT/CM=0.33730 CM*KT=0.09192 DTDZ0=0.10042482E+01

SUBS TS   TW  DLT VISS VISW  HFG     C  CDTO  BD/TW B/TW2    B    B/TW
 7  560. 530. 30. 188. 1000. 344. 0.585 0.051 9.359 1.766 16534.9 31.198
IT  ROHSN  HTCOF    DTDZ0   CMDOT   DLCOF F(1,,1)  TH(1)  TH(2)  TH(3)
 3 1.2452 1.13956 1.00425 1.12028 0.88126 1.20048 -0.709 -0.739 -0.699
  THETF
0.000004
```

TABLE IV

RESULTS FOR Z DEPENDENT FUNCTIONS INVOLVED IN THE NUMERICAL SOLUTION OF THE EFFECT OF TEMPERATURE DEPENDENT VISCOSITY ON CONDENSATION HEAT TRANSFER

Z(I)	THETA(I)	F(1,I)	F(2,I)	F(3,I)	F(4,I)	F(5,I)	DEVLINT	VEL/VELN
.00	-1.00000	1.00000	0.00000	0.00000	0.00000	0.00000	0.00000	0.00000
.02	-0.97992	1.01534	0.02015	0.00020	-0.00020	-0.00000	0.00850	0.02463
.04	-0.95983	1.03041	0.04061	0.00081	-0.00079	-0.00000	0.01699	0.04962
.06	-0.93975	1.04516	0.06137	0.00183	-0.00175	-0.00000	0.02548	0.07498
.08	-0.91966	1.05956	0.08242	0.00326	-0.00309	-0.00000	0.03397	0.10070
.10	-0.89958	1.07356	0.10375	0.00513	-0.00478	-0.00000	0.04244	0.12676
.12	-0.87949	1.08712	0.12536	0.00742	-0.00682	-0.00001	0.05090	0.15317
.14	-0.85941	1.10020	0.14723	0.01014	-0.00919	-0.00002	0.05932	0.17989
.16	-0.83932	1.11275	0.16936	0.01331	-0.01188	-0.00003	0.06771	0.20693
.18	-0.81924	1.12471	0.19174	0.01692	-0.01487	-0.00005	0.07605	0.23427
.20	-0.79916	1.13603	0.21434	0.02098	-0.01815	-0.00007	0.08433	0.26190
.22	-0.77907	1.14666	0.23717	0.02549	-0.02172	-0.00010	0.09253	0.28979
.24	-0.75899	1.15654	0.26021	0.03047	-0.02554	-0.00014	0.10063	0.31793
.26	-0.73891	1.16560	0.28343	0.03590	-0.02961	-0.00020	0.10862	0.34631
.28	-0.71884	1.17378	0.30682	0.04180	-0.03391	-0.00027	0.11648	0.37489
.30	-0.69876	1.18102	0.33037	0.04818	-0.03843	-0.00035	0.12418	0.40367
.32	-0.67868	1.18723	0.35406	0.05502	-0.04314	-0.00046	0.13170	0.43261
.34	-0.65861	1.19235	0.37786	0.06234	-0.04803	-0.00059	0.13902	0.46169
.36	-0.63854	1.19629	0.40174	0.07014	-0.05309	-0.00074	0.14611	0.49087
.38	-0.61847	1.19898	0.42570	0.07841	-0.05829	-0.00092	0.15294	0.52014
.40	-0.59841	1.20033	0.44969	0.08716	-0.06361	-0.00113	0.15948	0.54946
.42	-0.57834	1.20025	0.47370	0.09640	-0.06905	-0.00138	0.16569	0.57880
.44	-0.55828	1.19864	0.49760	0.10611	-0.07457	-0.00167	0.17155	0.60811
.46	-0.53823	1.19542	0.52164	0.11631	-0.08015	-0.00199	0.17701	0.63737
.48	-0.51818	1.19046	0.54550	0.12698	-0.08579	-0.00237	0.18205	0.66652
.50	-0.49813	1.18368	0.56924	0.13812	-0.09145	-0.00279	0.18661	0.69553
.52	-0.47809	1.17496	0.59283	0.14975	-0.09712	-0.00328	0.19066	0.72436
.54	-0.45806	1.16418	0.61623	0.16184	-0.10278	-0.00382	0.19416	0.75294
.56	-0.43803	1.15122	0.63939	0.17439	-0.10841	-0.00442	0.19706	0.78124
.58	-0.41801	1.13596	0.66226	0.18741	-0.11398	-0.00510	0.19931	0.80919
.60	-0.39799	1.11827	0.68481	0.20088	-0.11947	-0.00585	0.20088	0.83674
.62	-0.37798	1.09800	0.70698	0.21480	-0.12487	-0.00668	0.20169	0.86382
.64	-0.35798	1.07503	0.72871	0.22916	-0.13016	-0.00760	0.20172	0.89038
.66	-0.33799	1.04920	0.74996	0.24395	-0.13530	-0.00861	0.20090	0.91634
.68	-0.31801	1.02036	0.77066	0.25915	-0.14029	-0.00972	0.19918	0.94163
.70	-0.29803	0.98834	0.79075	0.27477	-0.14510	-0.01093	0.19650	0.96618
.72	-0.27807	0.95300	0.81017	0.29078	-0.14971	-0.01225	0.19281	0.98991
.74	-0.25812	0.91415	0.82885	0.30717	-0.15410	-0.01368	0.18805	1.01273
.76	-0.23818	0.87162	0.84671	0.32393	-0.15826	-0.01524	0.18216	1.03456
.78	-0.21825	0.82522	0.86369	0.34103	-0.16216	-0.01693	0.17507	1.05530

TABLE IV (Continued)

Z(I)	THETA(I)	F(1,I)	F(2,I)	F3,I)	F(4,I)	F(5,I)	DEVLINT	VEL/VELN
.80	-0.19833	0.77476	0.87969	0.35847	-0.16579	-0.01875	0.16673	1.07486
.82	-0.17843	0.72005	0.89465	0.37621	-0.16914	-0.02072	0.15708	1.09313
.84	-0.15854	0.66088	0.90847	0.39425	-0.17217	-0.02284	0.14604	1.11001
.86	-0.13866	0.59704	0.92105	0.41254	-0.17489	-0.02511	0.13355	1.12539
.88	-0.11880	0.52831	0.93231	0.43108	-0.17728	-0.02755	0.11955	1.13915
.90	-0.09896	0.45447	0.94215	0.44983	-0.17932	-0.03015	0.10397	1.15117
.92	-0.07913	0.37527	0.95046	0.46875	-0.18100	-0.03294	0.08674	1.16132
.94	-0.05932	0.29048	0.95712	0.48783	-0.18232	-0.03591	0.06780	1.16947
.96	-0.03953	0.19984	0.96204	0.50703	-0.18327	-0.03908	0.04708	1.17547
.98	-0.01976	0.10311	0.96508	0.52630	-0.18384	-0.04245	0.02450	1.17919
1.00	-0.00000	0.00000	0.96612	0.54562	-0.18403	-0.04602	0.00000	1.18046

APPENDIX C

CALIBRATION CURVES FOR MEASURING DEVICES AND EQUATIONS FROM LEAST SQUARES METHOD OF CURVE FITTING

The temperature (T) in degrees Fahrenheit corresponding to an experimentally obtained ice-point reference junction thermocouple reading (R_t) was calculated with the following equation:

$$T = 32.183 + 46.4846\ R_t - 1.24977\ R_t^2 + .049044\ R_t^3$$

This equation was obtained by applying the method of least squares to the data for Copper-Constantan thermocouples tabulated by Leeds and Northrup Company, as taken from the National Bureau of Standards Circula No. 561. The rms error for this equation is 0.000095 over the range of 70 F to 240 F.

The calibration curves and corresponding equations obtained by applying the method of least squares for the two flow measuring devices, and for the static pressure transducer are presented in Figures 42, 43 and 44.

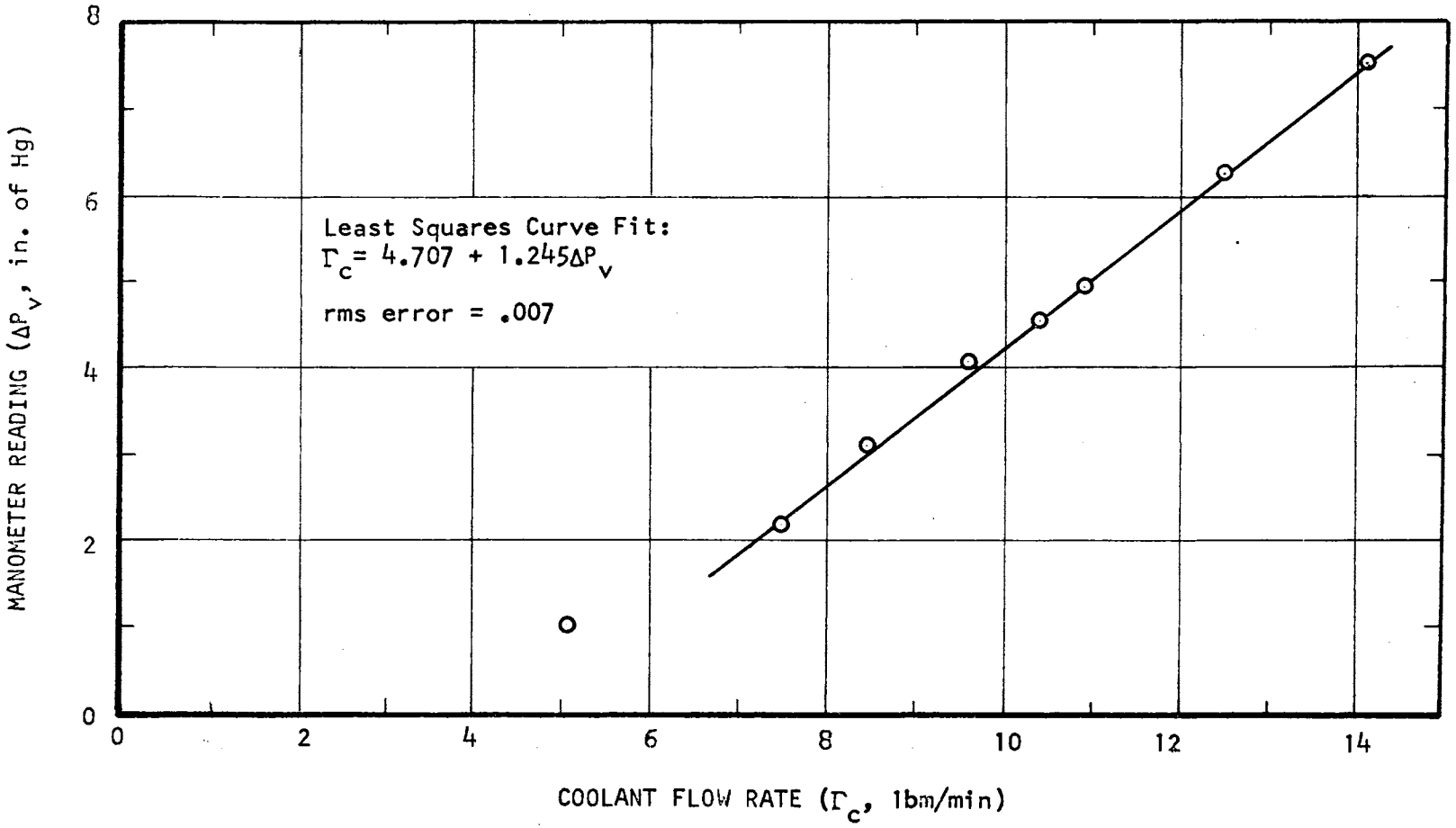

Figure 42. Calibration Curve for the Metering Venturi Used to Measure Coolant Flow Rate.

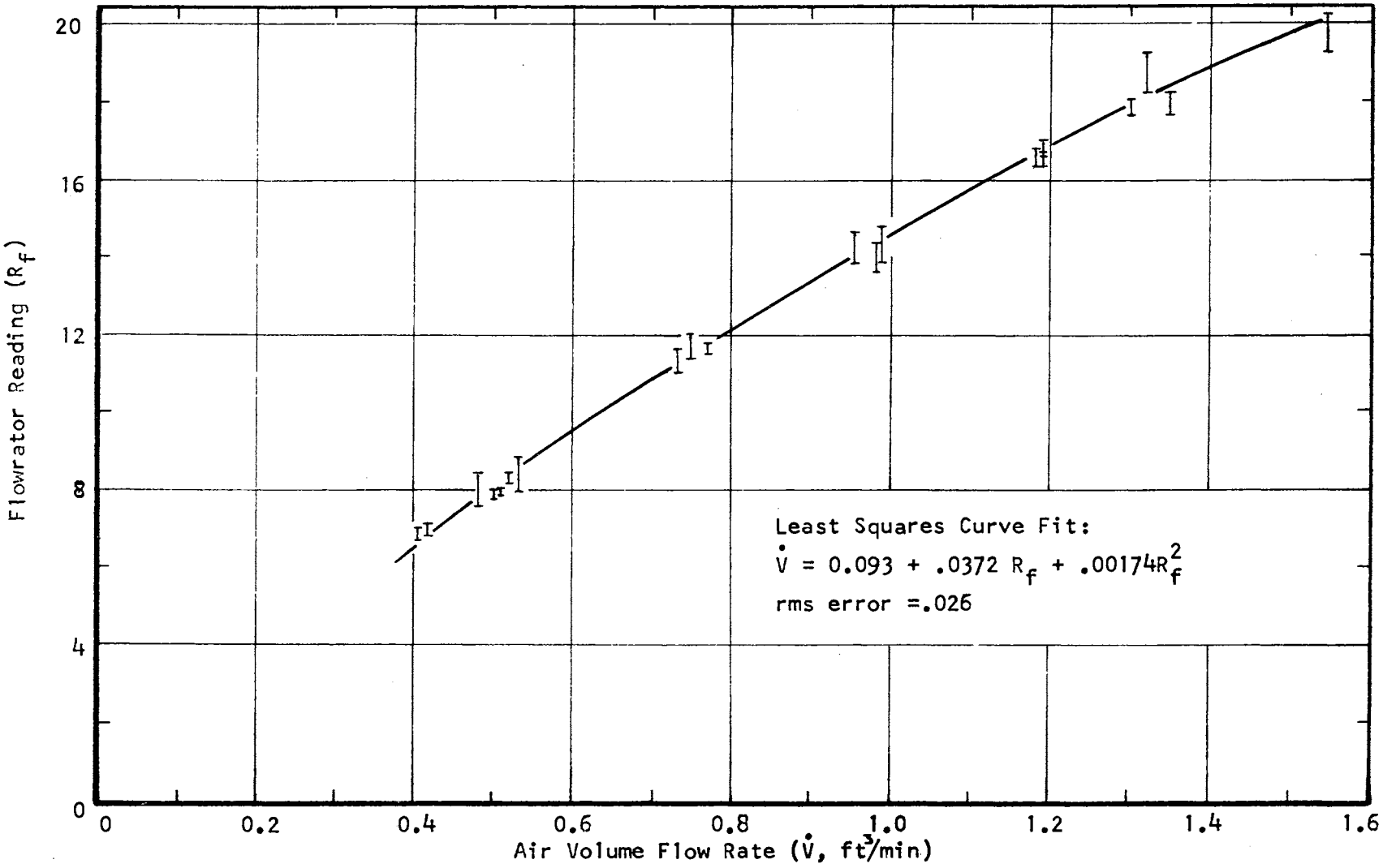

Figure 43. Calibration Curve for the Flowrator Arrangement used to Measure Air Flow Rate.

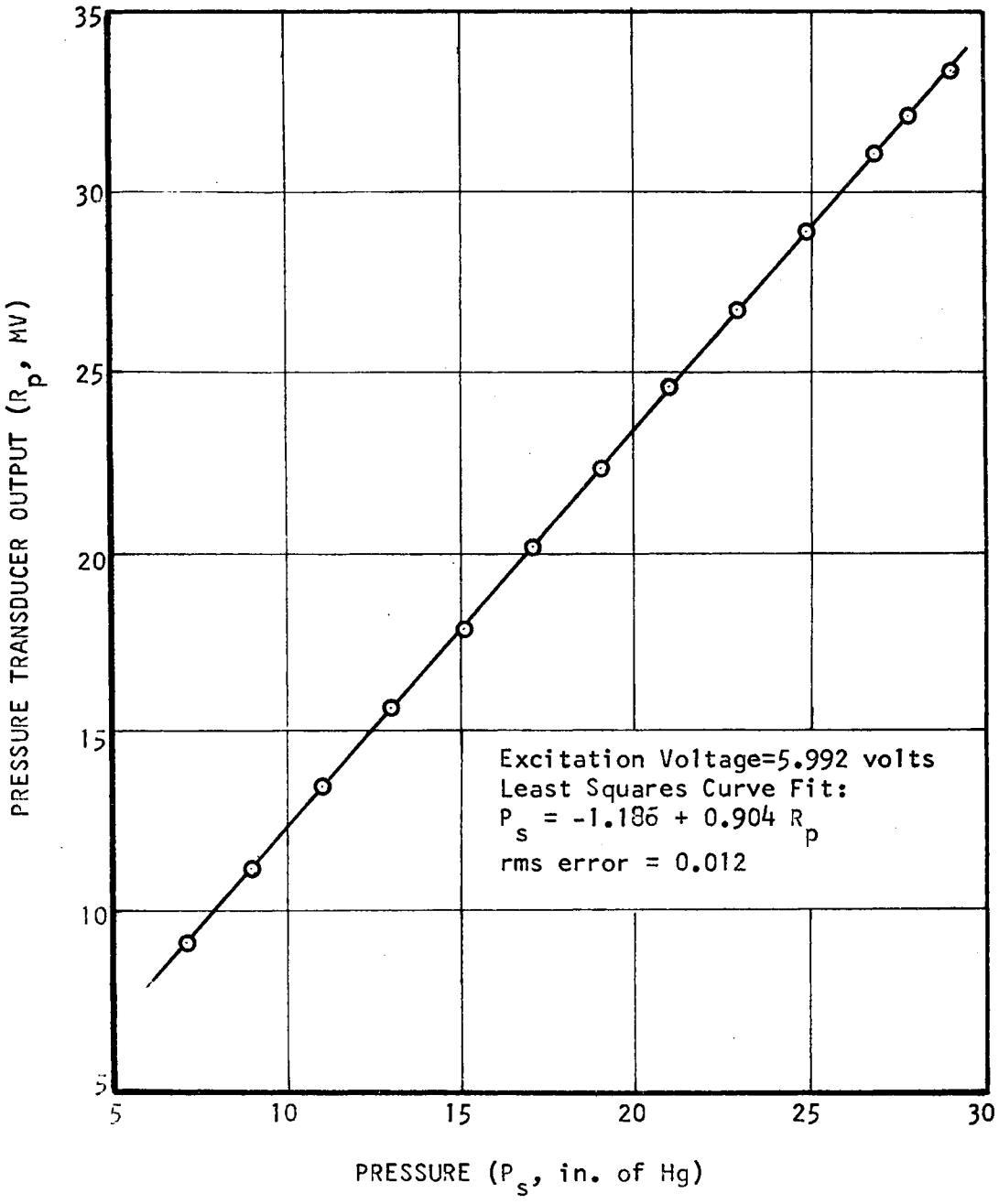

Figure 44. Static Pressure Transducer Calibration Curve.

VITA

Robert Lee Lott, Jr.

Candidate for the Degree of

Doctor of Philosophy

Thesis: THE EFFECT OF VAPOR-BORNE SOUND ON CONDENSATION HEAT TRANSFER

Major Field: Mechanical Engineering

Biographical:

Personal Data: Born in Dallas, Texas, September 27, 1936, the son of Robert Lee and Thelma Lucille Lott. Married Peggy Dee Gillespie, December 26, 1958, in Camden, Arkansas. The father of four children: a daughter, Susan Lynn, born October 10, 1959 in Dallas, Texas; a son, Robert Paul, born July 18, 1962 in Baton Rouge, Louisiana; a daughter, Lori Jon, born September 13, 1963 in Stillwater, Oklahoma; and a son, John Milton, born September 13, 1963 in Stillwater, Oklahoma.

Education: Graduated from Texarkana, Arkansas High School in 1954; attended Hardin-Simmons University during the Fall semester 1954; attended Louisiana State University from the spring semester 1955 through the summer session 1958, obtaining a pre-medical course background; attended Southern Methodist University under the co-op engineering program from August, 1958, until July, 1960, receiving a Bachelor of Science in Mechanical Engineering in August, 1960; received the Master of Science in Mechanical Engineering from the University of Arkansas in June, 1962; attended the 1962 summer session at Louisiana State University to participate in the National Science Foundation sponsored Institute in Radioisotope Methodology; completed requirements for the Doctor of Philosophy in May, 1969.

Professional Experience: Participated in the Southern Methodist University co-op program, gained experience in engineering while working at Chance-Vought Aircraft and Socony-Mobil Field Research Laboratory; employed as instructor of Mechanical Engineering at the University of Arkansas, while completing requirements for the Master of Science in

Mechanical Engineering; taught part-time and served as a research assistant while completing course work requirements for the Doctor of Philosophy; Instructor of Mechanical Engineering at Vanderbilt University from September, 1964 until September, 1966, and from September, 1967 until May, 1969. A member of the honorary organizations of Alpha Epsilon Delta, Pi Tau Sigma, Sigma Tau and Sigma Xi; a member of the American Society for Engineering Education since 1961; a member of the American Society of Mechanical Engineers since 1961, having served as vice-chairman of the Nashville sub-section from June, 1965 to September, 1965, chairman from September, 1965 to June, 1966, and adviser to the Vanderbilt Student Chapter since September, 1967.